AN ABSTRACT OF THE THESIS OF

Teresa King Hagelberg for the degree of Master of Science in Oceanography presented on August 25, 1989.

Title: The Response of Pliocene Climate to Orbital Forcing: Radiolarian Evidence from the Eastern Equatorial Pacific.

Redacted for privacy

Abstract approved: ______________________

Nicklas G. Pisias

A high resolution radiolarian record from eastern equatorial Pacific Deep Sea Drilling Project Site 572 spanning the time period from 1.8 to 4.9 Ma is examined. Paleoceanographic events before and after the onset of Northern Hemisphere glaciation near 2.47 ma, and before and after the closure of the Isthmus of Panama near 3.2 Ma are examined. The response of Pliocene climate to forcing from the Earth's orbital parameters is also evaluated.

A high resolution chronology is developed for site 572 based on orbital tuning methods. Multivariate statistical techniques are used to develop a sea surface temperature (SST) transfer function for this time interval that estimates past SST changes from downcore species abundances of radiolaria. These estimates indicate a mean cooling from lower to upper Pliocene but no significant changes near the onset of Northern Hemisphere glaciation and no abrupt changes before or after the closure of the Isthmus.

Spectral and cross-spectral analyses are used to examine frequency domain characteristics of this SST time series. The spectra indicate a concentration of variance within the precession (23 kyr^{-1}) and obliquity (41 kyr^{-1}) bands in several but not all time intervals. Most variance in the spectra is concentrated at lower frequencies. Cross spectral analysis of the SST time series and calculated orbital variations indicates that the SST record is not coherent with orbital variations.

The nonstationarity of the SST time series is next considered, and the amplitude modulation of the 23 kyr^{-1} and 41 kyr^{-1} components of the SST record is examined. High coherence is seen between the 23 kyr^{-1} component of SST and the amplitude modulation of precession. The amplitude modulation of the 41 kyr^{-1} component of the SST record is dissimilar to the amplitude modulation of obliquity, but extremely similar to and coherent with the 23 kyr^{-1} component of SST. The amplitude modulation of SST and $\delta^{18}O$ at a range of frequency bands have the same features, features which are similar to the modulation of precession. This suggests a strongly nonlinear response of equatorial Pacific SST and planktonic $\delta^{18}O$ to orbital forcing in the Pliocene. Such a response has not previously been seen in a paleoclimatic data set. Although the reasons for this response are still unclear, it is evident that strong nonlinearities in climate are present during this time.

The Response of Pliocene Climate to Orbital Forcing: Radiolarian Evidence from the Eastern Equatorial Pacific

by

Teresa King Hagelberg

A THESIS

submitted to

Oregon State University

in partial fulfillment of
the requirements for the
degree of

Master of Science

Completed August 25, 1989

Commencement June 1990

APPROVED:

Redacted for privacy

Professor of Oceanography in charge of Major

Redacted for privacy

Dean of College of Oceanography

Redacted for privacy

Dean of Graduate School

Date thesis is presented August 25, 1989

Typed by Teresa Hagelberg

ACKNOWLEDGEMENT

I'd like to thank Nick Pisias for support and advice as a major professor over the duration of this study. Guidance particularly in the later stages has provided inspiration for future work. Many thanks to Alan Mix for providing appropriate counterpoints and thought provoking observations and remarks along the way. Thanks also go to the rest of my committee, Dawn Peters and Jerry Heidel.

Pat Hays has been an instrumental and invaluable individual in many ways. She provided much of the essential background material for this work. She also was particularly helpful in the early stages of sampling cores and processing samples. Pat has supplied me with more pertinent advice then I could possibly recall.

Much appreciation goes to Adrienne Roelofs for teaching me about radiolaria and for providing the surface sediment data that is used in this study. I'm also grateful for all the laboratory assistance provided by Adrienne, Katy Condon, Kara Nelson, and Stacey Moore.

Mitch Lyle is thanked for being a good listener and for his helpful discussions. Rainer Zahn also supplied many interesting viewpoints. John Farrell was extremely helpful in providing me with his unpublished carbonate chronostratigraphy for site 572. Warren Prell supplied the isotope and carbonate data. Thanks also to the "computer guys" for their immense patience.

Leigh has been an ideal officemate and a great friend these past three years. Thanks for putting up with me. Hopefully I can return all of her help and support in the near future. Much gratitude also to Cherry and Sharmon for being sympathetic listeners and stress relievers.

Finally, Carl has provided me with infinite emotional support and encouragement, patience, and perspectives. Along with the rest of my family, he has helped to make this possible.

This research was funded by NSF grant OCE-8521815-01.

TABLE OF CONTENTS

LIST OF FIGURES

LIST OF FIGURES

LIST OF FIGURES

LIST OF TABLES

THE RESPONSE OF PLIOCENE CLIMATE TO ORBITAL FORCING: RADIOLARIAN EVIDENCE FROM THE EASTERN EQUATORIAL PACIFIC

INTRODUCTION

In the late 1970's, researchers confirmed that variations in the geometry of the earth's orbital components are a primary cause of late Pleistocene ice ages. Specifically, the ice age - orbit link was strengthened with oceanographic data from deep sea sediment cores which indicate a correlation between the earth's orbital parameters and climatic change (Hays et al., 1976). These parameters of precession, obliquity (tilt), and eccentricity and their corresponding fundamental periods of 23,000 and 19,000 years, 41,000 years, and 100,000 years respectively, account for much of the inferred changes in Pleistocene Northern Hemisphere ice sheet extent and sea surface temperature (Hays et al., 1976; Pisias and Moore, 1981; Imbrie et al., 1984; Martinson et al., 1987). As more and higher resolution data has become available, to a large extent due to the Deep Sea Drilling Project (DSDP), the Ocean Drilling Project (ODP), and the development of the hydraulic piston core (HPC), it is possible to extend high resolution paleoclimatic investigations beyond the Pleistocene, the period of most extensive Northern Hemisphere glaciation, to earlier periods.

The common goal of late Pleistocene studies of paleoclimatic data is the determination of mechanisms that operate within the climate system. These studies have led to the establishment of a high resolution time scale for the Pleistocene (Martinson et al., 1987). Further work includes strategies to decipher the response of the oceanic system to orbital forcing (Imbrie et al., 1989). Understanding the response of other components of the climate system such as sea surface temperature, and the relationships between different regions of the oceans has been a goal as well (McIntyre et al., 1989; Karlin et al., 1989).

An important component of Pleistocene climate is the interactions that are related to the presence of large Northern Hemisphere ice sheets. Dominance of a 100,000 year periodicity in Pleistocene climatic records is generally attributed to a nonlinear response of ice sheets to the eccentricity-modulated precession cycle (Hays et al, 1976; Imbrie and Imbrie, 1980). Results from modelling indicate that incorporation of ice sheet variations into paleoclimate models increase model sensitivity to orbital variations (Birchfield and Weertman, 1982).

Several modelers have presented plausible nonlinear mechanisms in which the 100,000 year oscillations are formed. These models consider both internally formed as well as externally forced oscillations (Birchfield and Grumbine, 1985; Saltzman and Sutera, 1984; Oerlemans, 1982). In any case, ice sheets appear to be a source of internal forcing that amplifies the climatic response to orbital forcing.

One important goal is to understand the relative importance of external orbital forcing versus internal ice sheet forcing to elements of the ocean - climate system . In this study I examine the climatic response of the tropical Pacific in the Pliocene epoch, a period in which major ice sheets are not a significant factor.

High resolution studies of foraminiferal assemblages in Pleistocene and upper Pliocene sections in the equatorial Atlantic suggest that the tropics may be climatically decoupled from higher latitudes (Karlin et al, in press). Equatorial Atlantic sea surface temperature estimates from both time intervals suggest that equatorial oceans respond linearly to precessional forcing independent of ice sheet forcing and modulation over the past 2.4 ma. A detailed study of the equatorial Pacific climatic response should provide a means of testing this hypothesis.

This study investigates the response of tropical Pacific climate to orbital forcing in the absence of major Northern Hemisphere ice sheets and the evolution of this response through the Pliocene. Two specific quesions are posed: (1) do the tropics respond to orbital forcing throughout the Pliocene, before and after the onset of Northern Hemisphere glaciation and before and after the closure of Isthmus of Panama, and (2) what factors may influence this response?

STUDY AREA

I. Physical Setting

A. Modern

One prerequisite to examining the above climatic responses is a study area with an absence of local effects so strong that long term trends are obscured, yet with a significant amount of oceanographic variability. The eastern equatorial Pacific is such a region; it is geographically removed from direct ice sheet forcing and it is a region with distinct oceanographic variability on annual time scales and beyond.

The surface ocean currents of the eastern tropical Pacific (Figure 1) generally reflect the trade wind system. Corresponding to the northeast and southeast trade winds are the westward flowing South Equatorial Current (SEC) and North Equatorial Current (NEC), respectively. The SEC, the strongest surface current in the equatorial Pacific, can be split into three branches lying between 0° and 4°N, 0° and 8°S, and south of 9°S (Wyrtki and Kilonsky, 1984). The NEC lies in the latitude range of 8°N to 20°N. Corresponding to the Intertropical Convergence Zone (ICTZ), a region of weak and variable winds that migrates seasonally with the southeast trades, is the eastward flowing North Equatorial Countercurrent (NECC). The NECC, which varies seasonally with the NEC, flows between 2°N and 9°N.

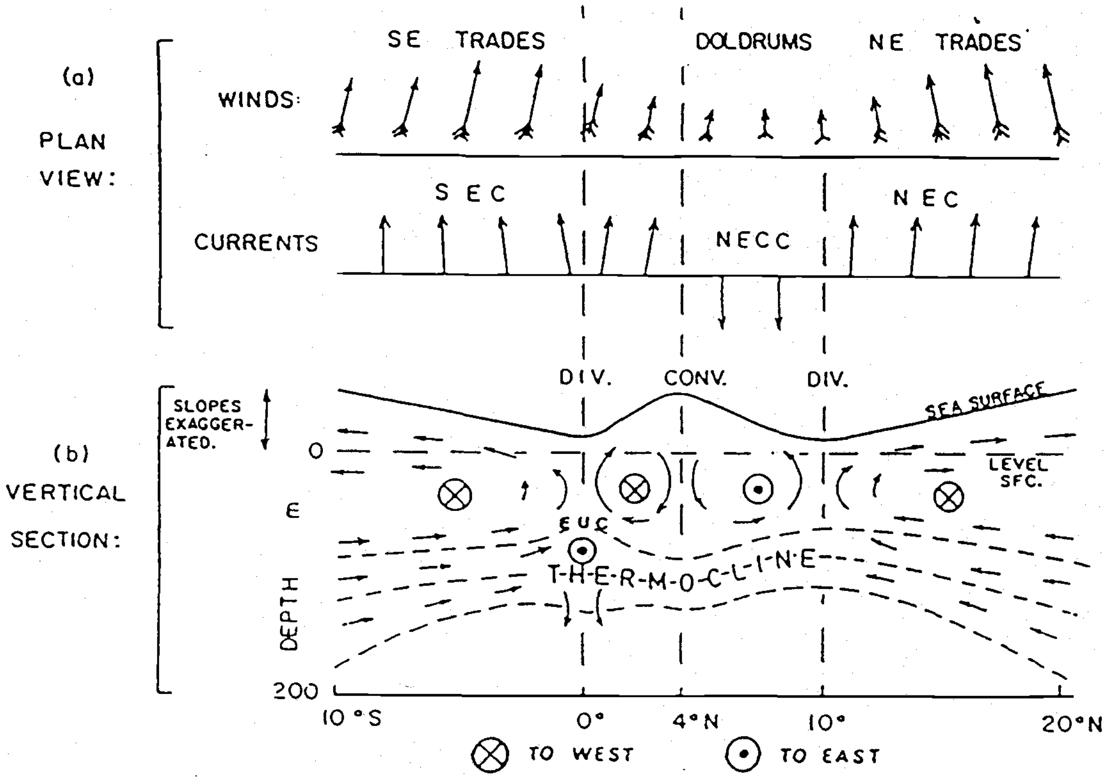

Figure 1: (a) Schematic diagram of prevailing winds and east-west surface currents in the equatorial Pacific.
(b) Vertical section indicating sea surface slopes (exaggerated), thermocline structure and current directions (from Pickard and Emery, 1982).

The subsurface, eastward flowing Equatorial Undercurrent (EUC) is also an important component of the equatorial current system. Situated beneath the SEC, the core of the EUC lies at the equator beneath the base of the mixed layer. Together with the thermocline, the EUC shoals eastward in the equatorial Pacific (Wyrtki, 1966; Philander, 1973; McPhaden, 1986; Hayes, 1987). The features of the EUC are consistent with a baroclinic zonal pressure gradient due to the dominance of trade winds which pile up warm water in the western Pacific and provide a source of eastward momentum for the current (Philander, 1973; McPhaden, 1986).

Associated with the EUC and the SEC is equatorial divergence brought about by the interaction of the Coriolis force with major current boundaries (Figure 1). This divergence provides a source of nutrient rich water along the equator. Features of equatorial divergence are reflected in surface and sediment distributions of plankton (Lombari and Boden, 1985).

The trade winds that force the equatorial surface currents undergo a seasonal cycle of location and intensity. In February the Northeast trades extend to approximately 5°N in the eastern Pacific and the Southeast trades extend across the equator (Figure 2). In August, however, the Northeast trades only extend to about 10°N while the Southeast trades extend to around 5°N (Figure 2).

Figure 2: February (top) and August (bottom) surface currents in the eastern equatorial Pacific. Vectors indicate velocity and direction of the currents; thin dashed lines indicate the Intertropical Convergence zone and thick dashed lines indicate current boundaries (From Wyrtki, 1965).

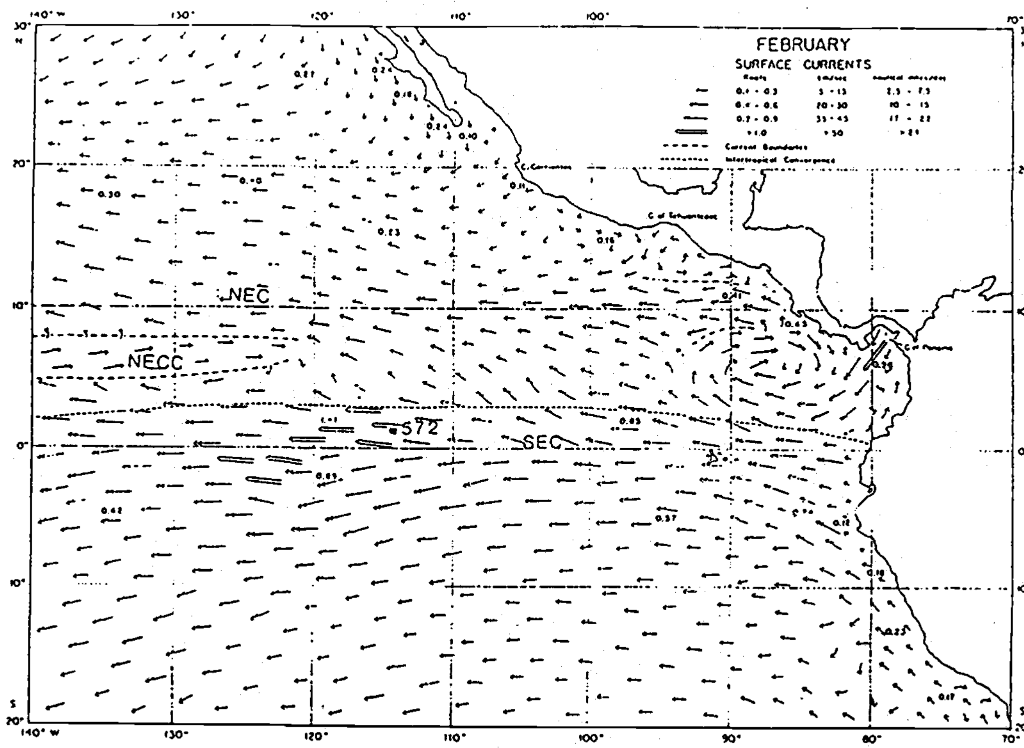
FEBRUARY
SURFACE CURRENTS
NEC
NECC
SEC
572

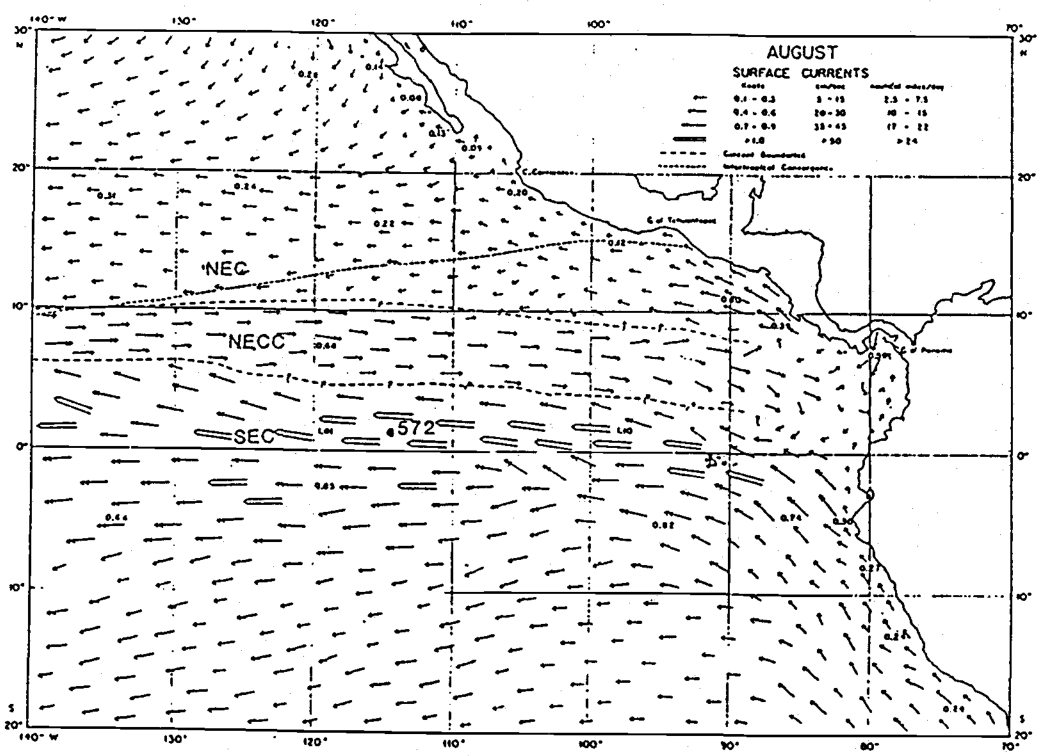
AUGUST
SURFACE CURRENTS
NEC
NECC
SEC
572

Figure 2

These variations are transferred to seasonal variations in the intensity of the SEC, EUC, and NEC, and in the migration of the Inter-Tropical Convergence Zone (Wyrtki, 1965; Hayes, 1987; Picard and Emery, 1982).

On annual scales, the eastern equatorial Pacific wind and sea surface temperature (SST) cycles are also related. Unlike non-equatorial regions where the annual sea surface temperature cycle is primarily due to the annual cycle in solar heating, in the eastern equatorial Pacific the annual SST cycle is related to the annual cycle in surface wind convergence through a series of feedbacks (Horel, 1982). Heat transport models of this region indicate that more significant heat is supplied through eastward flow than through heat gain from the atmosphere (Bryden and Brady, 1985).

B. Pliocene Setting

Two events which could have important implications for tropical Pacific ocean circulation occurred during the Pliocene: first, the closure of the Isthmus of Panama around 3.5-3.2 ma (Keigwin, 1982; Berggren and Hollister, 1974), ended equatorial circulation between the Atlantic and Pacific. Biogeographic and geochemical indicators suggest that surface water exchange between the Atlantic and Pacific became increasingly restricted at this time (Keigwin, 1982).

A second significant event occurring at about 2.47 ma was a shift in the oxygen isotopic ratios recorded in foraminifera that is believed to represent the onset of major Northern Hemisphere glaciation (Prell, 1984; Shackelton et al., 1984). At this time evidence in the Pacific for major ice rafting includes diatom floral changes (Rea and Schrader, 1985), and greater winds at 2.6 ma (Janacek, 1983). Increased input of ice rafted debris in the Norwegian Sea at around 2.56 ma is further evidence of large scale glaciation initiation at this time (Jansen et al, 1989).

II. Previous Results

Much of the previous paleoceanographic research in the eastern equatorial Pacific concerns the Pleistocene and the response of the region to the late Pleistocene ice ages (Molina-Cruz, 1977a, b; Romine, 1981; Schramm, 1985). These studies relied on quantitative techniques using microfossil proxy indicators to estimate the response of the tropical Pacific to climatic change.

In the Pliocene equatorial Pacific, much of the previous research is stratigraphic in nature (Nigrini, 1968; Hays et al., 1969; Dunn and Moore, 1981; Dunn, 1982). Paleoceanographic studies have focused on the timing of the onset of initiation of major Northern Hemisphere glaciation using oxygen isotope indicators from foraminifera (Shackelton and Opdyke, 1977; Prell, 1984; Prell, 1985).

Hays (1987) and Hays et al. (1989) compared the paleoceanography of the Pliocene eastern equatorial Pacific (DSDP sites 572 and 573) to that of the Pleistocene (piston cores RC10-65 and RC11-210). These studies used quantitative methods similar to those of late Pleistocene paleoclimatic studies and estimated paleotemperatures from radiolarian assemblages. Although this study was of relatively high resolution, the 20 cm sampling interval in sites 572 and 573 corresponds to a resolution on the order of approximately 15,000 years, which is too low to quantitatively discern orbital frequencies in the data without the possibility of sample aliasing (Pisias and Mix, 1988). In this study I increase the resolution of Hays (1987) and Hays et al. (1989) to include orbital frequencies.

III. Site 572

The high resolution paleoceanographic record used in this study is from DSDP Site 572, located at 1°26'N, 113°50'W. Situated within the SEC and EUC, Site 572 provides an appropriate oceanographic setting (Figure 2). The oceanographic location of site 572 has not changed significantly due to plate motion; over the past 4 million years it has remained between 0° and 1°N and has not moved more than 2° east (van Andel et al., 1975). Seasonality at site 572 has been found by Hays (1987) and Hays et al.

(1989) to be approximately the same over the past 4 million years making Pliocene seasonal thermal gradients comparable to Pleistocene and modern gradients at this site.

The hydraulic piston-cored site is marked by high core recovery and high but variable sedimentation rates (Mayer, et al, 1985). At a water depth of 3900m, its lithology of cyclic siliceous calcareous ooze chalk represents the "equatorial bulge" of productivity due to equatorial divergence. Carbonate content ranges from 45% to 90%, and provides a high resolution stratigraphic tool. The radiolaria at site 572 are well preserved (Nigrini, 1985). Unfortunately, no magnetostratigraphy is available for site 572 due to the very low intensities measured as well as overprinting due to chemical alteration (Mayer et al., 1985).

METHODS

I. Sampling

Samples of approximately $10cm^3$ were taken from Deep Sea Drilling Project cores 572a and 572c every 10cm, from 29.60m to 45.90m in 572a and from 48.59m to 69.09m in 572c. Core 572c was sampled in the lower portion of the record as 572a is marked by severe coring disturbance in this part of the section. The samples were freeze dried and split. From each sample, approximately 0.5 g was used to determine $CaCO_3$ for stratigraphic purposes, and 0.5 g was used to prepare radiolaria slides according to the random settling method of Roelofs and Pisias (1986). Calcium carbonate percentages for each sample were determined using the method of Dunn (1980); the data are in Appendix I.

II. Core Splicing

Another obstruction to pre-Pleistocene high resolution paleoclimatic work has been a lack of sediments of adequate resolution to examine orbital variations. Because the coring disturbance observed in the different holes drilled at DSDP site 572 and because of potential loss of sediment between successive cores, detailed stratigraphic analysis is necessary to produce a continuous composite Pliocene record. Here the development of this composite record is outlined.

Comparison of the 572a carbonate record to the corresponding 572c carbonate record of Pisias and Prell (1985) suggests that the amount of distortion in 572a relative to 572c varies downcore (Figure 3). It is advantageous to minimize this distortion as it can broaden spectral peaks or cause a data set to have extra spectral peaks when analyzing data in the frequency domain (Martinson, 1982). To correct this distortion and to accurately splice together 572a and 572c, the inverse correlation techniques of Martinson (1982) are used.

Inverse correlation is an objective method of correlating two signals. The technique relates a distorted signal to a reference signal via a mapping function. The coefficients of the mapping function are selected to maximize the correlation coefficient between two signals based on inverse techniques. In mapping the 572a downcore carbonate record onto 572c, 572c is chosen as the reference signal since there is less apparent coring disturbance downcore, as revealed by visual inspection of the cores. Thus it is assumed that 572c has experienced minimal distortion, and that 572a is the distorted signal.

The mapping function is used to assign to each sample in hole 572a an equivalent sub-bottom depth in 572c. In this way a composite depth scale is produced which yields a consistent sub-bottom depth to work with (hereafter referred to as 572 depth). The initial coherence of the

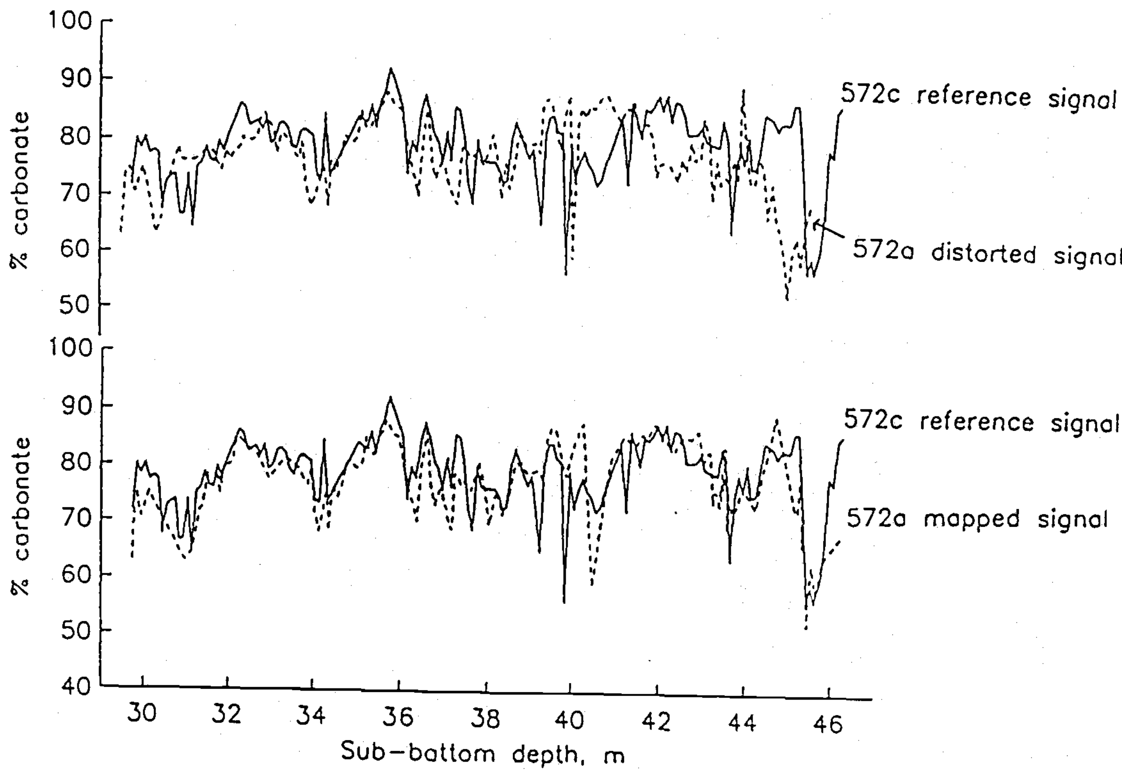

Figure 3: **Top:** Comparison of the Site 572c $CaCO_3$ record (Pisias and Prell, 1985) to the 572a $CaCO_3$ record.
Bottom: The 572a $CaCO_3$ record following mapping onto the 572c $CaCO_3$ record.

572a and 572c carbonate records was 0.41; after mapping 572a onto 572c, the coherence was increased to 0.68. Results of the mapping process are illustrated in Figure 3, and the mapping function is presented in Appendix II.

III. Chronostratigraphy

A. Initial Development

When analyzing time series of geologic data, the development of an accurate high resolution chronology is of utmost importance. Lack of such resolution can result in misidentification of important events, particularly in the frequency domain. Here the chronostratigraphic development of site 572 is outlined.

Biostratigraphy and carbonate stratigraphy places site 572 into an initial chronologic framework. Hays (1987) identified a set of radiolarian datums at site 572 and at DSDP site 573 (0° 30'N, 133° 19'W), 3 of which can be reliably located to within +/- 20 cm. These 3 datums are: *Theocalyptra davisiana var. davisiana* (FAD), *Sticho-corys peregrina* (LAD), and *Phormostichoartus doliolum* (LAD). These datums provided general biostratigraphic control for 572 and 573 in her study. Although these Pliocene radiolarian datums do not provide the detailed chronologic resolution necessary for this study, they can serve as a check on the final chronology. The locations of radiolarian datums identified to within +/- 10cm in this study are listed in Table 1.

Carbonate stratigraphy for Site 572 was developed by correlating carbonate events in Site 572c to carbonate and magnetostratigraphic events in nearby site 573 (Prell, 1985; Farrell, unpublished data). Carbonate events, defined by minima and maxima in $CaCO_3$ percentages, are high resolution stratigraphic tools in the equatorial Pacific. This correlation, together with the magnetostratigraphy available for site 573, provides the initial chronology for site 572 and is the basis for further fine scale adjustments.

B. Orbital Tuning

To develop a high resolution chronology, orbital tuning methods were employed. The basic assumption involved in orbital tuning of a time scale is that changes in the marine oxygen isotope record are related to changes in the obliquity of the earth's orbit via some time constant. The marine oxygen isotope record is a globally consistent signal in the Pleistocene (Imbrie et al, 1984), and since the calculated timing of orbital variations in eccentricity, obliquity (tilt), and precession are reasonably accurate during this time period (Berger, 1978, 1984), this relationship can be used to "tune" the oxygen isotope record to the time scale of the obliquity fluctuations. Assuming that obliquity affects the Pliocene planktonic and

Table 1: (Top) Location of important radiolarian events in Site 572 and comparison of previously established datums.

(Bottom) Comparison of established ages of magnetostratigraphic events ages estimated from the tuned chronology, as a measure of accuracy.

Biostratigraphic Events

Event	572 Depth (m)	Estimated Age (Hays, 1987)	Estimated age (This study)
FAD *T. davisiana*	37.70	2.4 Ma	2.42 Ma
LAD *S. peregrina*	41.88	2.7 Ma	2.66 Ma
LAD *P. doliolum*	57.00	3.6 Ma	3.62 Ma

Magnetostratigraphic Events

Event	572 Depth (m)	Estimated Age* (Farrell, unpub. data)	Estimated age (This study)
Matuyama/Gauss	38.00	2.47 Ma	2.44 Ma
upper Kaena	45.44	2.92 Ma	2.92 Ma
lower Kaena	46.84	2.99 Ma	2.99 Ma
upper Mammoth	47.64	3.08 Ma	3.06 Ma
lower Mammoth	49.04	3.18 Ma	3.17 Ma
Gauss/Gilbert	52.74	3.40 Ma	3.42 Ma
upper Cochiti	59.14	3.86 Ma	3.82 Ma
lower Cochiti	59.84	3.95 Ma	3.92 Ma
upper Nunivak	61.14	4.08 Ma	4.05 Ma
lower Nunivak	62.34	4.21 Ma	4.18 Ma
upper Sidufjall	63.64	4.35 Ma	4.29 Ma
lower Sidufjall	64.34	4.43 Ma	4.36 Ma
upper Thvera	65.14	4.52 Ma	4.45 Ma
lower Thvera	66.94	4.71 Ma	4.64 Ma

*Dates given are from Mankinen and Dalrymple (1979) benthic oxygen isotope records in a similar manner as the Pleistocene (although ice sheets are not as significant in amplifying the response), tuning of the site 572 chronology should increase timescale accuracy and should reduce distortions caused by variations in sedimentation rate.

This method assumes that solutions of the variations of orbital parameters are accurate over the time interval in question. Berger (1984) has analyzed the stability of the solutions of the orbital parameters, and claims that, in the frequency domain, the 400,000, 100,000, 41,000, 23,000, and 19,000 year elements do not deteriorate over the past 5 million years; thus the frequency characteristics of these orbital frequencies are sufficiently stable for this study. Beyond 5 ma, uncertainties in the calculations of the planetary system become significant (Berger, 1984).

Several studies have used variations in the calculated orbital record to tune the global oxygen isotope chronology in the Pleistocene (Kominz et al,1979, Hays et al, 1976, Morley and Hays, 1981). A number of various tuning approaches have been used and are summarized in Martinson et al. (1987). Imbrie et al. (1984) tuned a "stacked" oxygen isotope record (the SPECMAP stack) extending back 800,000 years.

Another important assumption made in tuning paleoclimate records is that the phase between the forcing (obliquity) and the response (oxygen isotope signal) is constant with time and is known. For Pleistocene studies this phase was determined based on independent radiometric dates (Hays et al., 1976). This phase (Φ) can be expressed in terms of a linear response of the climate system to orbital forcing:

$$\Phi = \tan^{-1}(2\pi)fT,$$

where T = the time constant, and f = the forcing frequency. As the frequency of the forcing is known, the problem with estimating phase lag lies in the estimation of the time constant. The estimate T = 17,000 years used by Imbrie and Imbrie (1980) is derived from radiometrically controlled data and is based on ice sheet changes in the last 127,000 years (Hays et al., 1976).

It is likely that there is some error present in using the same T for the past 5 million years. In this study however, the concern is not so much error in the estimate of T but rather error introduced by the assumption of a constant response time of climate. Analysis of late Pleistocene records indicates that error in the estimate of T of +/- 3000 years can introduce errors in time lag estimates of not more than 500 years (Imbrie et al., 1984). Because this error is small relative to the sampling interval in this study, possible error in the estimate of T will be disregarded.

The data set used to tune the Site 572 chronology is the 572c oxygen isotope data (Prell, 1985; Figure 4). This data is obtained from the planktonic foraminifer Globigerinoides sacculifera, and is spaced at 10 cm intervals. (This isotope data has a systematic per mil offset (J. Farrell, pers.comm.) which has not been corrected as it does not affect the outcome of the tuning method.)

The chronology developed in the previous section is used to provide initial time control. Conventionally, magnetic and tightly constrained biostratigraphic events are held fixed throughout the tuning process (Imbrie et al., 1984). In site 572, since magnetics are absent and the biostratigraphic data has a margin of error larger than the scale of the tuning, both of these constraints are relaxed. However, efforts are made to keep track of key stratigraphic control points as well as core breaks throughout the process.

The method of Imbrie and Imbrie (1980) is used to apply a time constant to the calculated obliquity cycle of the past 4.8 million years (Berger, 1978). This phase shifted obliquity signal and the oxygen isotope signal are related within a narrow frequency band of 41,000 years^{-1}. To compare these two signals they are bandpass filtered at a frequency centered at 41,000 years^{-1}. In the first tuning iteration, the filter covers a relatively wide frequency band in order to capture drift introduced by error in the initial oxygen isotope chronology. The band

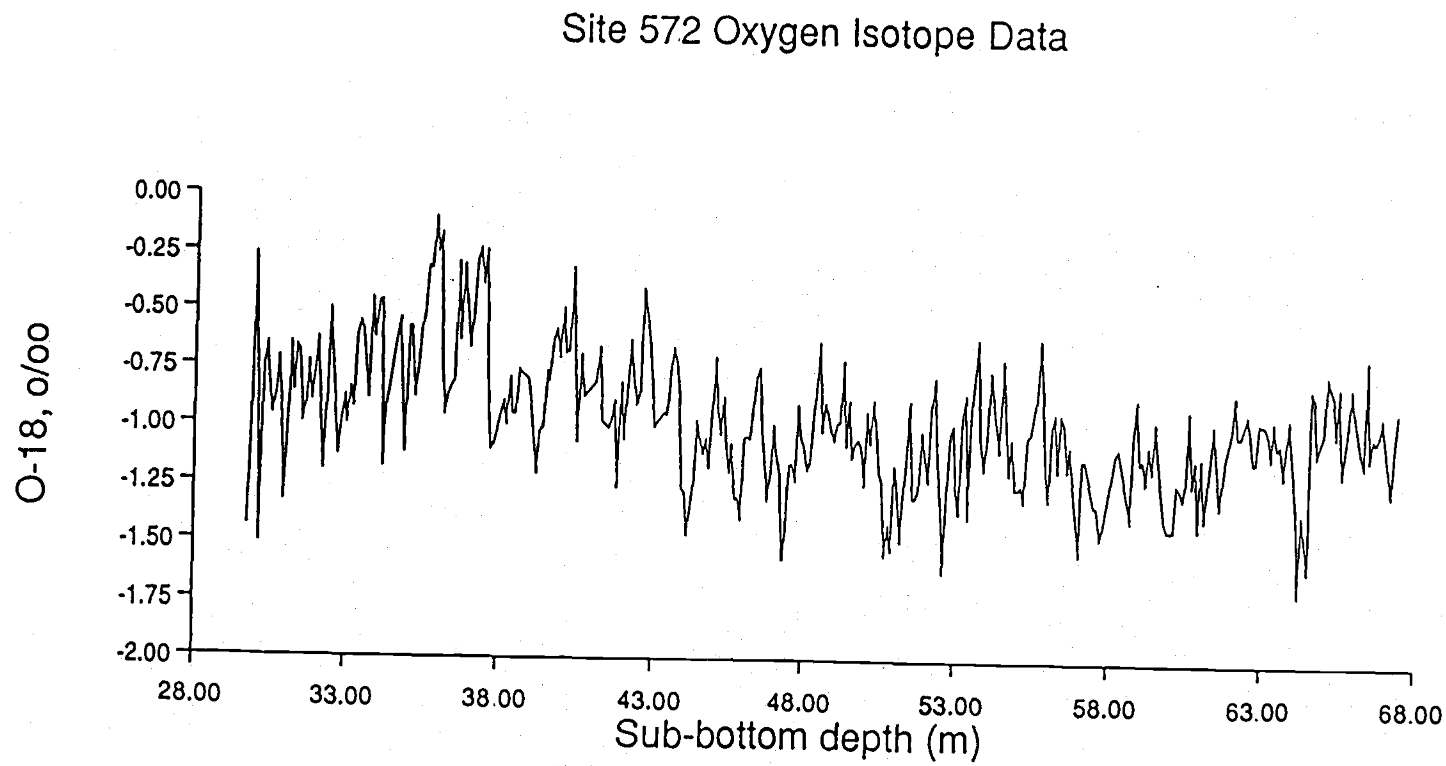

Figure 4: The site 572 $\delta^{18}O$ record (Prell, 1985).

is not so wide as to encompass other orbital frequencies which may be present in the data, however (Figure 5).

Adjusting the filtered oxygen isotope curve to better match the filtered obliquity curve ("tuning") produces a revised chronology for Site 572 (Figure 6). As a check, the unfiltered oxygen isotope data can be bandpass filtered again to insure that the amplitude variation of the signal is preserved. After this first iteration is satisfactory, the data can be tuned in progressively narrower bands to get a best fit. In this case, two iterations produced a chronology for Site 572 that is accurate within the range of uncertainty introduced by the sampling interval (Figure 6). Over the interval from 1.95 to 4.59 ma, the average adjustment to the initial chronology was 0.026 ma, the largest and smallest adjustments being 0.07 ma and 0 ma, respectively. Comparison with previous chronologies for this Site are presented in Figure 7. This comparison indicates only minor adjustments to the initial chronology.

There are a number of independent checks available to assess the accuracy of this chronology. Comparison of the ages of radiolarian events estimated from this chronology to previous estimates (Hays, 1987; Hays et al., 1989) indicates surprisingly good agreement considering the lower resolution of the earlier estimates (Table 1). Similarly, estimated ages of magnetostratigraphic events correlated via carbonate events in 572 and 573 indicates an error of

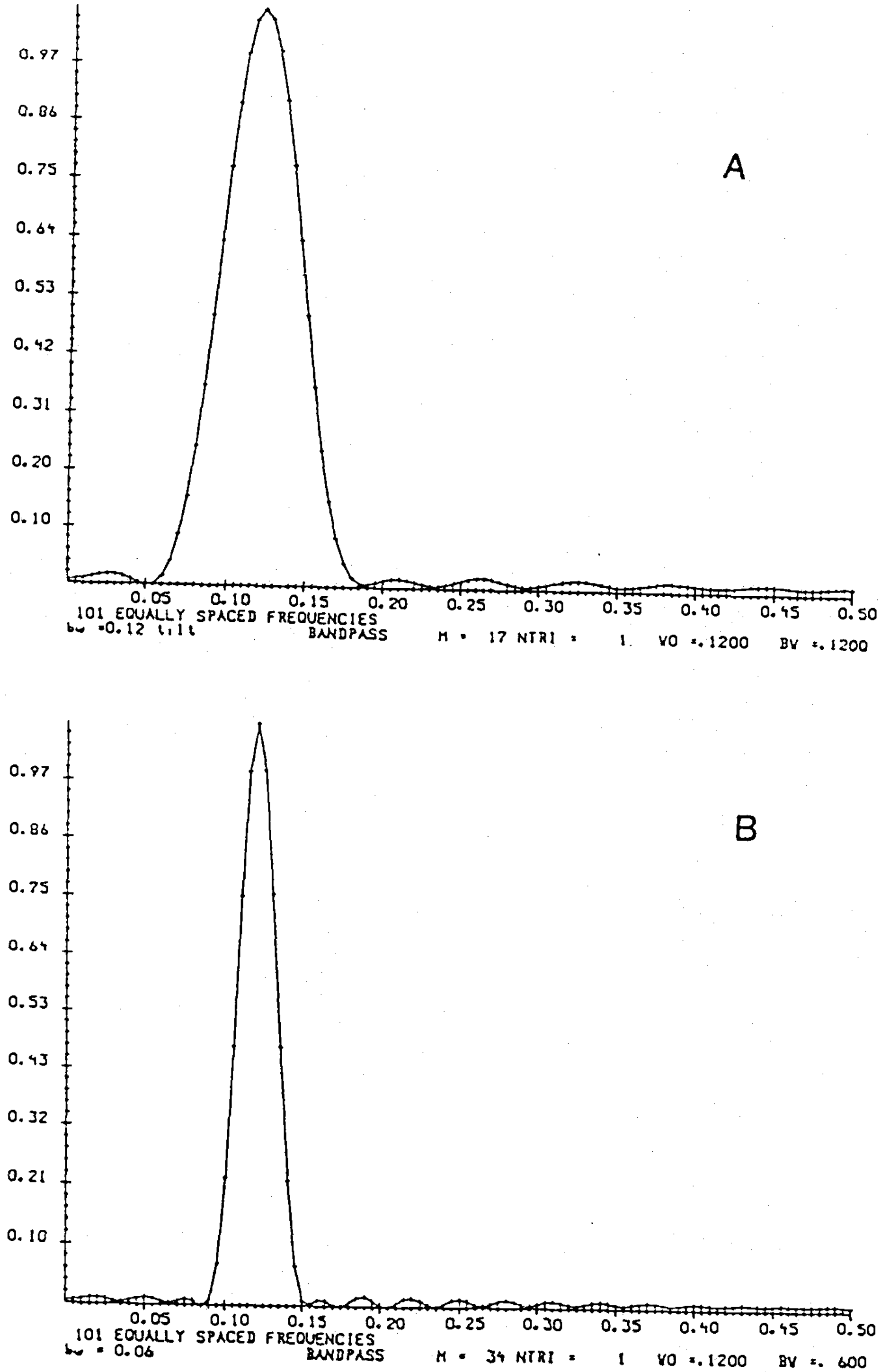

Figure 5: (a) "Wide" bandpass filter - initial iteration
(b) "Narrow" bandpass filter - second iteration

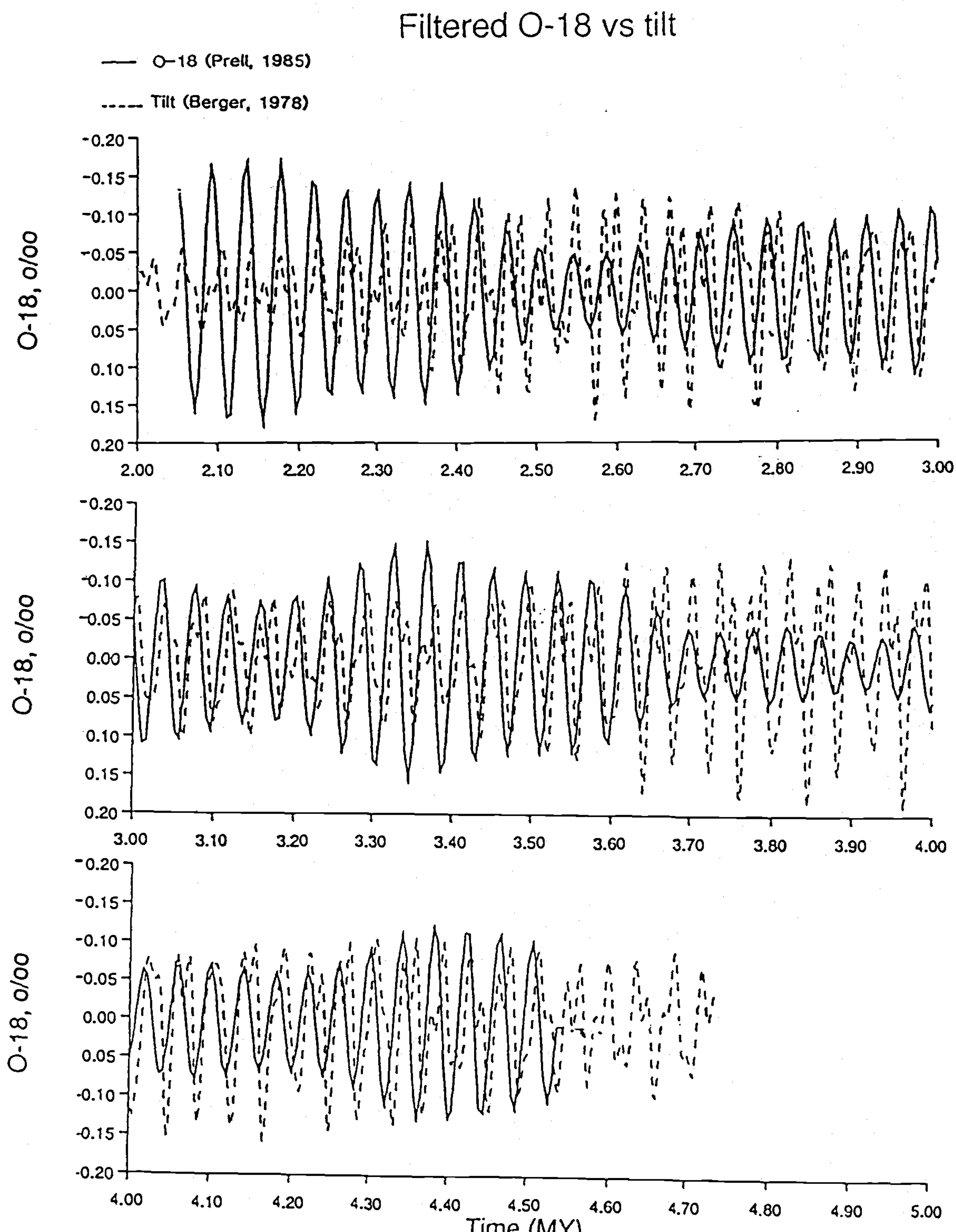

Figure 6: Bandpass filtered obliquity (dashed line) and $\delta^{18}O$ (solid line), 1.8 - 4.8 ma, with time constant applied using the method of Imbrie and Imbrie (1980).

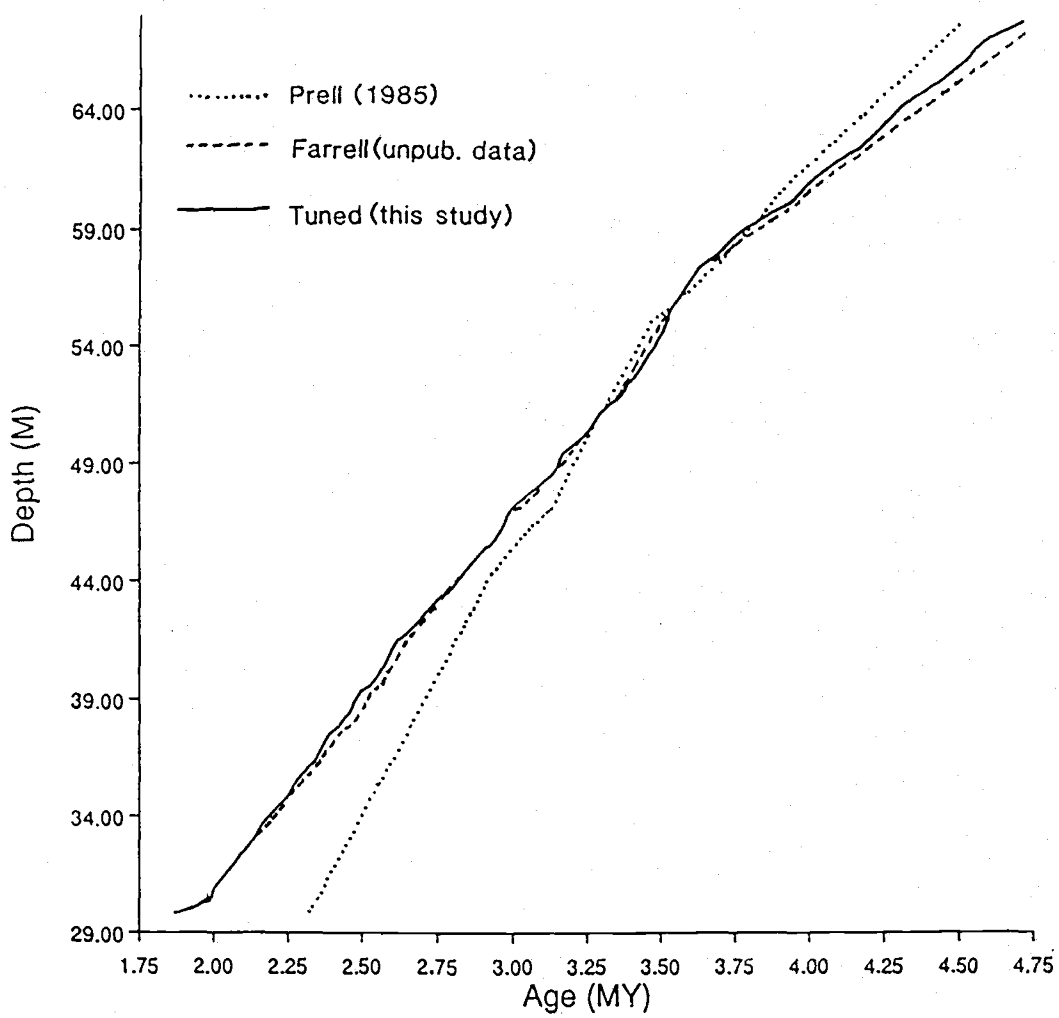

Figure 7: Comparison of tuned time scale with previous chronologies for 572 - Prell (1985), Farrell (unpub. data).

less than 1% from established dates (Mankinen and Dalrymple, 1979; Table 1). This error is well within the ability to correlate sites 572 and 573 and is within the margin of error of the paleomagnetic dates (Mankinen and Dalrymple, 1979).

The calculated cross-spectra of the oxygen isotope data and the orbital parameters provides another method of assessing the improvement of the tuned time scale over previous chronologies. The tuned $\delta^{18}O$ record has higher coherence with obliquity than the previous chronology (Figure 8). This indicates that although only minor adjustments were made to Farrell's chronology, large changes in coherency are seen. As a final check, comparisons in the interval from 1.88 - 2.4 ma suggest that this chronology for Site 572 is consistent with that of others (Raymo et al., 1989).

Considering that the resolution of Site 572 has definite technical limitations, the chronology resulting from orbital tuning provides very satisfactory results. In conclusion, it is useful to note that tuning to one frequency (obliquity) in one variable (oxygen isotope data) does not induce artificial spectral peaks in other independent variables (SST); it can however, enhance those frequencies that already exist (Pisias, 1983).

Figure 8: Cross-Spectra of $\delta^{18}O$ and etp: (a) Farrell chronology (b) tuned chronology. Solid line represents the spectra of orbital forcing (eccentricity + obliquity + precession, or etp) and the dashed line represents the spectra of the respective $\delta^{18}O$ records. The solid line with crosses represents the coherency of the orbital and isotopic time series at every frequency interval. Horizontal axis units in frequency cycles/ 5000 yr; Vertical axis units are coherency. Solid horizontal line gives level of the test statistic for nonzero coherency. Confidence interval, bandwidth, and number of lags (m) given at the top of the plot.

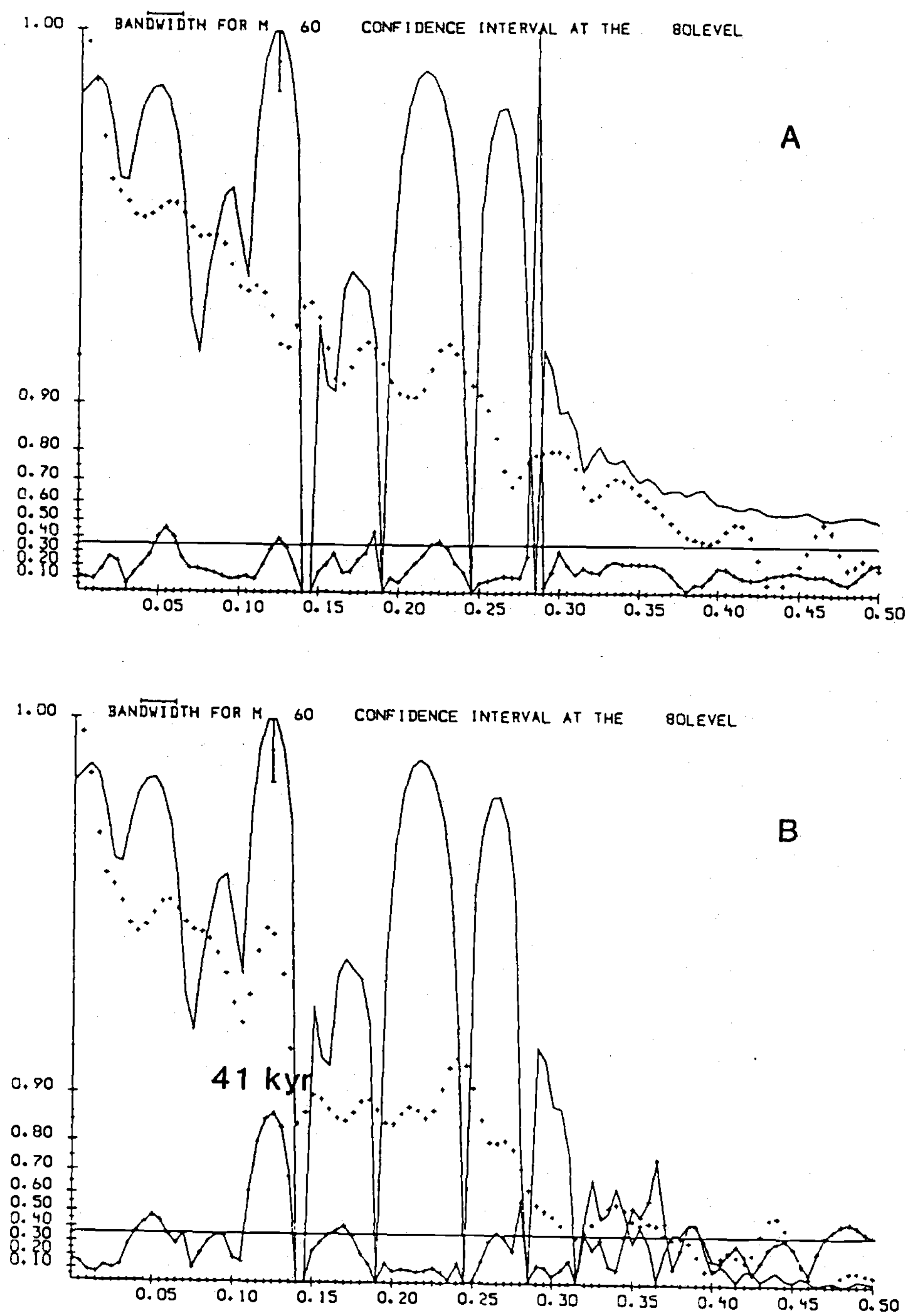
1.00
BANDWIDTH FOR M 60 CONFIDENCE INTERVAL AT THE 80LEVEL
A
0.90
0.80
0.70
0.60
0.50
0.40
0.30
0.20
0.10
0.05 0.10 0.15 0.20 0.25 0.30 0.35 0.40 0.45 0.50
1.00
BANDWIDTH FOR M 60 CONFIDENCE INTERVAL AT THE 80LEVEL
B
41 kyr
0.90
0.80
0.70
0.60
0.50
0.40
0.30
0.20
0.10
0.05 0.10 0.15 0.20 0.25 0.30 0.35 0.40 0.45 0.50

Figure 8

IV. High Resolution Paleoceanography

A. Radiolarian Species Selection

In the equatorial Pacific, radiolaria are excellent measures of oceanographic variability; they provide a more complete coverage of the water masses than other paleo-indicators (Moore, 1978); they are more diverse than foraminifera, and their siliceous skeletons are resistant to dissolution. Studies have demonstrated that the distribution of radiolaria in the surface sediments closely parallels surface water masses and currents (Moore, 1978; Pisias et al., 1986). Using radiolaria to quantitatively characterize past surface water distributions is a technique that has been demonstrated by Moore (1978) and other workers (Molina-Cruz, 1977a; Robertson, 1975).

In order to obtain a reasonably good estimate of the radiolarian population, 800 to 1000 individual radiolaria were counted in each sample. The relative percents of the species identified in each sample (50-60% of the total number counted) were calculated for use in statistical analyses.

In order to minimize the influence of taxonomic difficulties, this study uses only the surface sediment radiolarian data that has been recounted in the OSU lab. Only species whose taxonomy is well defined, whose counts can be duplicated by independent observations, and whose distribution maps are reasonable are included among the species counted. A total of 91 different species were counted in every sample (Table 2).

B. Transfer Function Development

Using quantitative multivariate statistical techniques developed by Imbrie and Kipp (1971), the relative abundances of radiolaria in the surface sediment can be used to infer past changes in oceanographic conditions. These techniques are used to develop a sea surface temperature (SST) transfer function for the Pliocene. This transfer function first employs Q-mode factor analysis with a VARIMAX rotation (Klovan and Imbrie, 1971; Klovan and Miesch, 1976) to partition surface sediment radiolarian assemblages into a set of linearly independent "factors".

The original data matrix $X_{n\times m}$, is transformed into a row-wise normalized matrix $U_{n\times m}$ (where n is the number of samples and m is the number of species), and described as the product of two matrices: $U_{n\times m} = B_{n\times f}F_{f\times m}$. $B_{n\times f}$ is the Factor Loading matrix, which describes the importance of each factor in each of n samples, and $F_{m\times f}$ is the Factor Score matrix, which describes the importance of the m original variables in defining each of f factors. $F_{m\times f}$ is used together with the downcore species data from site 572 to determine the time variation of the factors during the Pliocene.

Table 2: Radiolarian species counted in this study.

*S1	_Spongurus_ sp.
*S1A	_Spongurus cf. elliptica_
S3	_Actinomma medianum_ and _Actinomma arcadophorum_
*S4	_Actinomma leptodermum_
*S7	_Echinomma cf. leptodermum_
*S8	_Prunopyle antarctica_
S9	_Amphirhopalum ypsilon_
*S10	_Echinomma delicatum_
S11	_Collosphaera tuberosa_
*S12	_Euchitonia furcata/elegans_
*S13	_Polysolenia spinosa_
*S14	_Heliodiscus asteriscus_
S15	_Actinomma antarcticum_
*S17	_Hexacontium enthacanthum_ and _Hexacontium laevigatum_
*S18	_Hymenastrium euclidus_
S19	_Larcospira quadrangula_
S21	_Cenosphaera coronata_
*S23	_Didymocyrtis tetrathalamus tetrathalamus_
*S24	_Lithelius minor_
S29	_Larcopyle butschlii_
*S30	_Stylochlamydium asteriscus_
S32	_Polysolenia arktios_
S33	_Polysolenia lappacea_
*S34	_Polysolenia murrayana_
S36	_Dictyocorne truncatum_
*S36A	_Dictyocorne profunda_
*S36C	_Dictyocorne truncatum_ and _Euchitonia triangulum_
*S40	_Spongaster tetras tetras_
*S41	_Spongurus pylomaticus_
S42	_Spongocore puella_
*S43	_Spongopyle osculosa_
S44	_Spongotrochus glacialis_
*S47	_Stylodictya validispina_
*S48	_Porodiscus_ sp. B
S50	_Axoprunum stauraxonium_ and _Stylosphaera lithatractus_
*S51	_Stylatractus_ spp.
S52	_Styptosphaera spumacea_
S53	_Hexapyle_ spp.
*S54	_Octopyle stenozoa_ / _Tetrapyle octacantha_
C1N	_Collosphaera invaginata_
SLB	_Lithosphaera bacca_
*N1	_Liriospyris reticulata_
N2	Anthocyrtidium ophirense
N3	_Anthocyrtidium zanguebaricum_
*N4	_Carpocanistrum_ group
N5	_Lamprocyrtis nigriniae_
*N7	_Pterocorys minithorax_
N8	_Carpocanistrum papillosum_
GN8	_Loghospyris pentagona pentagona_

Table 2, continued

*N9	Giraffospyris angulata
N10	Eucyrtidium acuminatum
N11	Eucyrtidium hexagonatum
*N14	Tholospyris scaphipes
N15	Lamprocyclas junonis
N16	Lamprocyclas maritalis polypora
N17	Lamprocyclas maritalis maritalis
*N18	Botryocyrtis auritus/australis
N19	Botryocyrtis scutum
N24	Pterocanium spp.
*N27	Pterocanium praetextum, Pterocanium eucolpum
N28	Pterocanium trilobum
*N29	Pterocorys hirundo
N32	Phormostichoartus corbula
*N33	Botryostrobus aquilonaris
N35	Theocalyptra davisiana var. semeloides
*N35A	Theocalyptra davisiana davisiana
*N36	Theocalyptra bicornis
*N38	Theocalyptra bicornis
N39	Theoconus hertwigii
*N40	Pterocorys zancleus
N42	Theocorythium trachelium trachelium
N43	Dendrospyris borealis
E1	Lamprocyclas neoheteroporous
E2	Lamprocyclas heteroporous
E3	Theocorythium vetulum
E4	Didymocyrtis avita
E5	Didymocyrtis penultima
E6	Stylatractus universus
E7	Pterocanium prismatium
E8	Stichocorys peregrina
E9	Spongaster pentas
E10	Phormostichoartus fistula
E11	Phormostichoastus doliolum
E12	Botryostrobus bramlettei
E13	Lychnodictyum audax
E14	Phormostichoastus marylandicus
E15	Solenosphaera omnitubus
E16	Stichocorys delmontensis
E17	Stichocorys sp.

* - indicates species used in transfer function. (See 'Species Selection'). All of the species listed except for E1 - E17 (the extinct species) are described in Nigrini and Moore, 1979. The extinct species are described in Nigrini and Lombari, 1984.

Regression of these factors against modern August and February sea surface temperatures produces a set of equations that describe sea surface temperature in terms of the radiolarian assemblages. These equations can then be used to estimate paleotemperatures.

There are a number of restrictions to consider in developing a transfer function for the Pliocene. Species of radiolaria that go extinct or exhibit abundances for which there is no analog in the modern ocean cannot be used, thus narrowing the number of available species. An example of this is the species Theocalyptra davisiana, which has been recognized as an important indicator of western subarctic waters (Moore, 1978; Morley, 1980). The first appearance datum for T. davisiana is at about 2.4 ma, excluding it from the factor analysis used in this study.

The high diversity of radiolaria is reflected the large number of species having fairly low average abundances. Species averaging less than 1% (0.2 -1%) are included in the factor analysis only if their variation is consistent with that of more abundant species. Species with similar morphologies (S4, S7, and S8; see Table 2) are lumped when their surface sediment distributions are very similar and factor analysis suggests that the species act alike. Species used in this transfer function include those shown not to be greatly affected by dissolution in sediments (Pisias et al., 1986). Of the 74 extant species within the 91 different radiolarian species counted, 35 fit all of the above criteria. These species, noted in Table 2, are used in estimating paleotemperatures for Site 572.

The accuracy of these paleotemperature estimates cannot be evaluated without other independent measures. In Pleistocene equatorial Pacific sediment core RC13-110, independent estimates of paleotemperatures using radiolarian and foraminifera paleotemperature equations are in approximate agreement (Pisias and Mix, personal communication). This convergence of paleotemperature estimates from two different fossil groups suggests that a reasonable record of paleoceanographic change is measured by this technique.

C. Time Series Analysis

(1) Spectral Analysis

Using the estimated SST signal for Site 572 as a measure of Pliocene oceanographic variability, standard spectral analysis procedures outlined in Jenkins and Watts (1968) are used to examine variability in the frequency domain. Spectral analysis allows one to examine the distribution of variance or power at a range of frequency intervals. The concentration of variance in orbital frequency bands can be compared to other bands. These methods use an autocovariance function and a cross-covariance function to calculate the spectra and cross-spectra, respectively (see Jenkins and Watts, 1968).

This method requires that the time series data consist of equal time steps. Sediment core data, which is usually equally spaced in depth but unequally spaced in time must first be "resampled" at equal time intervals. Simple linear interpolation techniques are used here to resample the data; other interpolation techniques produce equivalent results in the variance spectrum.

For the Site 572 paleotemperature time series the average sample interval is approximately 8500 years which corresponds to a minimum resolvable period of 17,000 years (Nyquist frequency, or $1/2\Delta T$), which is adequate for resolving events in the orbital band. For convenience, a 5000 year sampling interval is used here in calculating the spectra, although the Nyquist frequency of 17,000 years^{-1} is observed.

In order to examine the evolution of the sea surface temperature response over time, successive intervals of 500,000 years in length are analyzed. Each successive interval overlaps the previous interval 250,000 years. These intervals span the interval from 1.8 ma to 4.89 ma, with the exception of a data gap from about 3.0 - 3.1 ma.

(2) Complex Demodulation

Complex demodulation is a useful procedure when a time series is nonstationary, that is, amplitude and phase at a particular frequency vary slowly over time. The instantaneous amplitude and phase of these frequencies as a function of time can be determined by this technique. The rationale used in complex demodulation is that if a SST record is significantly influenced by orbital forcing, the pattern of the amplitude changes of the SST response and the forcing function within a particular orbital frequency band should be similar.

This technique provides another quantitative means of summarizing the development of the SST response over time at discrete frequency bands. Assuming that a data set has a periodic perturbation,

$$x_t = R_t \exp \{i(\lambda t + \Phi_t)\}$$

(where R_t is amplitude, Φ_t is phase, and (λ) is the frequency of interest), complex demodulation is a means of extracting approximations to the two series $\{R_t\}$ and $\{\Phi_t\}$ using the complex analog of $\{x_t\}$. The series is smoothed by low-pass filtering the data to remove unwanted components (frequency components and harmonics greater than or equal to the frequency of interest). At every frequency λ that undergoes demodulation, a different low pass cosine filter is designed. These techniques are discussed further in Bloomfield (1976).

Complex demodulation is used here to examine the time progression of amplitude of the SST signal in the obliquity and precession bands. These amplitude modulations can be compared to the amplitude modulations of the calculated series of obliquity and precession.

RESULTS

I. Sedimentation Rates

Using the above defined chronology, F tests are used to detect any significant changes (α = 0.05) in variability of the carbonate content, linear sedimentation rates, or downcore sea surface temperature (see next section) records. These results are presented in Table 3. Significant changes in the variance of the carbonate record is seen before and after 2.48 ma, and no significant changes in the variance of sedimentation rates are seen. Significant changes in variance are also seen in the August SST record (see next section). Using t-tests, differences in the means of these variables are also compared. These results are also listed in Table 3. Significant changes in the mean are seen in August and February SST between the 2.48 - 3.20 Ma interval and the 3.21 - 4.93 Ma interval, and in sedimentation rates.

II. Transfer Function

A. Factor Analysis

Q-mode factor analysis with a VARIMAX rotation (Klovan and Imbrie, 1971; Klovan and Meisch, 1976) of surface sediment radiolarian species identified six factors. These six factors account for 49.9%, 12.2%, 12.1%, 4.8%, 11.4%, and 1.3% of the information in the

Table 3: General statistical results for site 572

Variable	Period	Mean	Std. Dev.	Range
Carbonate (%)	1.79 - 2.48 Ma	76.9	5.18	25.30
	2.48 - 3.20 Ma	76.6	8.21	37.08
	3.21 - 4.93 Ma	74.7	8.74	39.69
SST, August (°C)	1.79 - 2.48 Ma	20.8	1.57	7.01
	2.48 - 3.20 Ma	20.9	1.96	9.37
	3.21 - 4.93 Ma	21.7	1.56	9.25
	overall	21.3	1.71	10.25
SST, February (°C)	1.79 - 2.48 Ma	24.8	1.15	6.99
	2.48 - 3.20 Ma	24.9	1.33	6.82
	3.21 - 4.93 Ma	25.8	0.92	4.57
	overall	25.3	1.16	7.60
LSR (m/my)	1.79 - 2.48 Ma	17.1	6.1	27.45
	2.48 - 3.20 Ma	15.2	6.1	26.40
	3.21 - 4.93 Ma	12.4	5.6	34.00

Significant (95% CI) changes in variance exist in the following regions:

Carbonate: between 1.79-2.48 Ma and 2.48-3.20 Ma

August SST: between 1.79-2.48 Ma and 2.48-3.20 Ma and between 2.48-3.20 Ma and 3.21-4.93 Ma

February SST: between 1.79-2.48 Ma and 2.48-3.20 Ma and between 2.48-3.20 Ma and 3.21-4.93 Ma

LSR: no significant changes in variance

Significant (95% CI) changes in mean exist in the following regions:

LSR: between 1.79-2.48 Ma and 2.48-3.20 Ma and between 2.48-3.20 Ma and 3.21-4.93 Ma

August SST: between 2.48-3.20 Ma and 3.21-4.93 Ma

February SST: between 2.48-3.20 Ma and 3.21-4.93 Ma surface sediment data, respectively, with 91.75% of the total variance explained. The importance of each species in defining each factor is given in F, the factor score matrix (Table 4). This set of factors is similar to both the Modern seven factor model of Moore (1978) and the eight factor Pliocene model of Hays et al. (1989). Maps of the surface loadings of these factors (the factor loading matrix, B) are shown in Figures 9 through 14.

The first factor (F1; Figure 9) is a Tropical factor dominated by highest positive loadings of Octopyle stenozoa/ Tetrapyle octacantha (S54). This factor is equivalent to the Tropical factors of Moore (1978) and Hays et al. (1989).

The second factor (F2; Figure 10) represents the Subarctic. The highest loading species in this factor are Botryostrobus aquilonaris (N33), Lithelius minor (S24), Pterocorys zancleus (N40), and the lumped group Prunopyle antarctica + Actinomma leptodermum + Echinomma cf. leptodermum (S8 + S4 + S7) This factor resembles the Transitional factor of Moore (1978) in the high loadings of Lithelius minor (S24) and Pterocorys zancleus (N40) and the Transitional/Eastern Boundary factor of Hays et al. (1989) in the high loading of Echinomma delicatum (S10).

The third factor (F3), a Western Pacific factor, is dominated by Stylochlamydium asteriscus (S30) which is similar to the Western Pacific factors of Moore (1978) and

Table 4: Factor Score matrix [F] for the 6 factor model used in this study.

Species	Factors 1	2	3	4	5	6
S1	0.030	−0.020	−0.054	−0.107	0.271	0.285
S1A	−0.006	−0.007	0.075	0.063	−0.009	−0.019
S8	−0.015	0.524	0.007	−0.193	0.123	−0.111
S10	−0.016	0.334	0.006	0.150	−0.002	0.349
S12	0.044	−0.021	0.046	0.014	0.014	0.035
S13	−0.011	−0.006	0.132	0.097	−0.022	0.004
S14	0.031	−0.038	0.074	0.056	0.053	−0.097
S17	0.043	0.127	0.028	−0.074	−0.048	−0.033
S18	0.027	−0.007	0.031	−0.008	0.039	0.130
S23	0.168	−0.037	0.179	0.163	−0.079	0.114
S24	−0.024	0.290	−0.035	0.184	0.600	−0.223
S30	−0.001	0.000	0.945	−0.073	0.053	0.053
S34	0.093	0.002	−0.092	−0.050	0.018	0.377
S36A	−0.001	−0.001	0.042	0.004	−0.007	0.011
S36C	0.004	−0.002	0.082	0.009	−0.019	0.044
S40	0.009	−0.003	0.103	0.003	−0.024	0.007
S41	−0.007	0.070	0.006	0.003	−0.035	0.017
S43	−0.052	−0.222	0.008	−0.011	0.573	−0.024
S47	−0.041	0.145	0.045	−0.057	0.272	0.105
S48	0.015	0.132	0.004	−0.034	0.000	0.142
S51	−0.063	0.066	0.004	0.879	0.008	0.078
S54	0.956	0.023	−0.012	0.062	0.047	−0.100
N1	0.029	−0.009	0.003	0.055	−0.009	−0.028
N4	0.066	0.023	0.005	0.081	−0.018	−0.060
N7	0.103	−0.009	−0.077	−0.090	0.015	0.527
N9	0.059	−0.013	0.011	0.025	−0.016	−0.042
N14	0.026	−0.110	−0.014	−0.062	0.260	0.298
N18	0.041	0.012	−0.016	−0.058	0.009	0.197
N27	0.059	−0.001	−0.007	−0.017	−0.012	−0.026
N29	−0.001	0.087	−0.001	−0.003	0.018	0.079
N33	−0.029	0.541	0.016	0.002	−0.205	0.070
N35A	−0.014	0.113	0.007	−0.004	−0.010	0.127
N36	−0.007	−0.008	−0.006	−0.033	0.115	−0.027
N38	−0.002	0.191	0.013	−0.038	−0.044	0.033
N40	0.087	0.224	−0.035	−0.168	0.049	−0.238

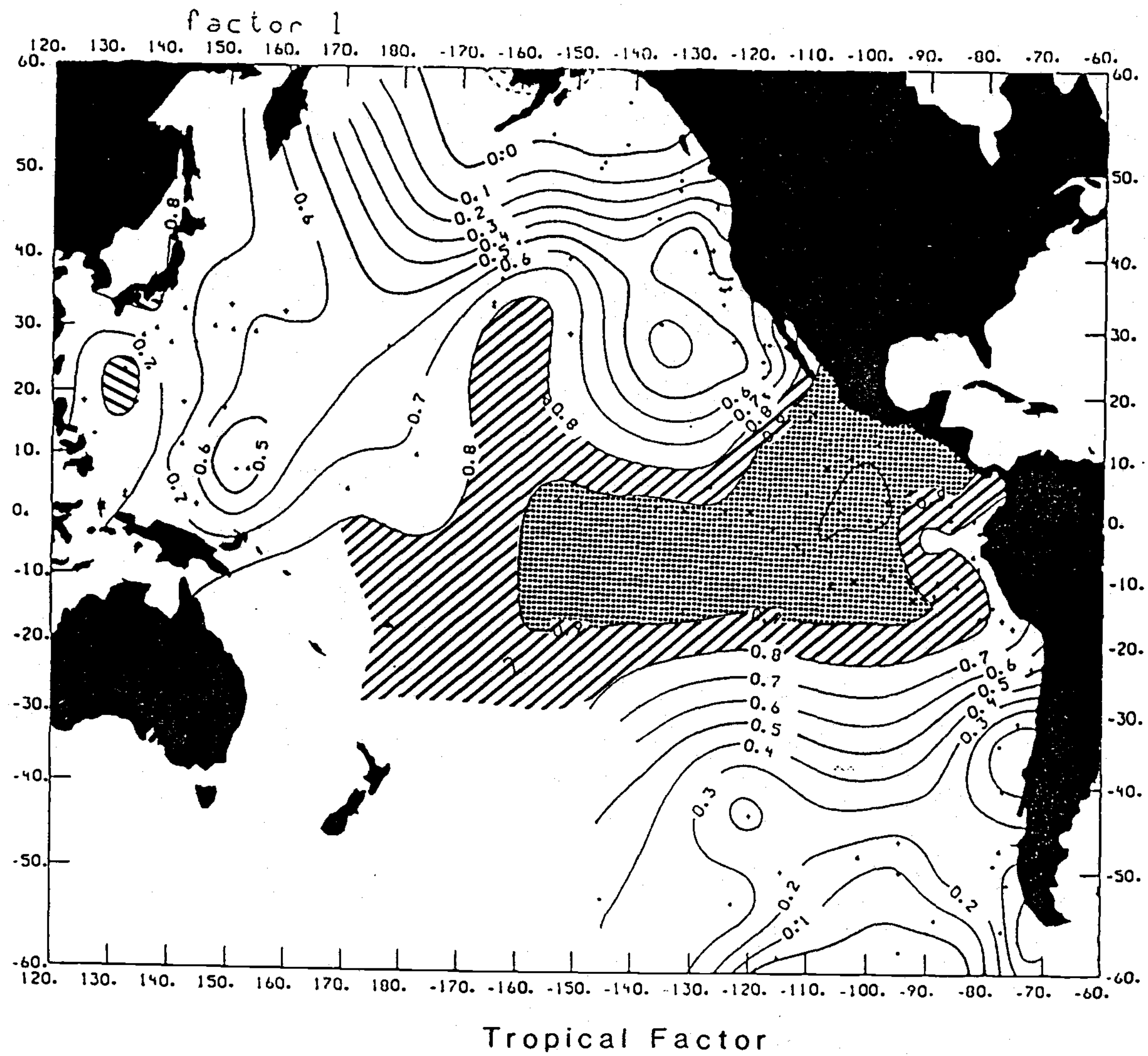

Figure 9: Factor 1 - Tropical factor. Values contoured are the surface loadings of this factor. Dotted area represents geographic area of highest loading.

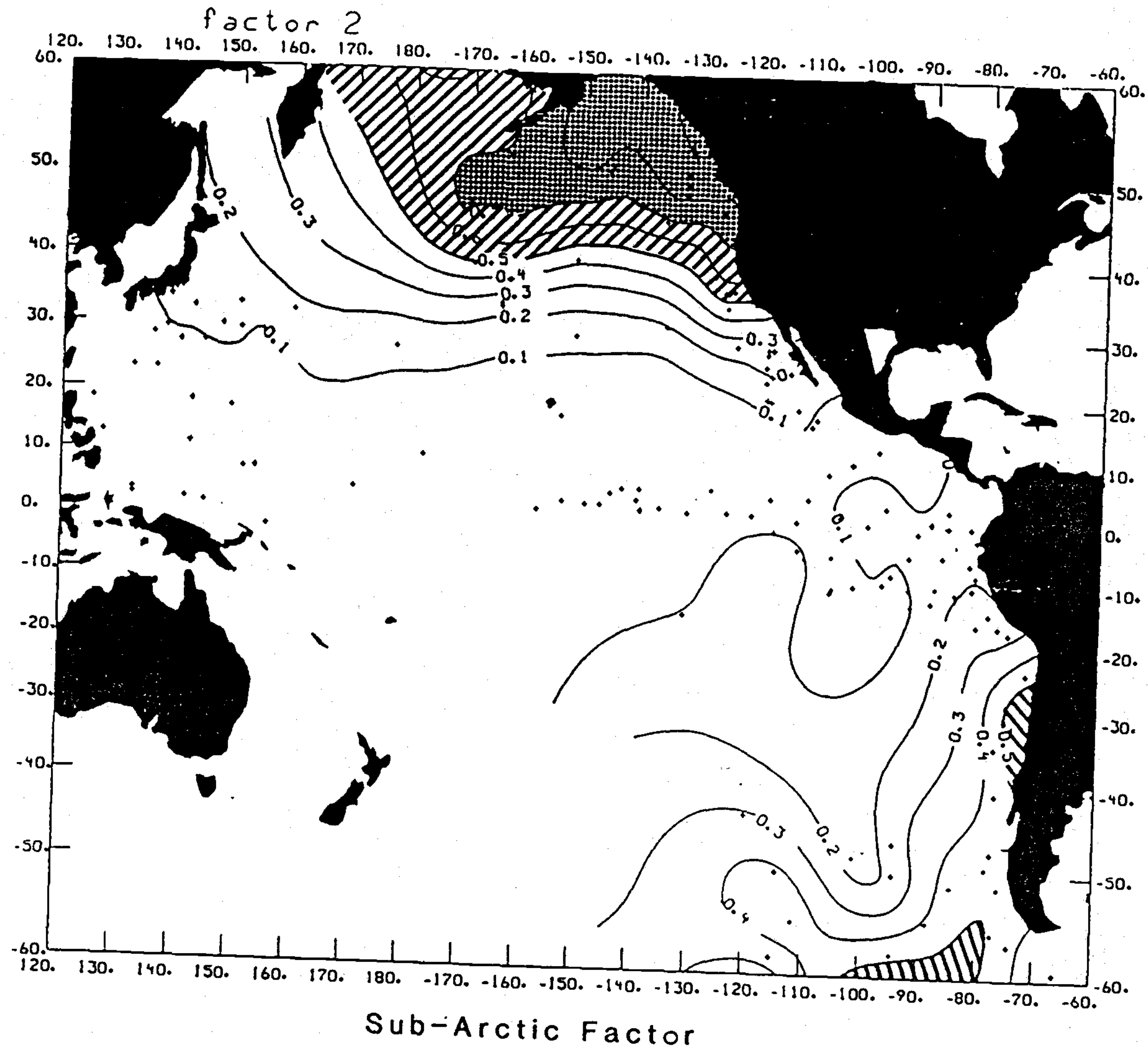

Figure 10: Factor 2 - Subarctic. See Figure 9 caption for details.

Hays et al. (1989) (Figure 11). The factors of Moore (1978) and Hays et al. (1989) which are calculated for Modern and upper Pliocene transfer functions, respectively, have high loadings of Didymocyrtis tetrathalamus (S23) in this factor. This species is less important in this study because it evolves gradually in the late Miocene and early Pliocene and is easily confused with very similar species Didymocyrtis avita and Didymocyrtis penultima, which go extinct by the Pleistocene. As a result, it has a lower relative abundance and is therefore less important.

The fourth factor (F4; Figure 12), dominated by Stylatractus spp. (S51) is a Gyre factor. Loadings are highest in the mid-ocean gyres, and the dominant species is a heavily silicified, dissolution-resistant species group. This species was not used in the data sets of Moore (1978) or Hays et al. (1989), so this factor does not appear in their analyses.

The fifth factor (F5) is a Sub-Antarctic factor (Figure 13). The two dominant species that define the Antarctic factor of Moore (1978) are not included in this factor analysis due to their rarity at Site 572 (see methods). This factor is characterized by high loadings of Spongurus sp. (S1), Lithelius minor (S24), Spongopyle osculosa (S43), Stylodictya validispina (S47), and Tholospyris scaphipes (N14), and it maps as a broad maximum in the high latitudes of the Southern Hemisphere.

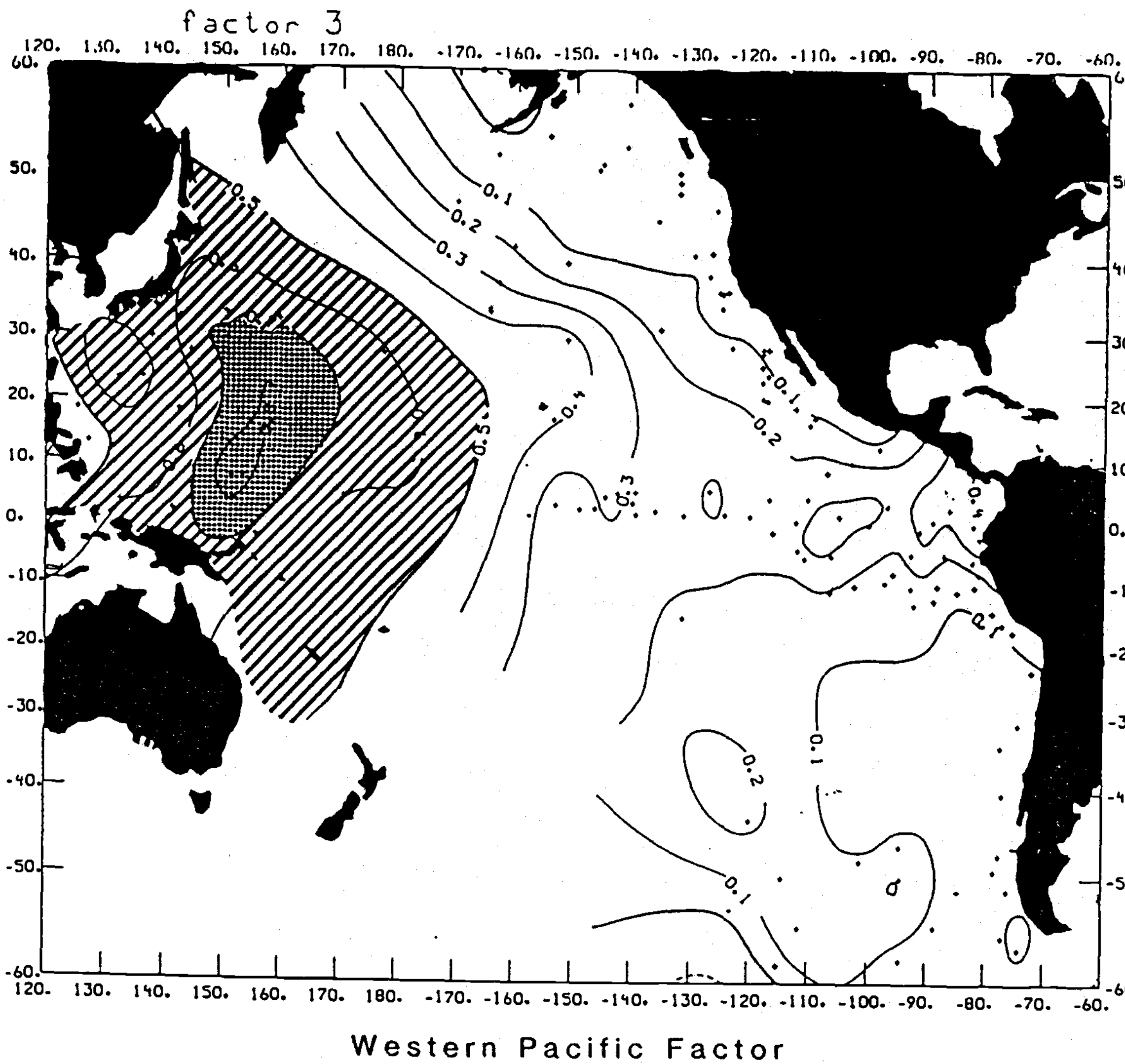

Figure 11: Factor 3 - Western Pacific. See Figure 9 caption for details.

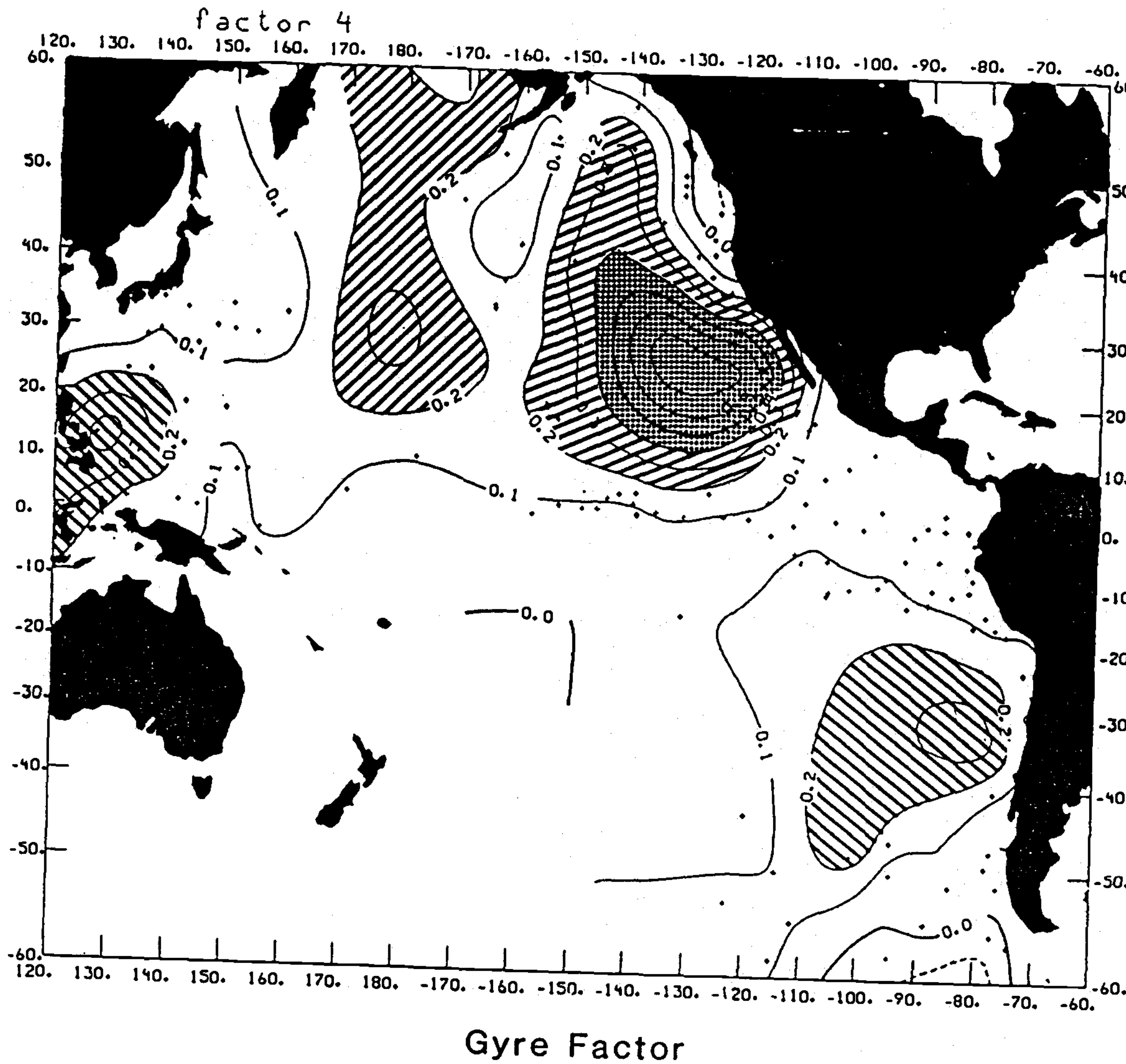

Figure 12: Factor 4 - Gyre. See Figure 9 caption for details.

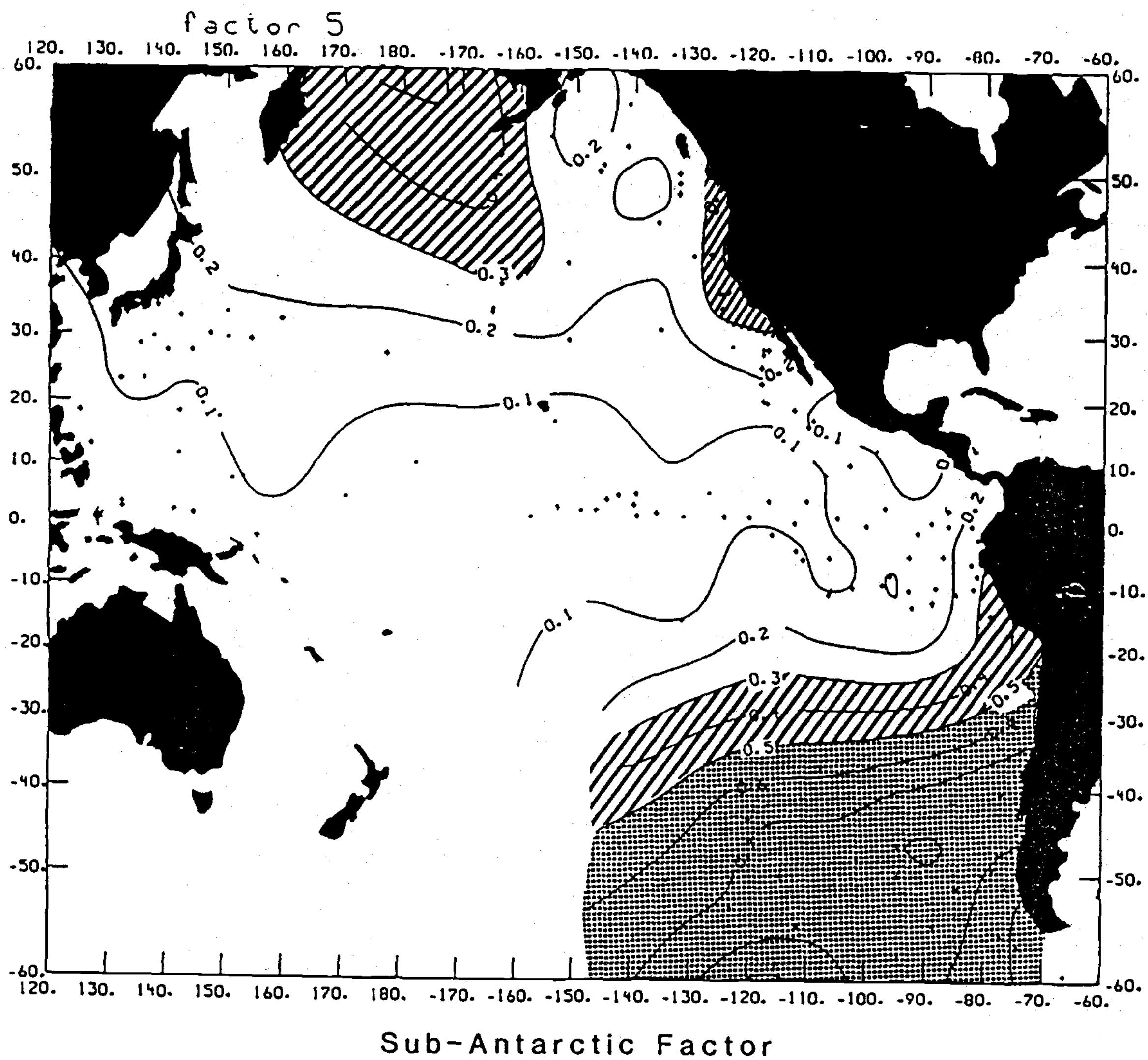

Figure 13: Factor 5 - Sub-Antarctic. See Figure 9 caption for details.

Factor six (F6), the Arctic/Peru Upwelling factor (Figure 14) is unlike any one factor of Moore (1978) or Hays et al. (1989). It is distinctly different from the Subarctic factor (F2) in that the strongest loadings are in the Peru upwelling region. Significant species in this factor are Pterocorys minithorax (N7), Polysolenia murrayana (S34), Spongurus sp. (S1), and Echinomma delicatum (S10).

These six factors explain 91.75% of the variance within the surface sediment data set used here, which is a reduced data set comprised of 35 species that range throughout the Pliocene (see Methods). For comparison, the seven factors of Moore (1978), which is a modern assemblage, accounts for 93.4% of the total variance in the Pan-Pacific data set, and the eight factor matrix of Hays et al. (1989) which is an upper Pliocene assemblage, accounts for 95% of the variation in that data set.

Downcore plots of these factors at Site 572 are shown in Figure 15. These downcore factors have an average communality of 0.942 +/- 0.027. The Tropical factor (F1) appears to have undergone a decrease in weighting from 4.55 ma to about 4.2 ma, after which it increases and fluctuates about a constant level up to 1.8 ma. The Subarctic factor (F2) appears to have had increased strength at Site 572 from 4.9 to 4.2 ma, after which it decreased and then gradually increased to its level at 1.8 ma. The Western

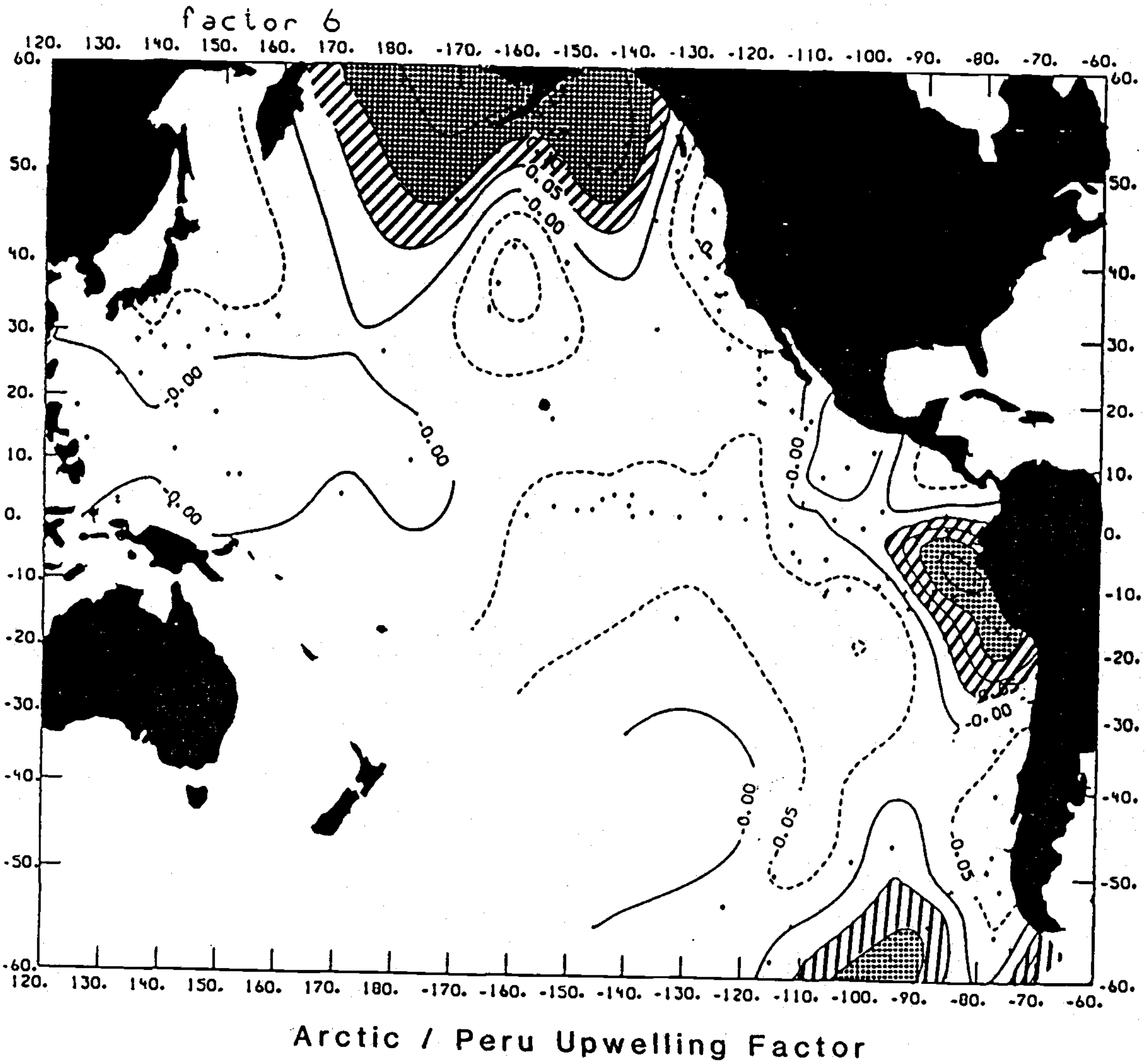

Figure 14: Factor 6 - Arctic/Peru upwelling. See Figure 9 caption for details.

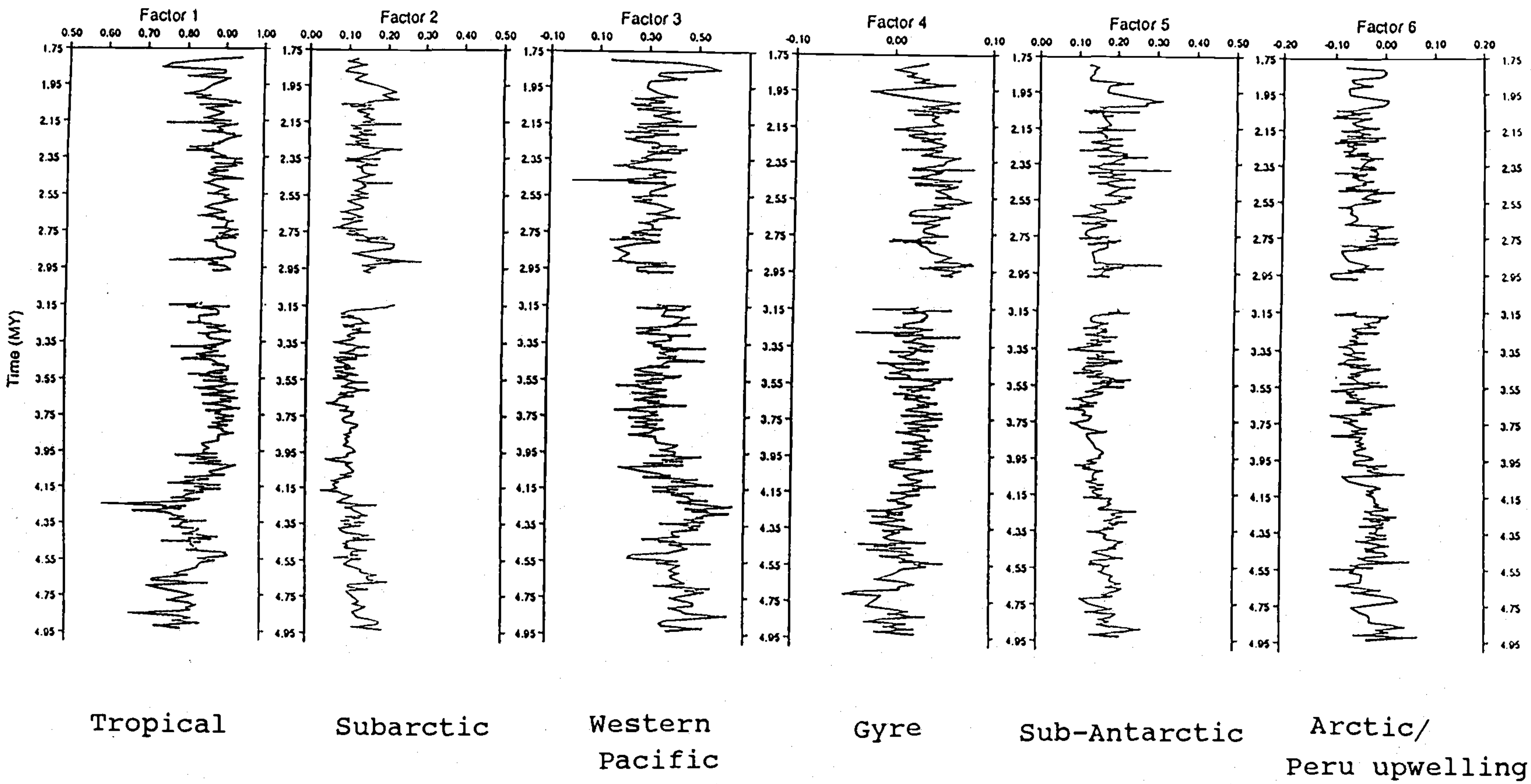

Figure 15: Downcore factor plots. Surface loadings are applied to the downcore radiolarian data set.

Tropical factor (F3) has the largest variations over time. The Antarctic factor (F5) is weakly varying from 4.9 to 3 ma, with maximum strength from 2.6 to 1.9 ma, and the Gyre factor (F4) and the Arctic/Peru upwelling factor (F6) remain relatively constant throughout the time interval examined here.

B. Paleotemperature Equations

Pliocene paleotemperature equations produced by regression of these factors against modern August (cool season) and February (warm season) sea surface temperatures (Levitus, 1982) are presented in Table 5. Comparison of the modern SST estimates from these equations and the atlas values is illustrated in Figure 16. Application of these equations to the downcore factors produces August (T_C) and February (T_W) paleotemperature estimates for Site 572 (Figure 17). Table 3 summarizes the general statistics for the SSTs.

The two paleotemperature records vary downcore in a similar manner. Although the standard deviation of the temperatures (see Table 3) is larger for the August (cool) SST record than for the February (warm) record, the range of the cool SSTs is more than 2°C larger. Compared to the Modern August and February mean SSTs of 21.5°C and 24.5°C respectively (Robinson, 1976), the mean Pliocene SSTs are a very similar 21.3°C and 25.3°C. The estimated Pleistocene

Table 5: Sea surface paleotemperature equation for February (T_{warm}) and August (T_{cool}).

Season	Paleotemperature Equation
February (warm)	$T_W = 6.4828\ (F1)^2 + 41.0495\ (F1*F6) + 18.5245\ (F4*F5) + 10.8188\ (F3) - 16.7554\ (F5) - 20.6855\ (F6) + 20.0826.$
August (cool)	$T_C = 8.2722\ (F4)^2 - 16.3620\ (F1*F2) - 11.1540\ (F1*F5) - 28.2659\ (F2 * F6) - 34.1633\ (F3* F5) + 86.8732\ (F3*F6) + 18.2466\ (F1) + 13.3553\ (F3) + 7.4015$

Percentage of Variation Explained:
February: 91.025%
August: 89.933%

Standard Error of Estimate of equation:
February: 2.09
August: 2.48

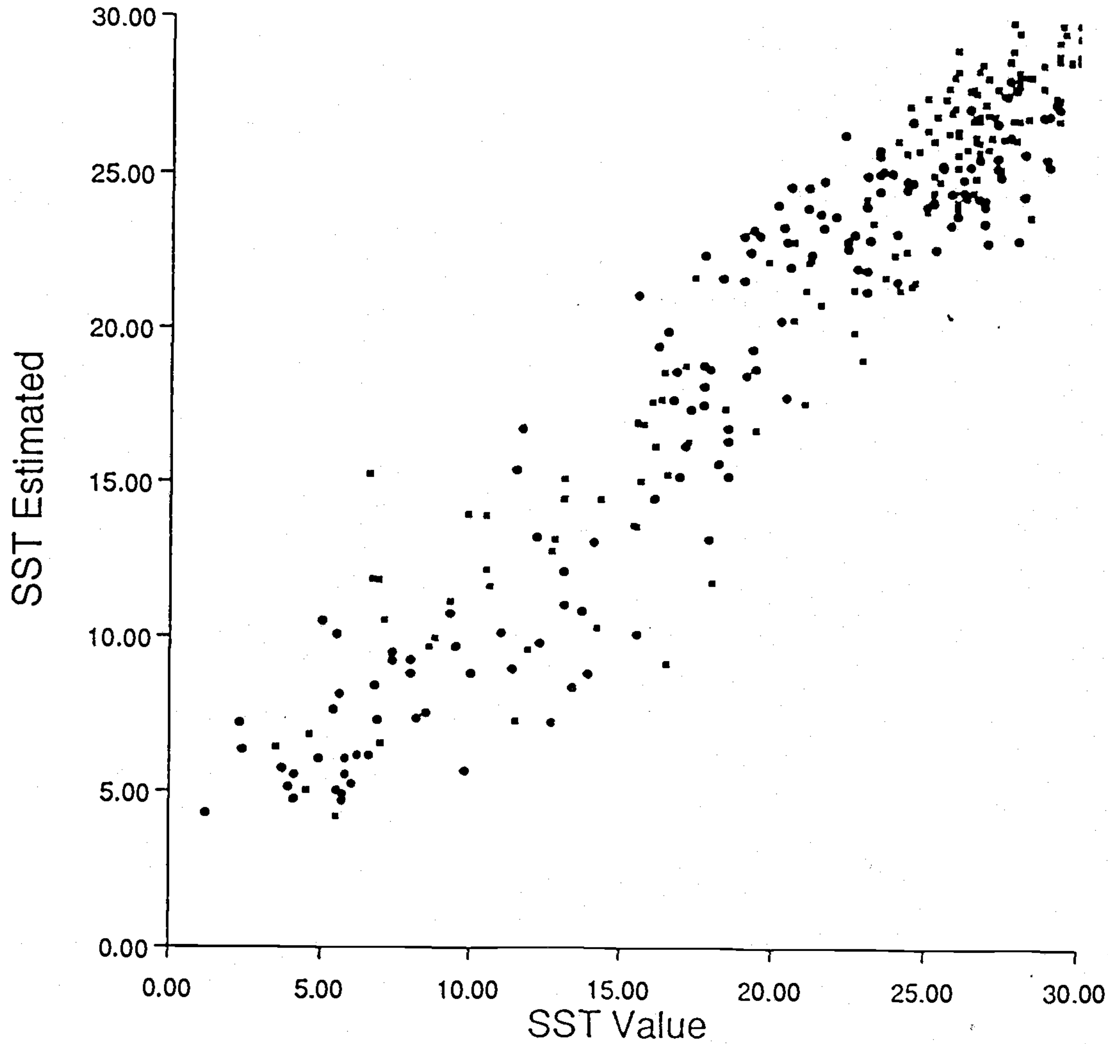

Figure 16: Comparison of actual modern SSTs to those predicted by regression equations.

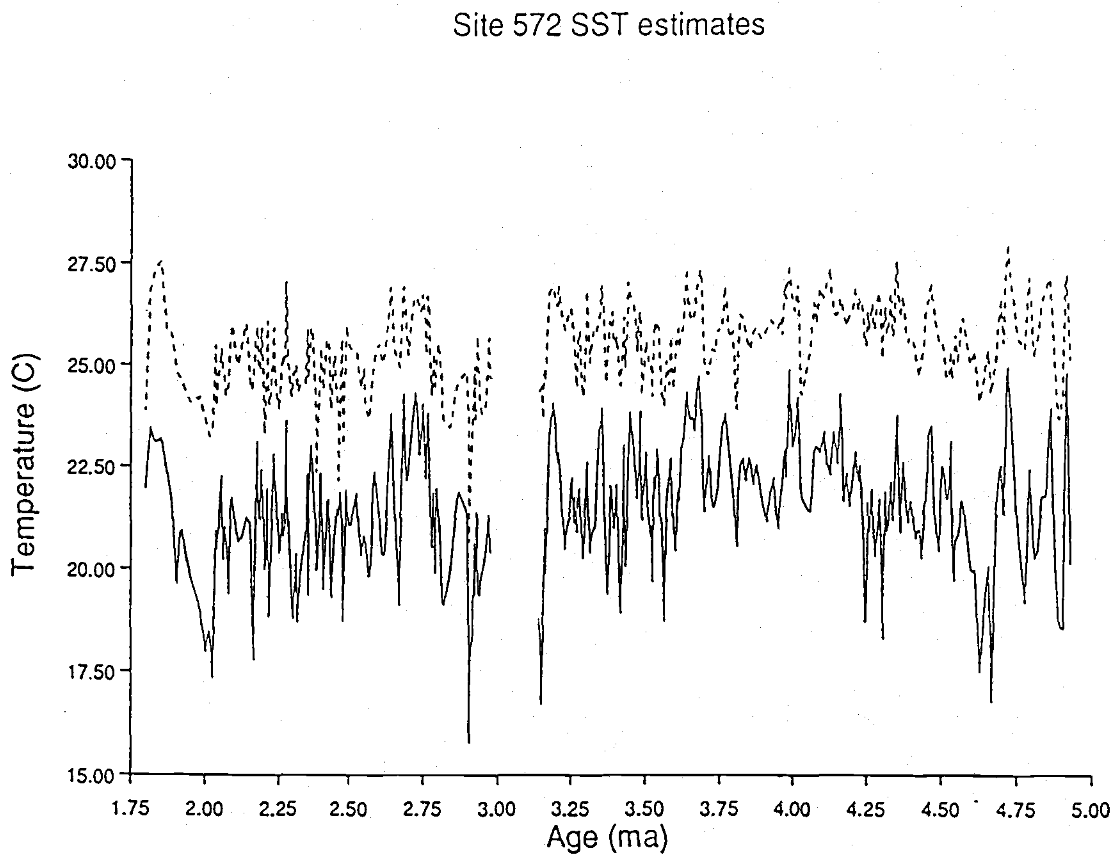

Figure 17: Downcore sea surface temperature (SST) estimates. The dashed line is the February estimate, T_{warm}, and the solid line is the August estimate, T_{cool}.

SSTs in this region, which are estimated from a different equation, are 23.6°C in August and 26.4°C in February (Hays, 1987, and Hays et al., 1989). The SST estimates produced here are comparable to the results of Hays (1987), who used a different paleotemperature equation to estimate a mean August temperature at site 572 of 19.4°C and a mean February temperature of 22.5°C over the period from 2.4 to 3.7 ma.

III. Spectral Analysis

Using the methods outlined above, the spectra of successive and overlapping 500,000 year intervals of the SST record is examined. The results are plotted on identical scales in Figures 18 through 22. In most intervals the spectra of the August and February SST are similar, although the August SST signal has higher variance. In every interval, variance is concentrated at some frequencies that are unrelated to orbital parameters; most of the variance in each interval is also concentrated at very low frequencies. Consequently, sorting out the significance of power in orbital bands compared to other frequencies is complicated. Intervals which have a significant concentration of variance in the obliquity and precession bands (within an 80% confidence interval) are summarized in Table 6.

In the obliquity band, both the August and February

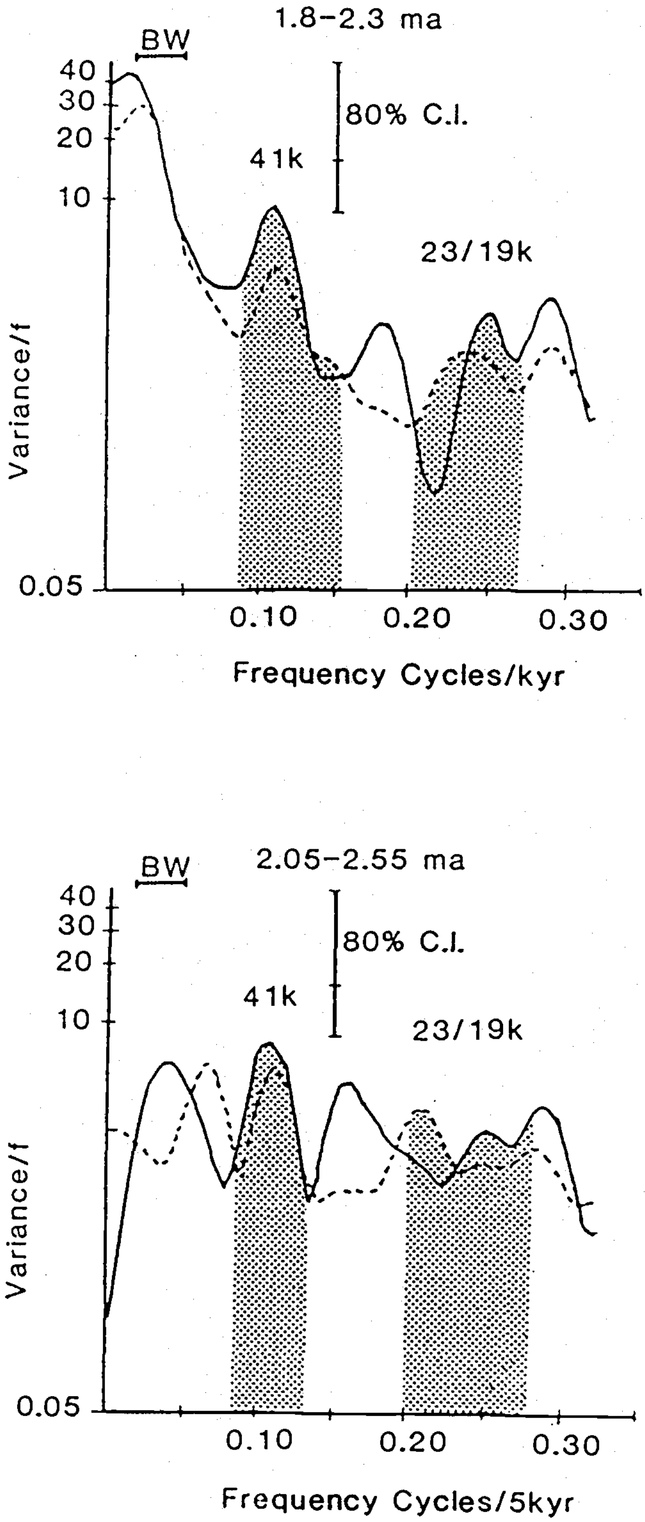

Figure 18: August (solid line) and February (dashed line) SST spectra. (a) 1.8 - 2.3 Ma; (b) 2.05 - 2.55 Ma. The stippled areas represent the obliquity (41k) and precession (23/19k) frequency bands, respectively. Bandwidth and 80% confidence interval given at top of each plot.

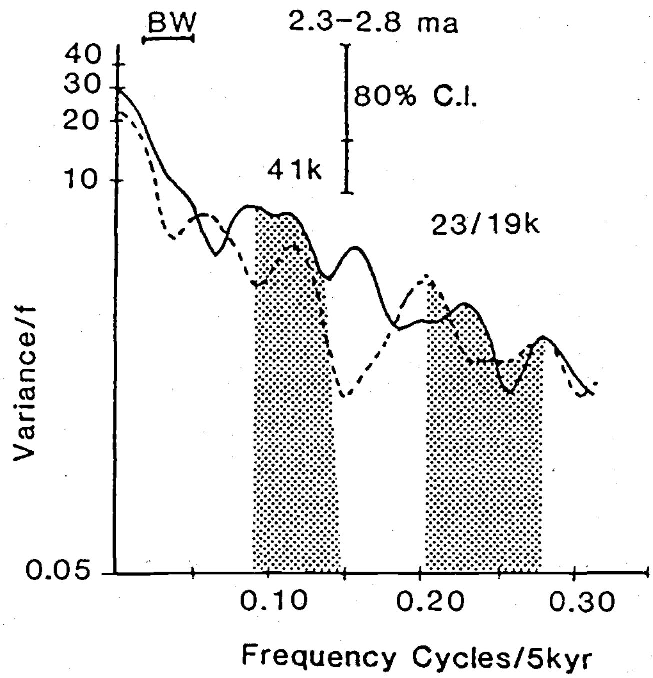

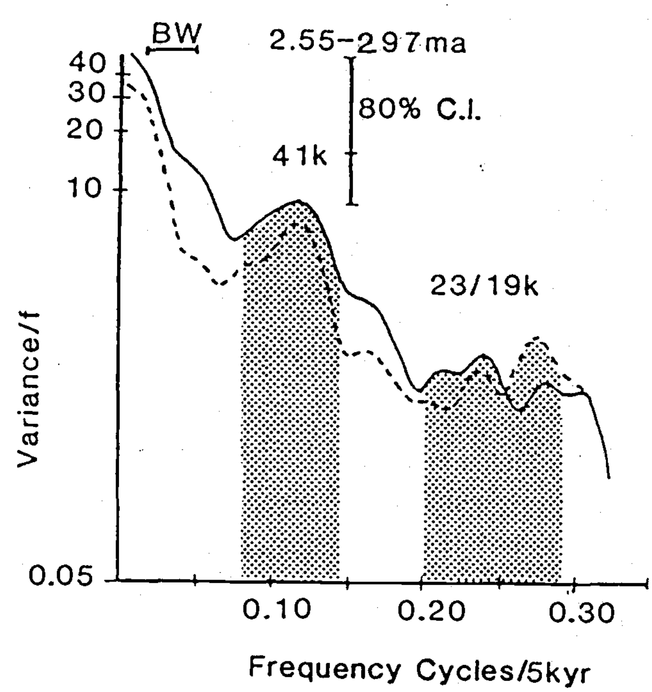

Figure 19: August (solid line) and February (dashed line) SST spectra. (a) 2.3 - 2.8 Ma; (b) 2.55 - 2.97 Ma. Labeling convention and amplitude scale the same as figure 18.

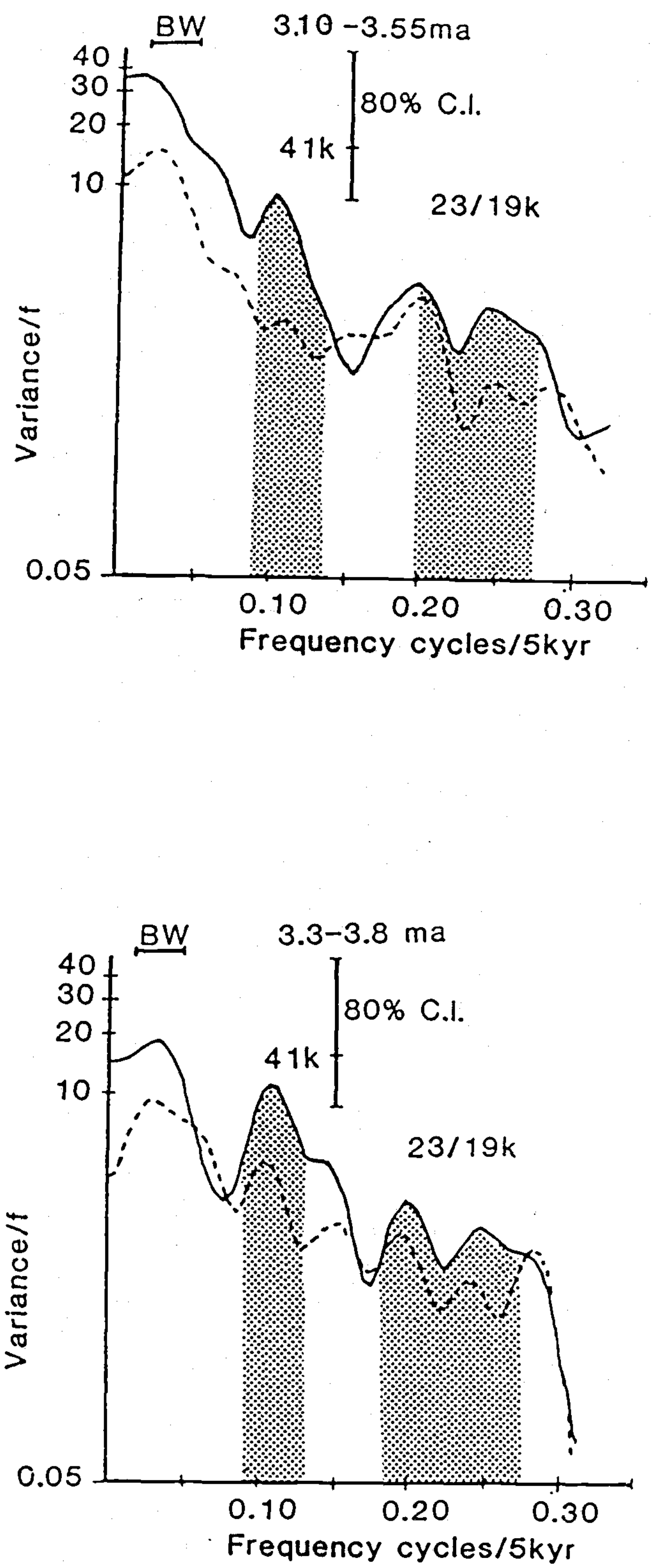

Figure 20: August (solid line) and February (dashed line) SST spectra. (a) 3.10 - 3.55 Ma; (b) 3.3 - 3.8 Ma. Labeling convention and amplitude scale the same as figure 18.

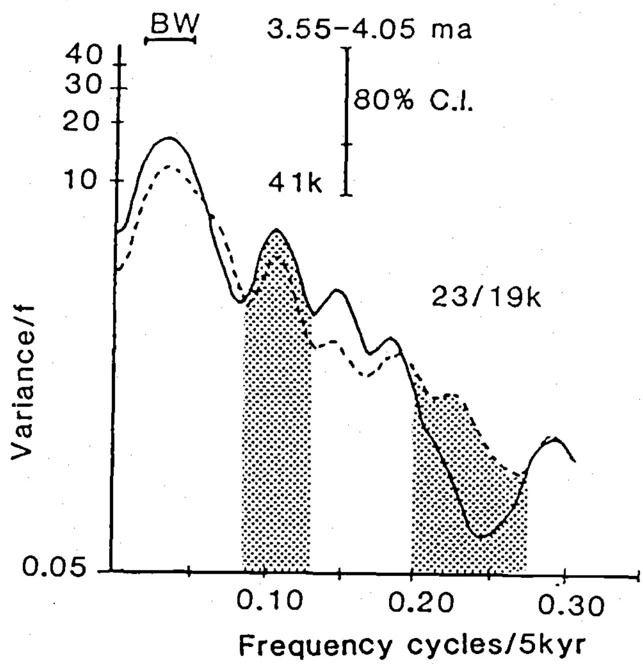

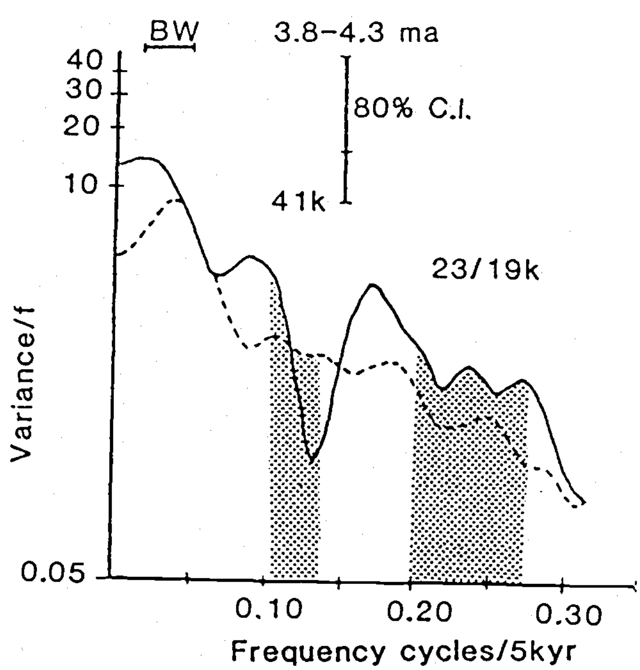

Figure 21: August (solid line) and February (dashed line) SST spectra. (a) 3.55 - 4.05 Ma; (b) 3.8 - 4.3 Ma. Labeling convention and amplitude scale the same as figure 18.

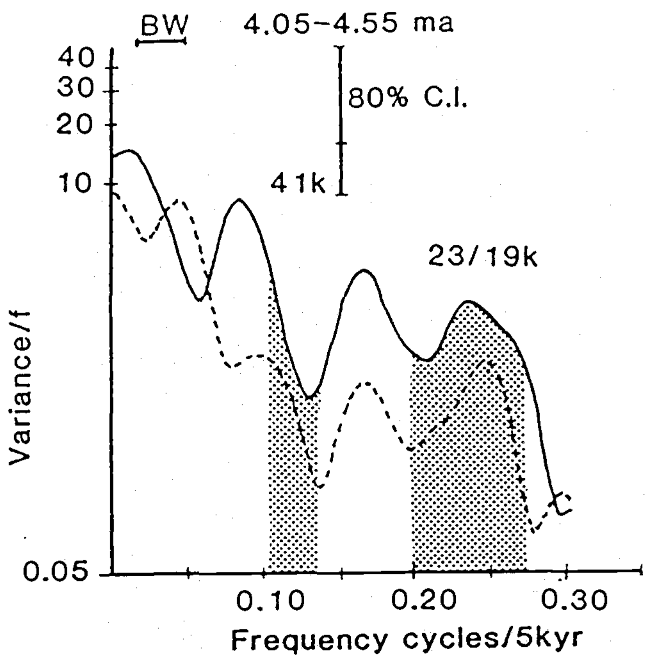

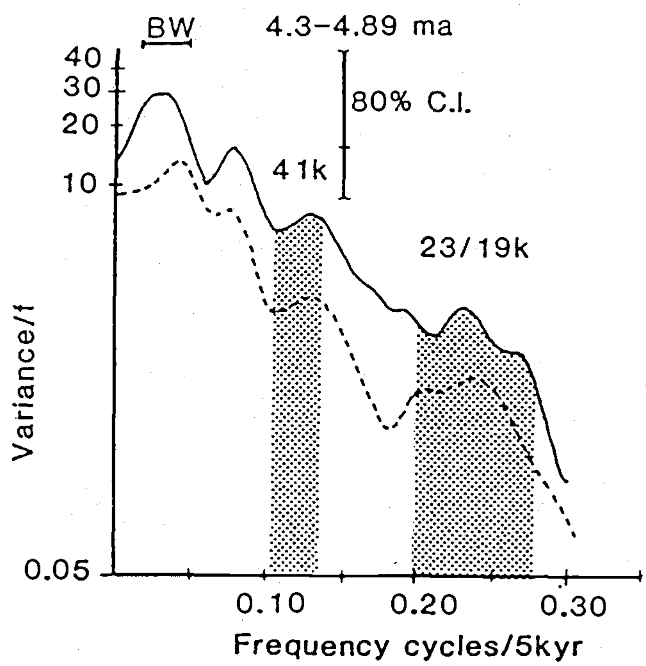

Figure 22: August (solid line) and February (dashed line) SST spectra. (a) 4.05 - 4.55 Ma; (b) 4.3 - 4.89 Ma. Labeling convention and amplitude scale the same as figure 18.

Table 6: Summary of spectral results for Site 572 SST (Figures 19 - 28). etp refers to eccentricity, tilt, and precession. T_C and T_W refer to August and February SST estimates, respectively. A "yes" indicates a significant concentration of variance, a "no" indicates no significant concentration or no coherency, and a "?" indicates inconclusive results.

Time Interval (ma)	41k power T_C	41k power T_W	23k power T_C	23k power T_W	Coherence with etp T_C
1.80 - 2.30	yes	yes	yes	yes	no
2.05 - 2.55	yes	yes	no	?	e only
2.30 - 2.80	yes	yes	?	no	e only
2.55 - 2.97	yes	yes	no	?	t, p
3.10 - 3.55	yes	no	yes	?	e only
3.30 - 3.80	yes	yes	yes	yes	no
3.55 - 4.05	yes	yes	no	no	no
3.80 - 4.30	no	no	no	no	no
4.05 - 4.55	no	no	yes	yes	no
4.30 - 4.89	no	no	yes	yes	e only

SSTs have a significant concentration of variance in the 1.8 -2.3 ma, 2.05-2.55 ma, 2.3 - 2.8 ma, 2.55 - 2.97 ma, 3.3 - 3.8 ma, and 3.55 - 4.05 ma intervals. In the interval from 3.15 - 3.55 ma there is significant concentration of variance in the obliquity band for the August SST signal but not for the February signal, and from 3.8 - 4.3 ma, 4.05 - 4.55 ma, and 4.3 - 4.89 ma there is no concentration of variance at this band in either signal.

In the precession band, any concentration of variance in both the August and the February SST signals is questionable throughout the intervals examined. In the intervals from 1.8 - 2.3 ma, 3.15 - 3.55 ma, 3.3 - 3.8 ma, 4.05 - 4.55 ma, and 4.3 - 4.89 ma there is a concentration of variance in the precession band in both August and February SST signals. The remaining time intervals are inconclusive, however.

Cross-spectral analysis of the August SST signal and the orbital parameters (eccentricity + tilt + precession, or etp; Imbrie et al., 1984) (Figures 23 - 27) indicates that in most cases the records are not significantly coherent within an 80% confidence interval, although individual SST spectra have peaks corresponding to these orbital values (Figures 18-22). Cross-spectral analysis of the August SST signal and the site 572 $\delta^{18}O$ record indicates that these records lack significant coherency with orbital bands as well (Figure 28).

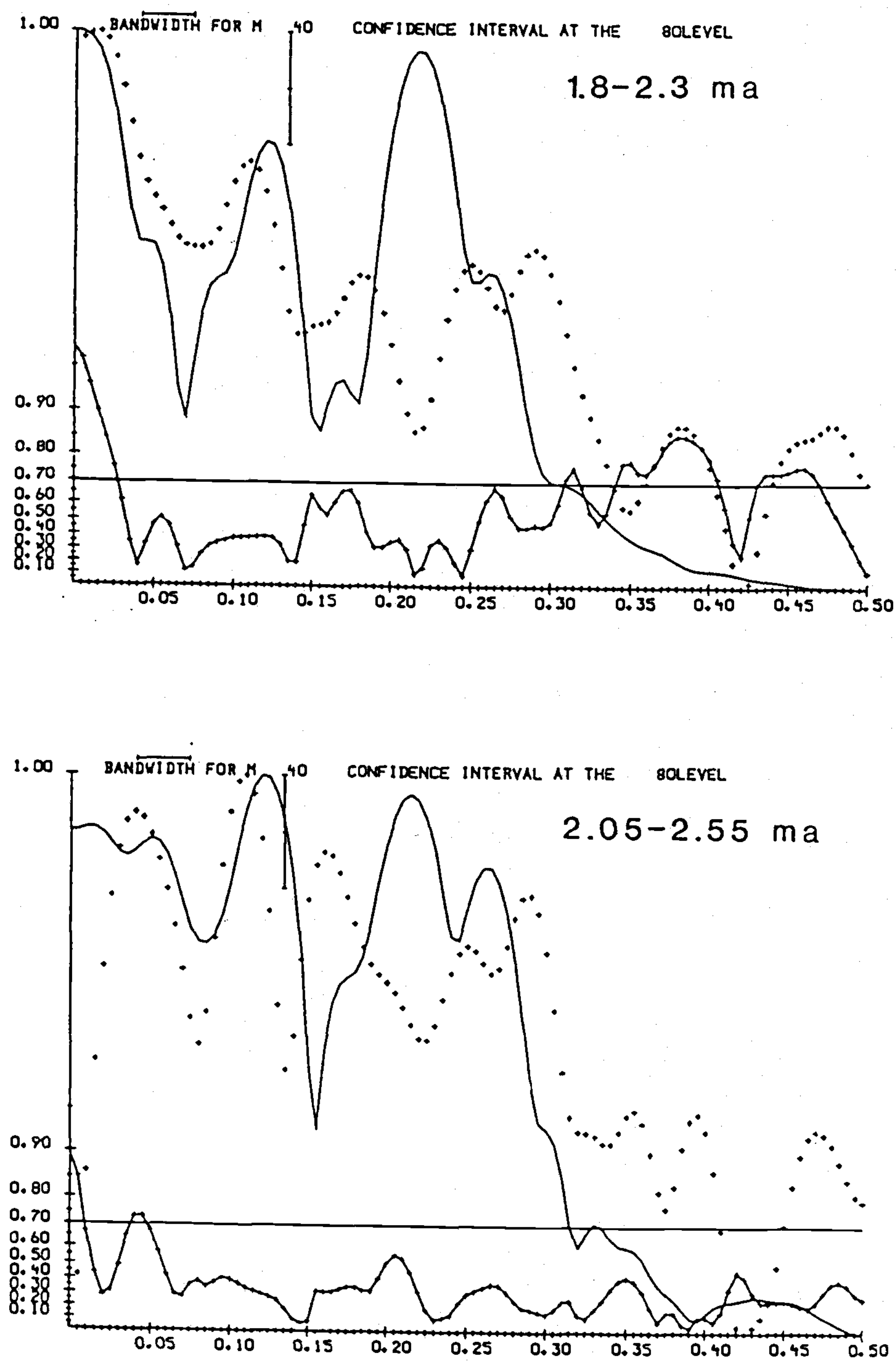

Figure 23: Cross spectra of August SST (dashed line) and eccentricity + obliquity + precession (etp; solid line). (a) Cross-spectra, 1.8 - 2.3 Ma. (b) Cross-spectra, 2.05 - 2.55 Ma. Labeling convention the same as for figure 8.

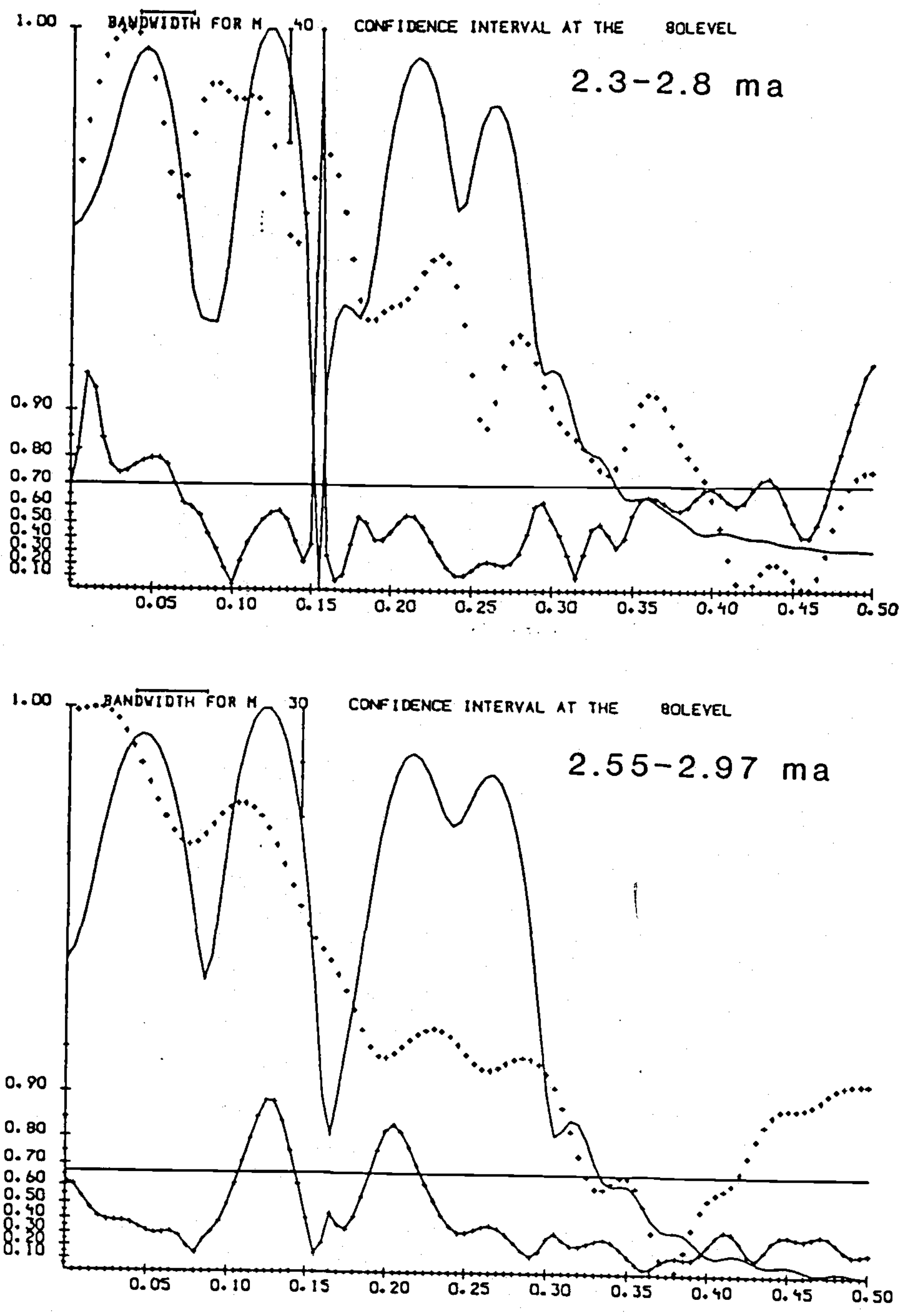

Figure 24: Cross spectra of August SST (dashed line) and eccentricity + obliquity + precession (etp; solid line).(a) Cross-spectra, 2.3 - 2.8 Ma. (b) Cross-spectra, 2.55 - 2.97 Ma. Labeling convention the same as for figure 8.

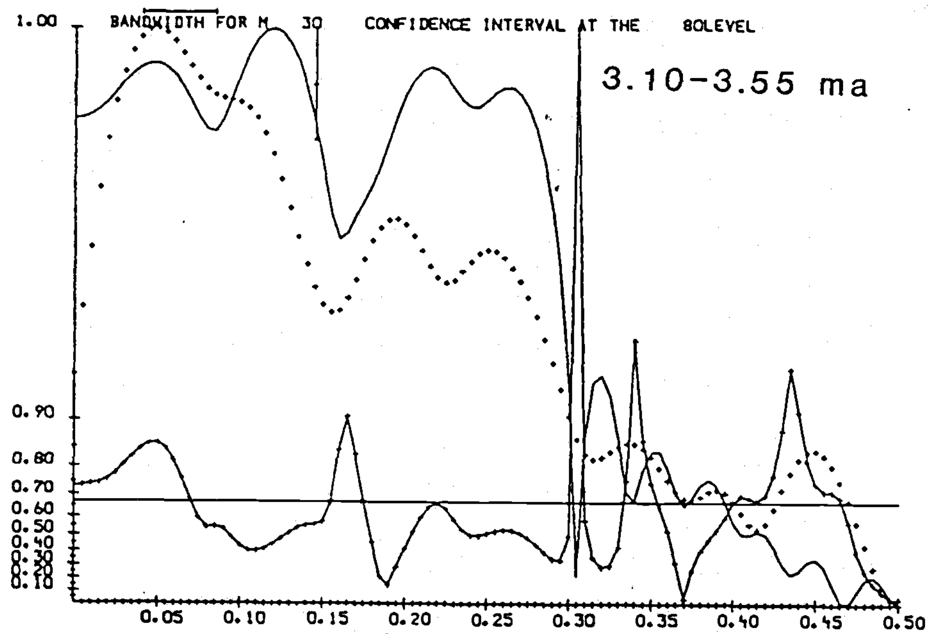

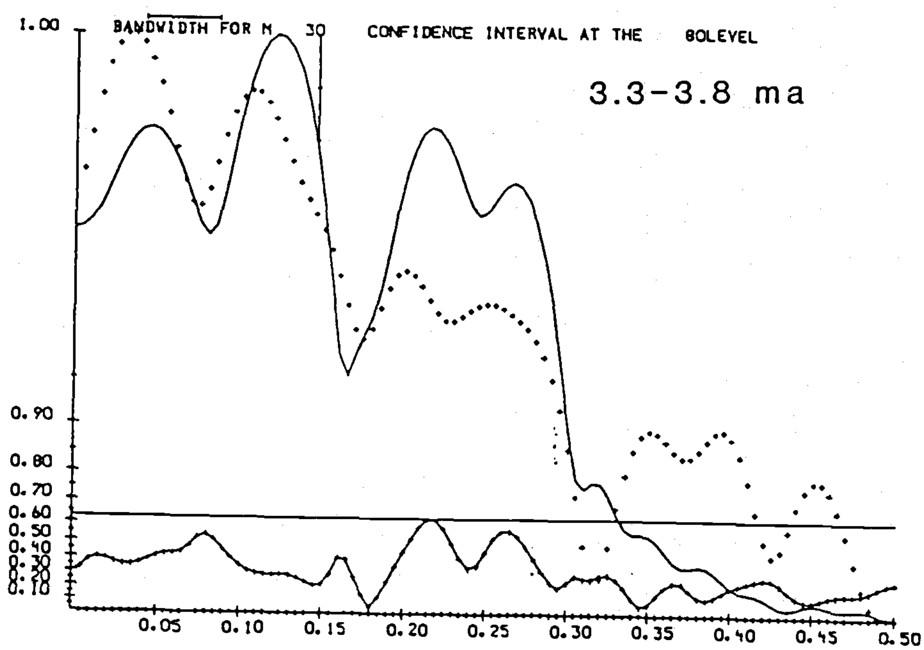

Figure 25: Cross spectra of August SST (dashed line) and eccentricity + obliquity + precession (etp; solid line).(a) Cross-spectra, 3.10 - 3.55 Ma. (b) Cross-spectra, 3.3 - 3.8 Ma.Labeling convention the same as for figure 8.

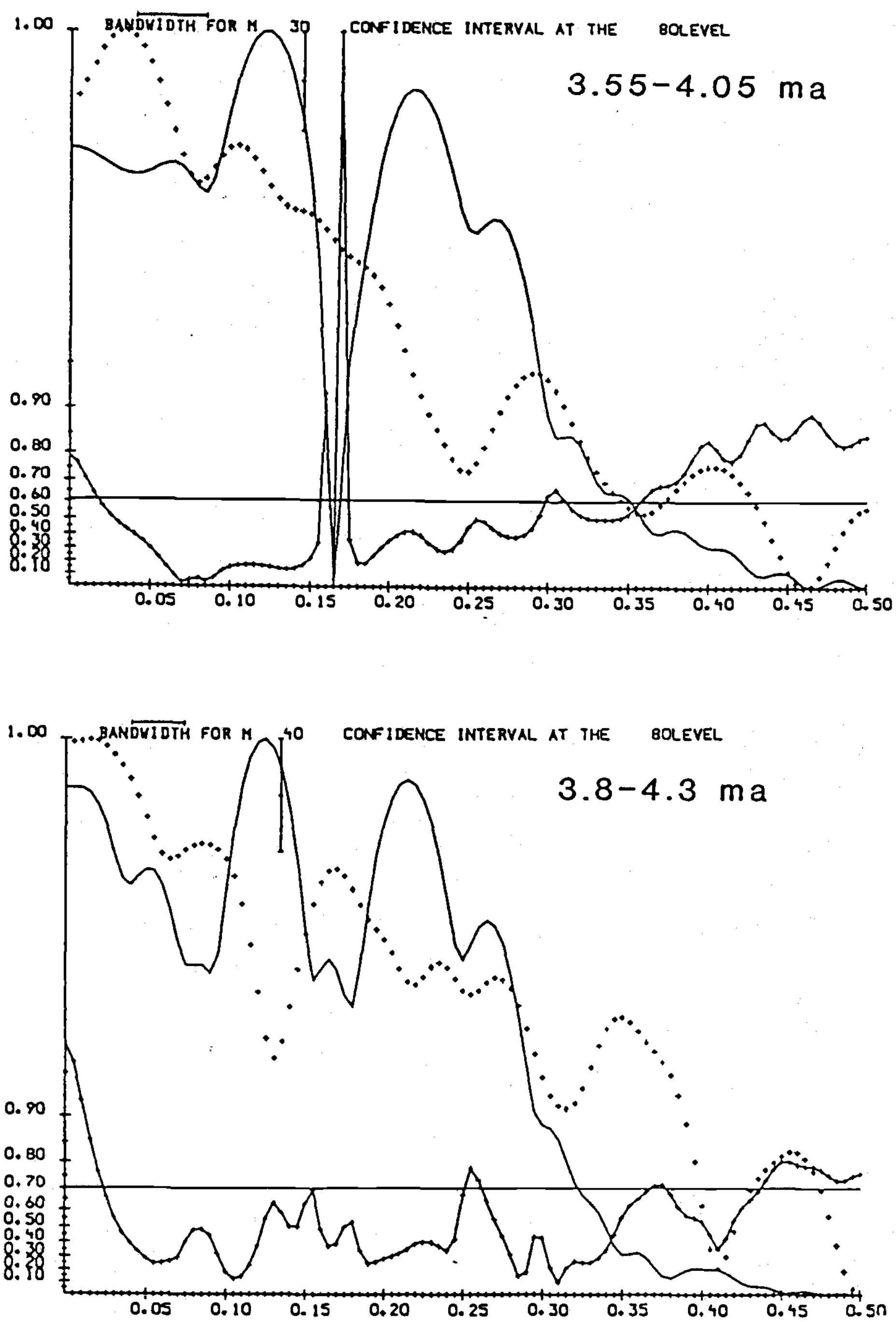

Figure 26: Cross spectra of August SST (dashed line) and eccentricity + obliquity + precession (etp; solid line).(a) Cross-spectra, 3.55 - 4.05 Ma. (b) Cross-spectra, 3.8 - 4.3 Ma.Labeling convention the same as for figure 8.

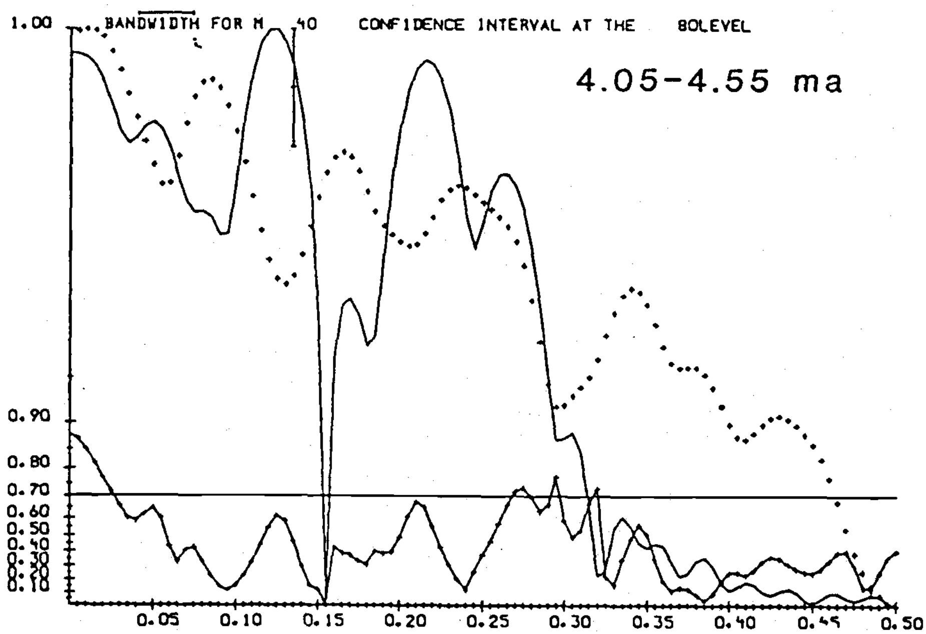

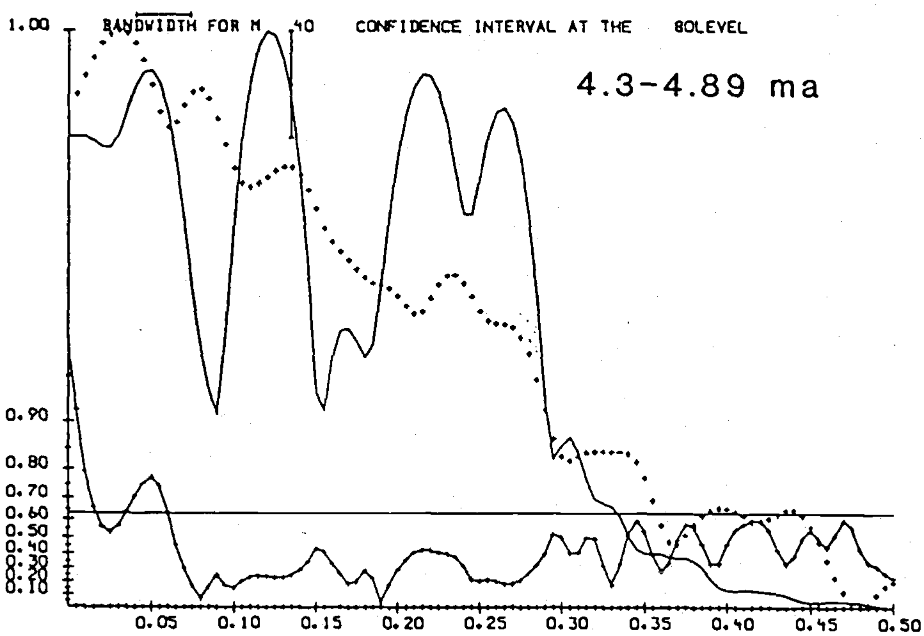

Figure 27: Cross spectra of August SST (dashed line) and eccentricity + obliquity + precession (etp; solid line).(a) Cross-spectra, 4.05 - 4.55 Ma. (b) Cross-spectra, 4.3 - 4.89 Ma.Labeling convention the same as for figure 8.

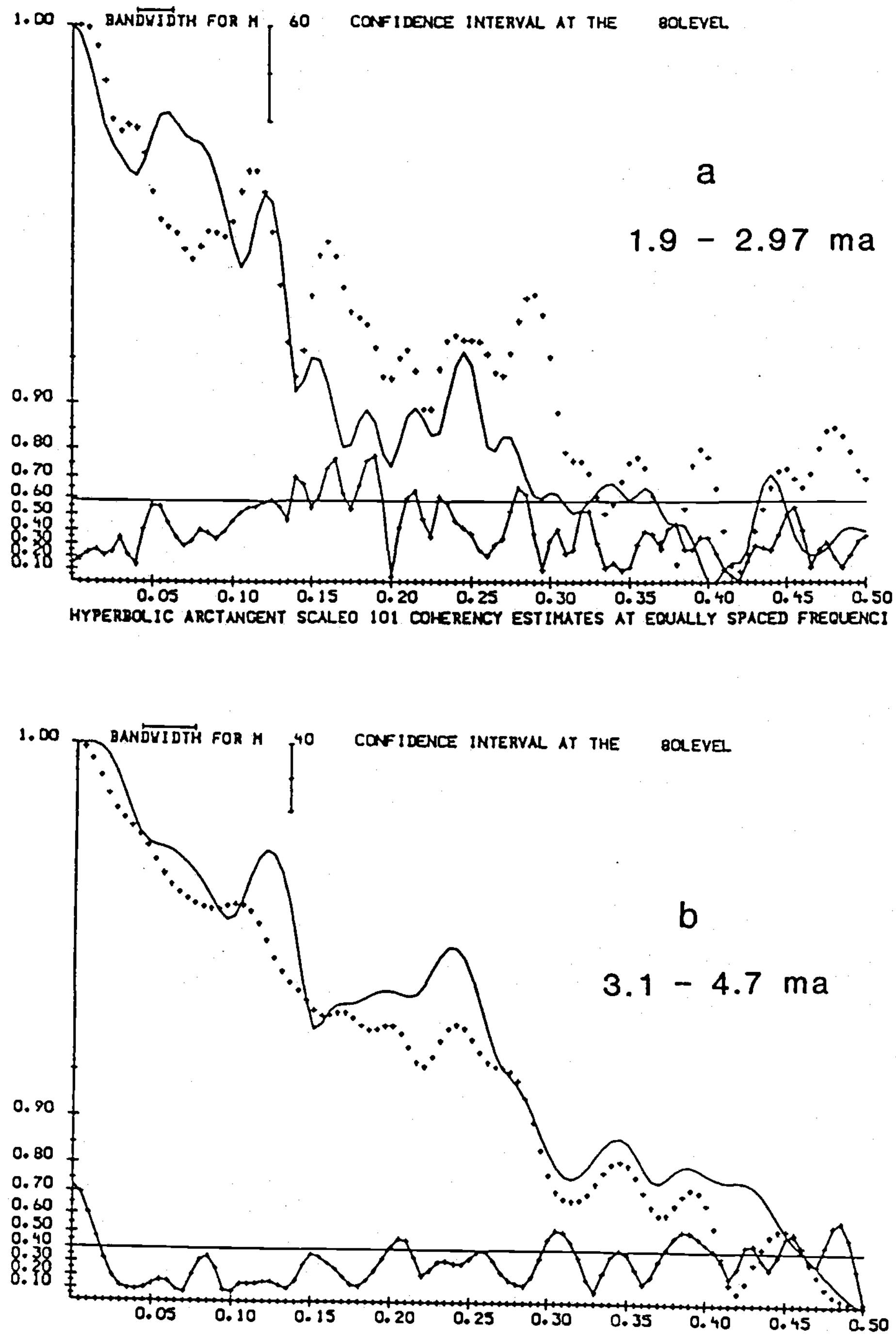

Figure 28: (a) Cross-spectra, August SST (dashed line) and $\delta^{18}O$ (solid line), 1.9 - 2.97 Ma. (b) Cross-spectra, August SST (dashed line) and $\delta^{18}O$ (solid line), 3.1 - 4.7 Ma. Labeling convention the same as for figure 8.

This lack of significant coherence in the orbital band raises some doubt as to the presence of direct orbital forcing of the SST signal. The possibility of a more subtle relationship to orbital forcing cannot be excluded at this point, however. More refined methods are now employed to determine if any relationship between the SST signals and orbital forcing can be detected.

IV. Complex Demodulation

Complex demodulation of the August SST record in the precession (23 kyr^{-1}) and obliquity (41 kyr^{-1}) frequency bands are compared to the amplitude modulation of precession and obliquity, respectively, in Figures 29 and 30. Note that the amplitude modulation of precession is, by definition, eccentricity (Berger, 1978).

In the precession band, it is apparent that the amplitude modulation of the August SST response is similar to the amplitude modulation of precession throughout the time interval. Cross spectra of the amplitude of precession (eccentricity) and the amplitude of the SST in the 23kyr^{-1} frequency band indicates that although coherence at $100{,}000^{-1}$ years exists between the two in the upper part of the record, it decreases in lower parts of the record (Figure 31).

In the obliquity band the amplitude modulation of SST is entirely dissimilar to the amplitude modulation of ob-

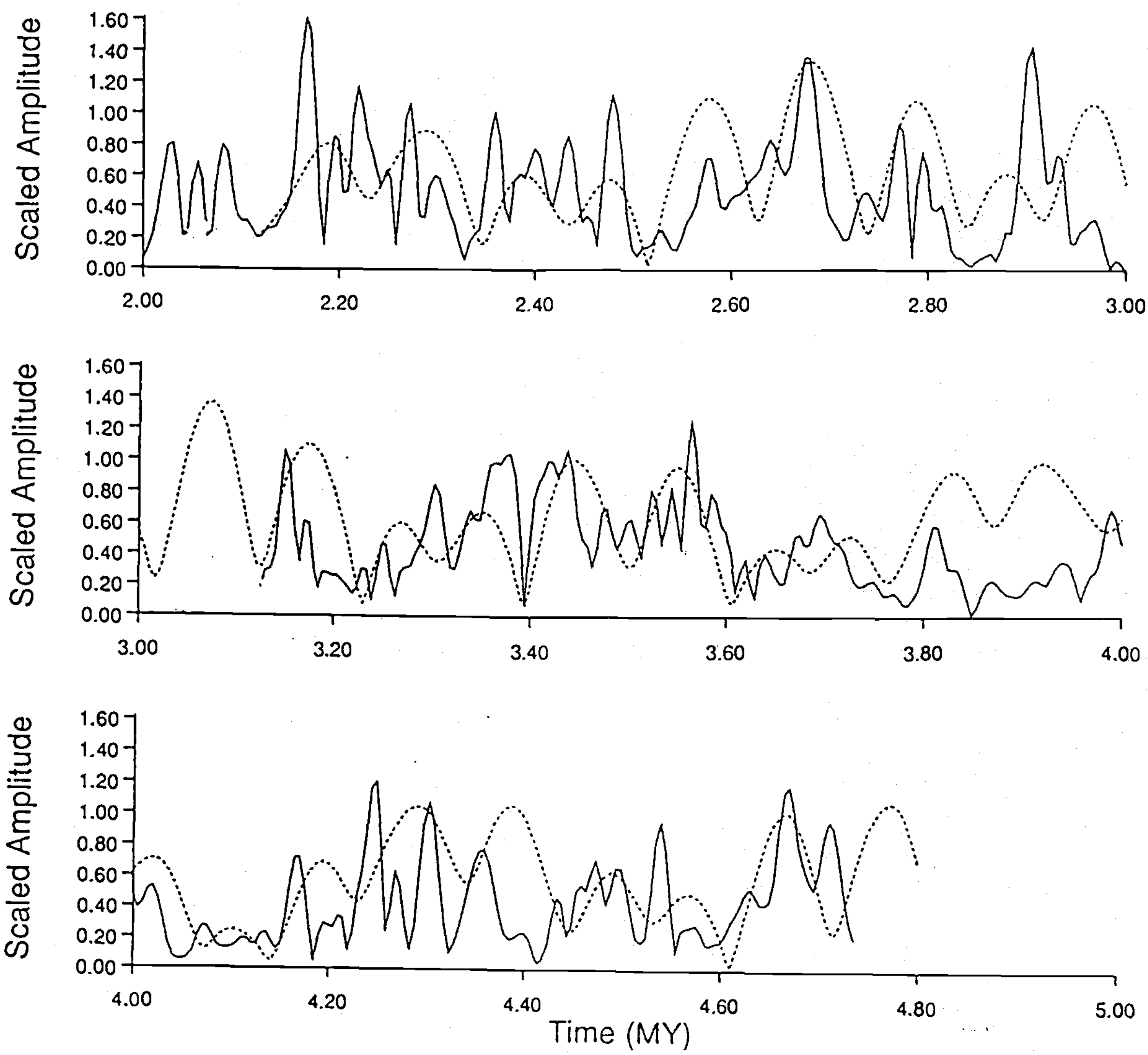

Figure 29: Demodulated amplitude of precession (dashed line) and August SST (solid line) in the precession band. The amplitude of precession has been scaled for comparison to SST.

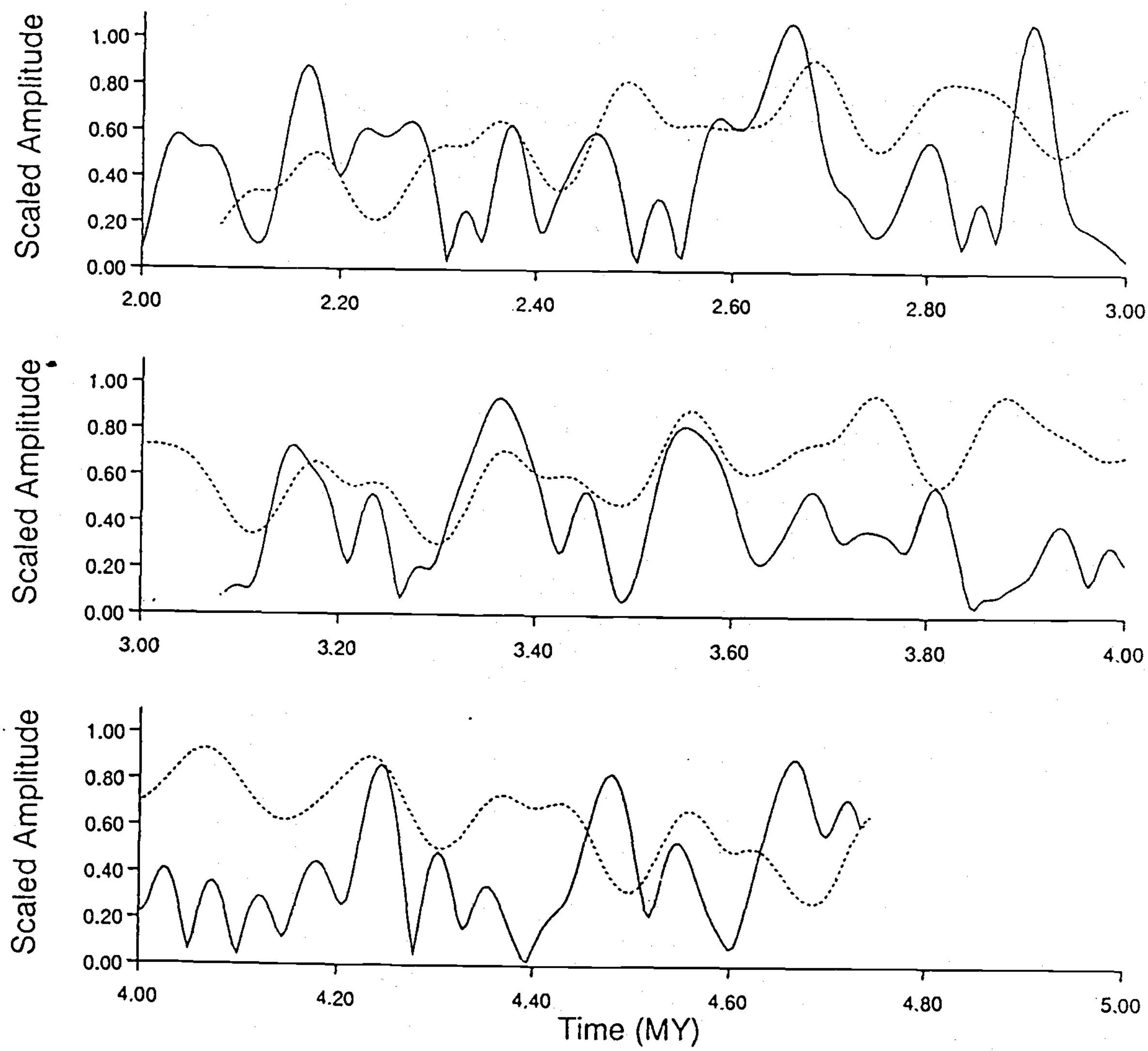

Figure 30: Demodulated amplitude of obliquity (dashed line) and August SST (solid line) in the obliquity band. Amplitudes have been scaled for comparison.

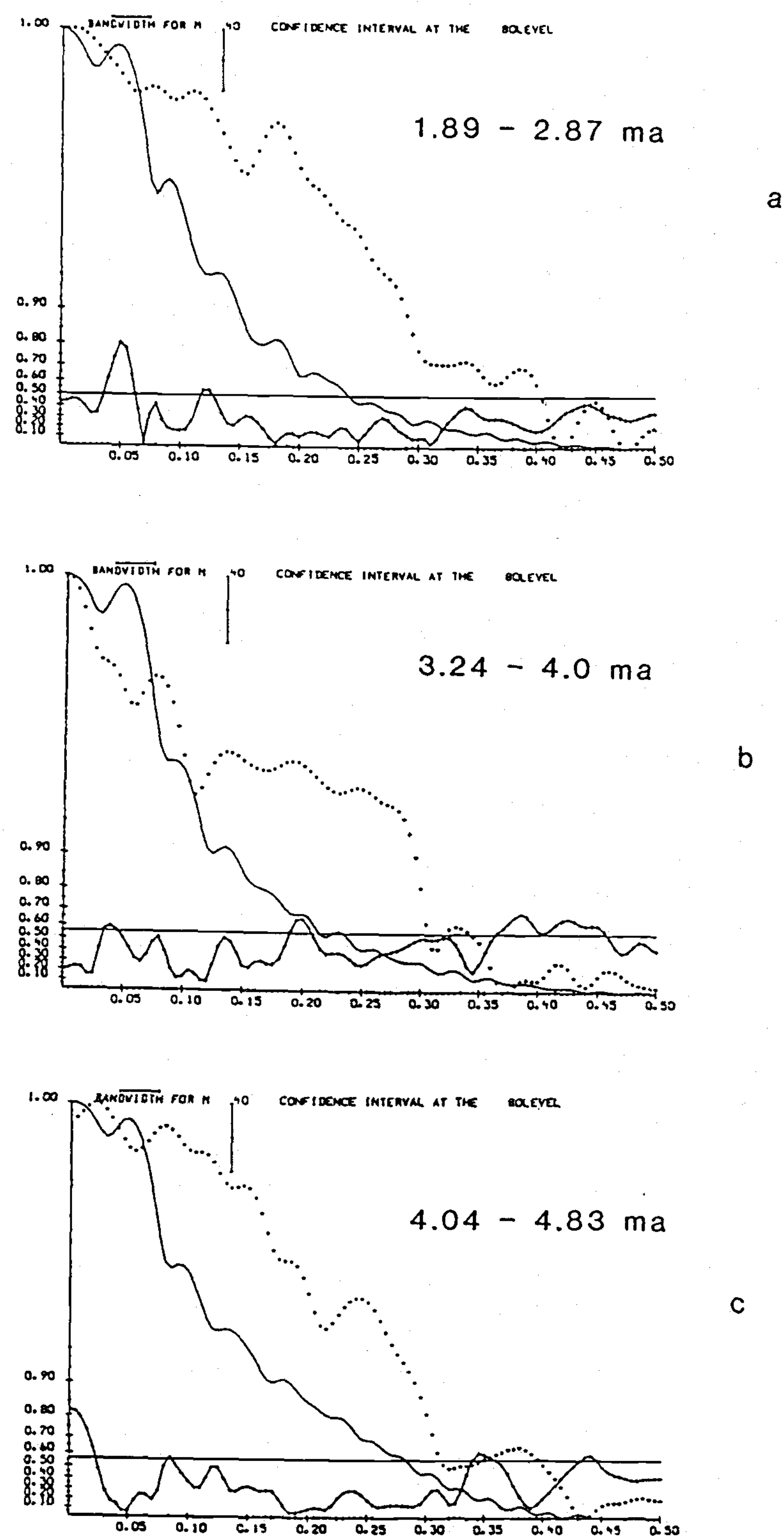

Figure 31: Cross spectra of the amplitude of precession (solid line) and the amplitude of the precession band component of SST (dashed line), (a) 1.9 - 2.97 ma. (b) 3.2 - 4.0 ma (c) 4.04 - 4.8 ma. Labeling convention the same as figure 8.

liquity (Figure 30). A particularly intriguing result is seen in comparing the modulation of the 41kyr^{-1} component of SST amplitude to the 23kyr^{-1} amplitude component (Figure 32). The similarity in the amplitudes over time is striking; furthermore, the coherence of these records is strong at low frequencies, where they are also in phase (Figure 33).

This phenomena is seen in other frequency bands that are not harmonics (multiples) of orbital frequencies, such as 60 kyr^{-1} and 35 kyr^{-1}. The amplitude modulation of SST at these frequencies is similar to and coherent with the amplitude modulation at 23 kyr^{-1} and 41 kyr^{-1} (Figure 34). These frequencies all follow the same amplitude modulation as precession.

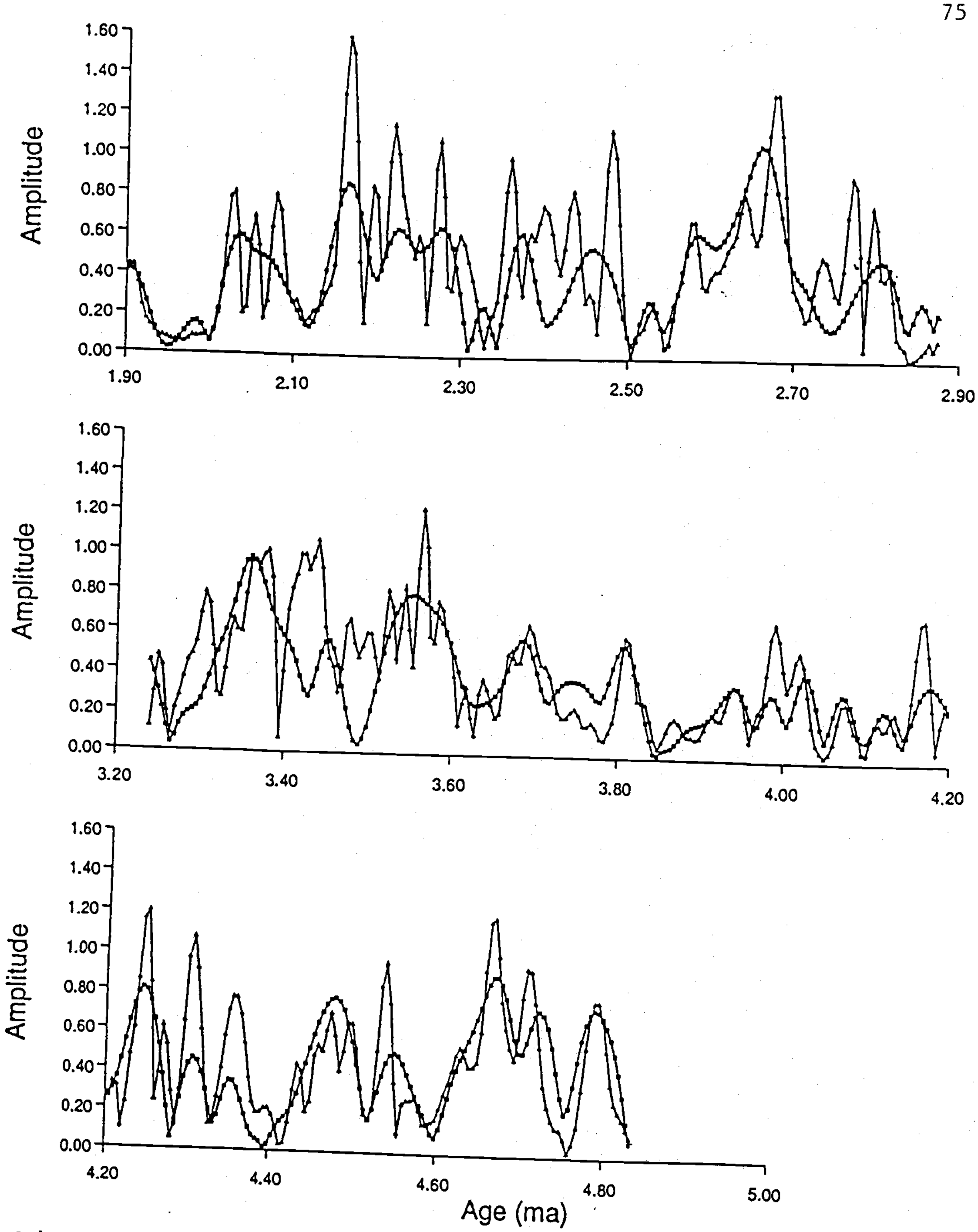

Figure 32: Demodulated amplitude of the precession band ($23kyr^{-1}$) component of August SST (triangles) and the $41kyr^{-1}$ component of August SST (squares).

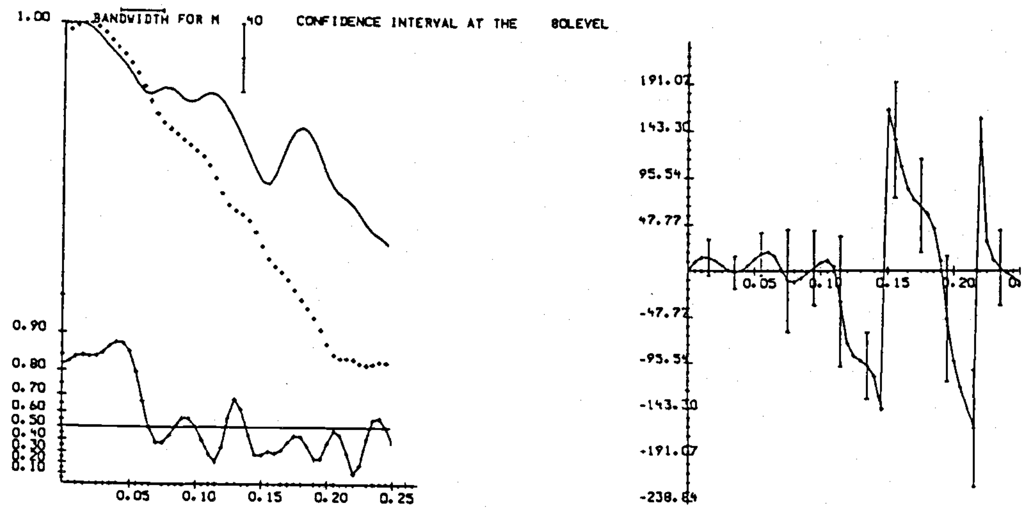

a 1.89 - 2.87 ma

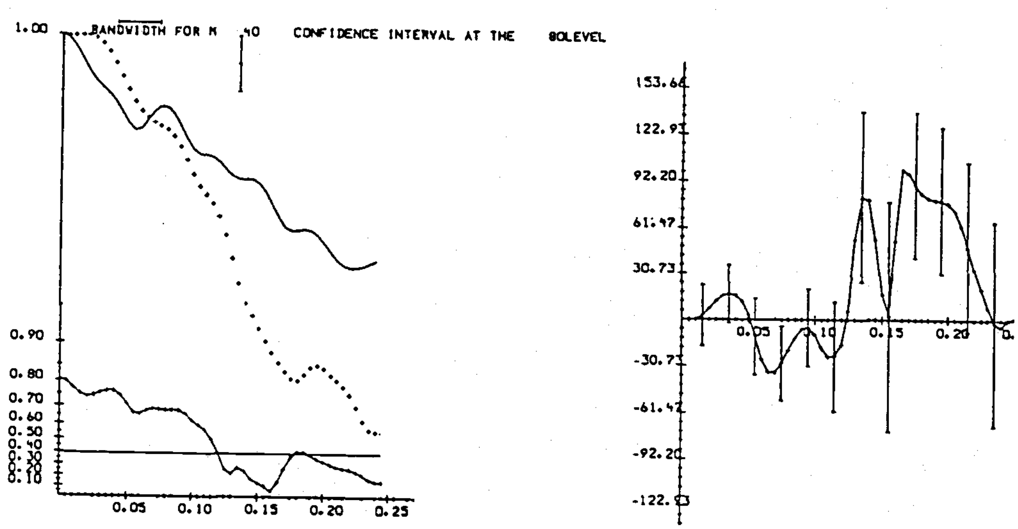

b 3.24 - 4.83 ma

Figure 33: Cross-spectra and phase of of $23kyr^{-1}$ (solid line) and $41kyr^{-1}$ (dashed line) components of August SST (a) 1.8 -2.9 ma (b) 3.1 - 4.8 ma. Labeling convention the same as figure 8 for cross-spectra, and phase is in degrees.

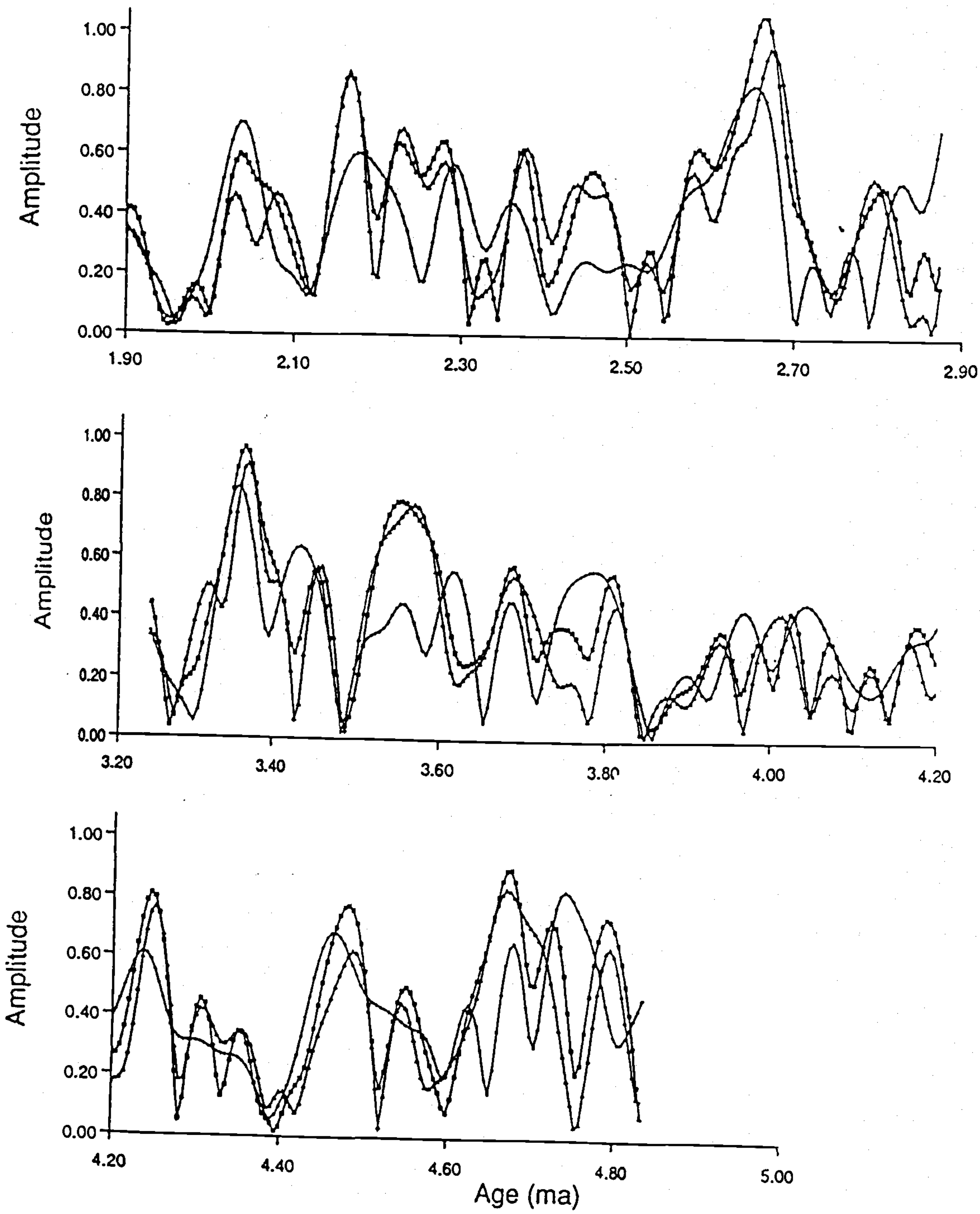

Figure 34: Demodulated amplitudes of $35kyr^{-1}$ (triangles) + $41kyr^{-1}$ (squares) + $60kyr^{-1}$ (dots) components of August SST.

DISCUSSION

Transformations of site 572 radiolarian data have produced a SST record which is a proxy for equatorial Pacific climatic change from 1.8 ma to 4.9 ma. Here the changes observed in this proxy over time as well as the nature of the climatic response to orbital forcing are explored.

Between the interval preceding the onset of Northern Hemisphere ice sheets, 2.48 - 3.2 ma, and the interval following the onset of glaciation (1.8 - 2.48 ma), the mean August and February SST estimates do not change significantly (Table 3). Before and after 3.2 ma, the latest estimated date of the closing of the Isthmus of Panama, a significant 0.8°C decrease in August SST and 0.9°C decrease in February SST is seen. Although this change in mean SST between 3.21 - 4.93 ma and 2.48 - 3.2 ma is significant ($\alpha = 0.05$), the temperature decrease does not appear to be a sharp transition. Instead, a gradual cooling of the surface waters from the lower to the upper Pliocene is indicated (Figure 17).

The observed SST changes before and after 3.2 ma coincide temporally with observed changes in the mean of benthic foraminiferal $\delta^{18}O$ records (Prell, 1984). This positive and rapid shift in the mean of the benthic isotopic record was not observed in site 572 and other low latitude planktonic isotopic records from the same time interval. When ice volume is a controlling factor of the ocean's isotopic composition, the planktonic and benthic records ordinarily covary; this benthic isotopic shift is thus interpreted to represent a sudden cooling of bottom waters at about 3.2 ma (Prell, 1984).

Although this shift in the mean benthic isotopic record should not affect the planktonic isotopic record if bottom water cooling occurs (Prell, 1984), the observed decrease of site 572 SST before and after 3.2 ma should theoretically influence the planktonic record (Mix, 1987). This is consistent with the observed slight increase in the mean of the site 572 $\delta^{18}O$ that is seen after 3.2 ma (Prell, 1984). This change in $\delta^{18}O$ is also not steplike in nature, however.

In addition to evidence for a global decrease of bottom water temperatures preceding the onset of Northern Hemisphere glaciation (Prell, 1984; Hodell et al, 1985; Keigwin, 1986), several other results suggest that before the onset of Northern Hemisphere glaciation, important climatic and atmospheric changes occurred as precursors. In the Antarctic there is evidence for cooling of surface waters at around 3.2 ma (Ciesielski and Grinstead, 1986). At equatorial Pacific DSDP site 573 (located to the west of site 572), a stepwise decrease in the depth of the thermocline occurred at around 2.9 ma (Hays, 1987; Hays et al., 1989). Previous to this time, the cool tongue associated with equatorial upwelling was located eastward of the modern location, suggesting lower average SEC intensity, reduced equatorial upwelling, and lower wind stress in the Pliocene.

In this study a gradual cooling of SST is seen at site 572, but no abrupt or distinct changes before and after the onset of Northern Hemisphere glaciation or the shoaling of Panama are evident. This lack of distinct change in the climate regime at 2.47 ma supports the idea that there may be significant decoupling of low latitudes from high latitude processes (Karlin et al, in press). Because a sharp transition in mean SST is absent at 3.2 ma, closure of the Isthmus of Panama did not perturb sea surface conditions at site 572 as significantly as other areas (Keigwin, 1982).

Examination of results in the precession band provides further evidence for the decoupling of low latitude responses from high latitude processes. The response of August SST to precessional forcing is of fairly low amplitude when the spectra are examined (Figures 18-22), and although the coherence between the two is nonsignificant in the precession band (Figures 23-28), the results of complex demodulation indicate that the amplitude modulation of precession and the 23 kyr^{-1} component of SST are similar (Figure 29). The only mild deviation of the SST modulation at this frequency from the precession modulation suggests that the SST is sensitive only to variations in precession throughout this interval, and that other oceanographic events have little effect.

Lack of coherence between the cross-spectra of SST and orbital variations in the obliquity band can be attributed to the nature of the SST data. Spectral analysis identifies frequencies by decomposing data into sinusoidal terms; when the data series is modulating or is nonsinusoidal, spectral peaks at these frequencies may be poorly defined by this analysis (Bloomfield, 1976, Ch.5). The strong amplitude modulation of the SST record at this frequency may cause the spectra to lose power at fundamental frequencies and lose coherence with obliquity.

The lack of coherence between SST and orbital cross-spectra in the precession band may reflect sensitivity to small errors in the time scale (Figures 23 - 27). Coherence between precession and SST requires a chronology accurate to less than the 23,000 year frequency of precession. The high coherency seen between the modulated signals (Figure 31) indicates that much less severe error limits are necessary when comparing the amplitudes of these components. This suggests that in analysis of time periods where a highly accurate chronology is uncertain, comparison of amplitude modulations may be a less sensitive means of gaining information than direct cross-spectral analysis.

A notable result of this study is the coinciding amplitude modulation of different frequency components of the SST data. The amplitude of the SST record in the 23 kyr^{-1} band is coherent with the amplitude of precession during the upper Pliocene (Figure 31), indicating a response to orbital forcing. In addition, the amplitude modulation of SST in the 41 kyr^{-1} band is coherent with the amplitude modulation of the 23 kyr^{-1} band (Figures 32 and 33). Furthermore, this similarity of amplitude modulation is seen at frequency bands not normally associated with orbital forcing (Figure 34). Thus, the amplitude modulation at each frequency band of the SST data that has been examined coincides with every other frequency band in its amplitude modulation at frequencies near 100 ky^{-1}.

This behavior is not unique to SST. Examination of the site 572 planktonic $\delta^{18}O$ record indicates a pattern of amplitude modulation at the 41 kyr^{-1} frequency band that is similar to the 23 kyr^{-1} frequency band modulation which in turn is similar to the amplitude modulation of precession (Figure 35). This amplitude modulation is again dissimilar to the amplitude modulation of obliquity.

These results imply that the equatorial Pacific may be sensitive to orbital forcing not only in the 23 kyr^{-1} band, but in a range of frequency bands throughout the Pliocene. This sensitivity overshadows significant climatic events such as the initiation of large ice sheets in the Northern Hemisphere and the closure of the Isthmus

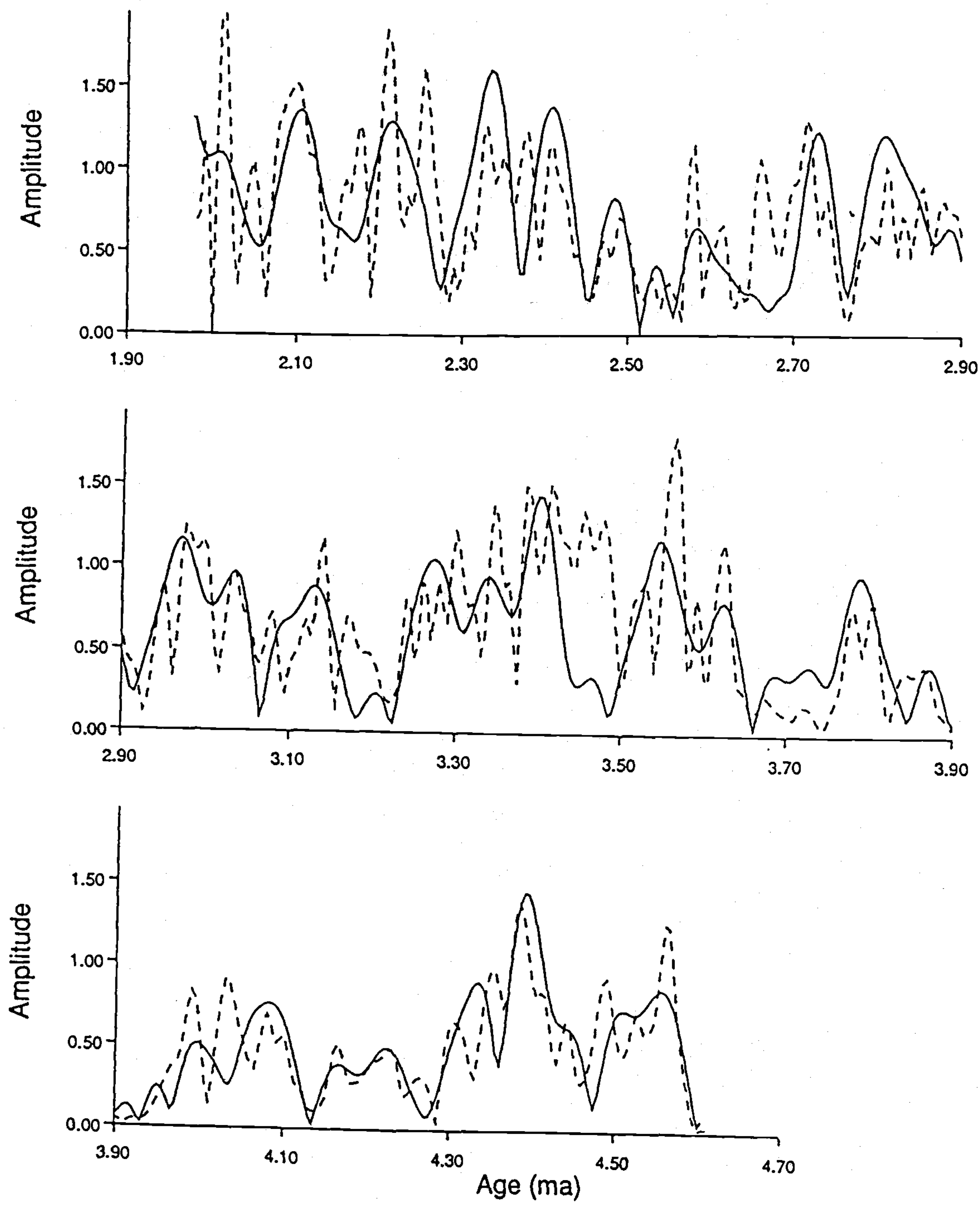

Figure 35: Demodulated amplitudes of 23kyr^{-1} component (dashed line) and 41kyr^{-1} component (solid line) of site 572 $\delta^{18}O$.

of Panama. It is present in the surface ocean temperature response and in the planktonic oxygen isotopic response.

While the response of SST at the $23ky^{-1}$ band may reflect a linear response to precessional forcing, the similar modulation at other frequencies in the SST and $\delta^{18}O$ record requires nonlinear behavior of the climatic system. This identical modulation of paleoclimatic signals across a range of frequency bands may be due to a series of harmonics and subharmonics created by a nonlinear response to orbital forcing. Such behavior has not been shown previously in a paleoclimatic data set, although the possibility of such behavior has been considered (Pisias and Leinen, 1984).

These results suggest significant differences between the dynamics of Pleistocene and Pliocene climatic regimes. Pleistocene evidence suggests a climatic system in which the response of the global oxygen isotope record to orbital forcing is predominantly linear (Imbrie et al., 1984). Discussion of nonlinearities in the Pleistocene system is primarily centered around the 100,000 year response in the upper Pleistocene (Hays et al., 1976; Imbrie and Imbrie, 1980), although nonlinearities in the obliquity band have been addressed as well (Pisias et al., in prep.). In the Pliocene regime presented in this study, a climatic system may exist in which at least two climatic variables, $\delta^{18}O$ and SST, respond to orbital forcing in a very different and highly nonlinear fashion than is seen in the Pleistocene regime.

A first order question arising from the results seen here is: How widespread in time and in geographic distribution is this behavior? Although the well-studied $\delta^{18}O$ record of the Pleistocene suggests a linear response of climate (Imbrie et al., 1984), the possibility of similar nonlinear behavior in other climatic variables during the Pleistocene cannot be ruled out. If similar behavior of the climatic system is discovered in the Pleistocene, new interpretations of the orbital influence on climate may thus be necessary. On the other hand, if this behavior is unique to the Pliocene, the notion that there are at least two different modes of climatic response to orbital forcing operating arises. The possibility arises that the Pleistocene may be characterized by a predominantly linear mode of response to orbital forcing, whereas the Pliocene may be dominated by a nonlinear response which affects a range of frequency bands other than the primary forcing frequency.

The possibility arises that what may be distinct Pleistocene / Pliocene differences may be due to a change in the response of the oceanic system to orbital forcing as the resonant frequencies of the climatic system itself changes. The climatic system may be responding nonlinearly to external forcing in the Pliocene and in a more linear manner in the Pleistocene, when the system's resonance may coincide with the external forcing. This nonlinear response of climate has been addressed by modelers, particularly in reference to the 100,000 year cycle in the late Pleistocene (Ghil, 1984; Ghil and Le Treut, 1981; Nicolis, 1984).

It is necessary to demonstrate that these results are not likely to be an artifact of the data or the techniques used. The technique of complex demodulation itself is considered first. Using the same techniques as in this study, random realizations of the SST data set were found not to have amplitude modulation similar to the SST data at any frequency band. In addition, no study that has used this technique with Pleistocene data sets has shown similar behavior (e.g. Pisias and Moore, 1981; Pisias et al., in prep.).

The possibility that orbital tuning of the chronology has produced such amplitude modulation must also be considered. Two lines of evidence indicate that this is not the case. The amplitude modulation of the site 572 $\delta^{18}O$ record was examined using the initial (untuned) chronology (Figure 36). It is apparent that this amplitude modulation was present before and after the tuning slightly modified the chronology. As a further check, an experiment was performed in which an artificial record was tuned to obliquity, and the spectra examined to determine if harmonics or subharmonics are produced by this process. Tuning of the artificial record, (a 1 million year record of obli-

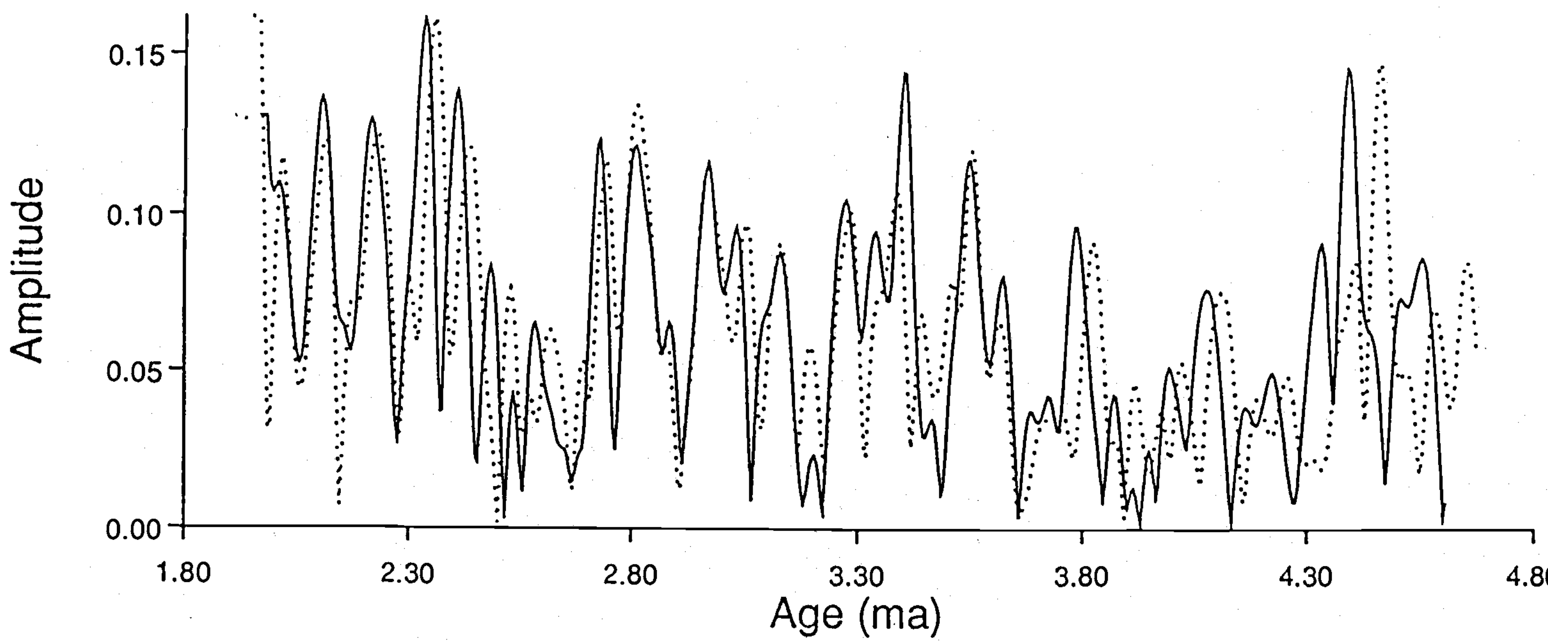

Figure 36: Comparison of 41kyr^{-1} component of $\delta^{18}O$ in the untuned chronology (dotted line) to the same component in the tuned chronology (solid line).

quity modulated by eccentricity plus a high frequency component), fails to produce a pattern of amplitude modulation at any frequency similar to results observed here.

The influence of potential error in the orbital calculations of eccentricity, obliquity, and precession on these results is also thought to be relatively insignificant. Berger (1982) and Berger and Pestiaux (1982) note that errors may be incurred in the amplitude and phase of the orbital calculations after about 3 ma; however, the coherence of amplitude modulation of the SST data at a range of frequency bands independent of the modulation of precession is in itself significant.

Finally, it must be noted that this pattern of amplitude modulation is seen in independent data sets (SST and $\delta^{18}O$), and is seen throughout the 1.9 - 4.8 ma interval. If data processing techniques were to create an artifact, one would expect the 572a portion of the SST record to differ from the 572c portion, for example. Likewise, if errors in radiolarian counts were thought to influence these modulations, one would not expect to see such similar modulations in the $\delta^{18}O$ record.

It has been demonstrated in this study that the eastern equatorial Pacific is responding to orbital forcing throughout the Pliocene. The climatic response to this forcing is entirely different than responses previously seen in the Pleistocene. These results suggest that the evolution of the climatic response to orbital forcing from the Pliocene to the Pleistocene is quite complex. In addition, the Pliocene climatic response appears insensitive to significant physical changes in boundary conditions, and sensitive only to changes in precession.

Further research is required to determine the physical mechanisms that could produce this type of oceanic response. Focusing attention on the evolution of the climatic response of the equatorial Pacific from such a highly nonlinear mode as is seen here into a predominantly linear mode as is seen in the Pleistocene should provide clues to these mechanisms.

CONCLUSIONS

(1) No distinct difference in sea surface temperature (SST) response at site 572 is observable before and after the initiation of Northern Hemisphere glaciation, suggesting a decoupling of the equatorial Pacific from high latitude processes.

(2) No direct influence of closure of the Isthmus of Panama is directly observable at site 572. Although a gradual cooling occurs prior to 3.2 ma, no sudden perturbation of the SST record is seen.

(3) The amplitude modulations of SST and $\delta^{18}O$ at a range of frequency bands are similar to one another and are highly coherent; at these frequencies, equatorial Pacific climate modulates near a 100 kyr^{-1} cycle in the Pliocene.

(4) The amplitude modulation of SST at a range of frequency bands including the orbital bands of 23 kyr^{-1} and 41 kyr^{-1} is similar to eccentricity, the amplitude modulation of precession, suggesting that equatorial Pacific climate responds nonlinearly to orbital forcing throughout the Pliocene.

(5) More study is necessary to determine the temporal and spatial extent of this behavior and the physical mechanisms by which sea surface temperature and planktonic $\delta^{18}O$ are responding in this way.

BIBLIOGRAPHY

Berger, A.L., 1984. Accuracy and frequency stability of the Earth's orbital elements during the Quaternary. In: A.L. Berger, J. Imbrie, J. Hays, G. Kukla, and B. Saltzman (eds.) Milankovitch and Climate, Part 1. Dordrecht: D. Riedel Publishing Company, pp. 3-39.

Berger, A.L., 1978. Long-term variations of caloric insolation resulting from the Earth's orbital elements. Quaternary Research 9: 139-167.

Berger, A.L. and P. Pestiaux, 1984. Accuracy and stability of the Quaternary terrestrial insolation. In: A.L. Berger, J. Imbrie, J. Hays, G. Kukla, and B. Saltzman (eds.) Milankovitch and Climate, Part 1. Dordrecht: D. Riedel Publishing Company, pp. 83-111.

Berggren, W.A., and C.D. Hollister, 1974. Paleogeography, paleobiogeography, and the history of circulation in the Atlantic Ocean. In: W.W. Hay (ed.), Studies in Paleoceanography. Tulsa, Oklahoma: Society for Economic Paleontologists and Mineralogists Special Publication No. 20, pp. 126-186.

Birchfield, G.E. and R.W. Grumbine, 1985. "Slow" physics of large continental ice sheets and underlying bedrock and its relation to the Pleistocene Ice Ages. Journal of Geophysical Research, 90 (B13): 11,294-11,302.

Birchfield, G.E. and J. Weertman, 1982. A model study of the role of variable ice albedo in the climate response of the Earth to orbital variations. Icarus, 50: 462-472.

Bloomfield, P., 1976. Fourier Analysis of Time Series: An Introduction. New York: Wiley and Sons, 258 pgs.

Bryden, H.L., and E.C. Brady, 1985. Diagnostic model of the three-dimensional circulation in the upper equatorial Pacific Ocean. Journal of Physical Oceanography, 15: 1255-1273.

Ciesielski, P.F. and G.P. Grinstead, 1986. Pliocene variations in the position of the Antarctic convergence in the Southwest Atlantic. Paleoceanography, 1 (2): 197-232.

Davis, J.C., 1986. Statistics and data Analysis in Geology, 2nd edition. New York: John Wiley and Sons. 646 pgs.

Dunn, D.A., 1982. Change from "Atlantic-type" to "Pacific-type" carbonate Stratigraphy in the middle Pliocene Equatorial Pacific Ocean. Marine Geology, 50: 41-60.

Dunn, D.A., 1980. Revised techniques for quantitative analysis using the "Karbonat-Bombe" and comparison to other quantitative carbonate analysis methods. Journal of Sedimentary Petrology, 50: 631-637.

Dunn, D.A. and Moore, T.C., 1981. Late Miocene-Pliocene (Magnetic Epoch 9 - Gilbert Magnetic Epoch) calcium carbonate stratigraphy of the equatorial Pacific ocean: summary. Geological Society of America Bulletin 92 (1): 104-107.

Ghil, M., 1984. Climate sensitivity, energy balance models, and oscillatory climate models. Journal of Geophysical Research, 89 (D1): 1280-1284.

Ghil, M., and H. Le Treut, 1981. A climate model with cryodynamics and geodynamics. Journal of Geophysical Research, 86 (C6), 5262 - 5270.

Hayes, S.P., 1987. The circulation of the equatorial Pacific ocean. In Further Progress in Equatorial Oceanography - Report of the 1986 US TOGA Workshop of the Dynamics of the Equatorial Oceans, E.J. Katz and J.M. Witte, eds. Ft. Lauderdale: Nova University Press, pp. 145-164.

Hays, J.D., J. Imbrie, and N.J. Shackelton, 1976. Variations in the Earth's orbit: Pacemaker of the Ice Ages. Science, 194: 1121-1132.

Hays, J.D., T. Saito, N.D. Opdyke and L.H. Burckle, 1969. Plio-Pleistocene sediments of the equatorial Pacific: their paleomagnetic, biostratigraphic, and climatic record. Geological Society of America Bulletin, 80: 1481-1514.

Hays, P., 1987. Paleoceanography of the Eastern Equatorial Pacific during the Pliocene: A high resolution radiolarian study. M.S. thesis (unpublished), Oregon State University.

Hays, P.E., N.G. Pisias, and A.K. Roelofs, 1989. Paleo ceanography of the eastern equatorial Pacific during the Pliocene: a high resolution study. Paleocean ography, 4 (1): 57-74.

Hodell, D.A., D.F. Williams, and J.P. Kennett, 1985. Late Pliocene reorganization of deep vertical watermass structure in the western South Atlantic: Faunal and isotopic evidence. Geological Society of America Bulletin, 96 (4): 495-503.

Horel, J.D., 1982. On the annual cycle of the tropical Pacific atmosphere and ocean. Monthly Weather Review, 110: 1863- 1878.

Imbrie, J., 1985. A theoretical framework for the Pleistocene ice ages. Journal of the Geological Society of London, 142: 417-432.

Imbrie, J., J.D. Hays, D.G. Martinson, A. McIntyre, A.C. Mix, J.J. Morley, N.G. Pisias, W.L. Prell, and N.J. Shackelton, 1984. The orbital theory of Pleistocene climate: support from a revised chronology of the marine d O-18 record. In: A.L. Berger, J. Imbrie, J. Hays, G. Kukla and B. Saltzman (eds.), Milankovitch and Climate, Part 1. D. Riedel Publishing Co., Dordrecht, pp. 269-305.

Imbrie, J. and J.Z. Imbrie, 1980. Modeling the climatic response to orbital variations. Science, 207: 943-953.

Imbrie, J. and N.G. Kipp, 1971. A new micropaleontological method for quantitative paleoclimatology: Application to a Late Pleistocene Caribbean core. In: K.K. Turekian (ed.), The Late Cenozoic Glacial Ages. Yale University Press, New Haven, pp. 71-181.

Imbrie, J., A. McIntyre, and A. Mix, in press. Oceanic response to orbital forcing in the late Quaternary: Observational and experimental strategies. In: J.-C. Duplessy, A. Berger, and S.H. Schneider (eds.), Climate and Geosciences. Dordrecht: Riedel Publishing Company.

Janacek, T.R., 1983. The history of eolian sedimentation and atmospheric circulation during the late Cenozoic. Unpublished Ph.D. dissertation, University of Michigan. 176 pgs.

Jansen, E., J. Sjoeholm, U. Bleil, and J. Erichsen, 1989. Neogene and Pleistocene glaciations in the Northern Hemisphere and Miocene-Pliocene global ice-volume fluctuations: Evidence from the Norwegian Sea. To be published in: Geologic History of the Polar Oceans: Arctic versus Antarctic (U. Bleil and Theide, J., eds). Kluwer Academic Publishers, NATO ASI Series.

Jenkins, G.M. and D.G. Watts, 1968. Spectral Analysis and its applications. San Francisco: Holden-Day, Inc. 525 pgs.

Karlin, K., W.F. Ruddiman, and A. McIntyre, in press. Comparison of Late-Pliocene and Late-Pleistocene sea-surface temperature responses in the Equatorial Atlantic divergence. Paleoceanography.

Keigwin, L.D., Jr., 1987. Pliocene stable-isotope record of Deep Sea Drilling Project Site 606: Sequential events of 18O enrichment at 3.1 Ma. In: R.B. Kidd, W.R. Ruddiman, et al., Initial Reports of the Deep Sea Drilling Project, 94: Washington (U.S. Government Printing Office), pp. 911-920.

Keigwin, L.D., Jr., 1986. Pliocene stable isotope record of Deep Sea Drilling Project Site 606: sequential events of $\delta^{18}O$ enrichment at 3.1 Ma. In: R.B. Kidd, W.R. Ruddiman, et al.,Initial Reports of the Deep Sea Drilling Project, 94: Washington (U.S. Government Printing Office).

Keigwin, L.D., Jr., 1982. Isotopic paleoceanography of the Caribbean and East Pacific: Role of Panama uplift in late Neogene time. Science, 217: 350-353.

Klovan, J.E. and J. Imbrie, 1971. An algorithm and fortran IV program for large-scale Q-mode factor analysis and calculation of factor scores. Mathematical Geology, 3 (1): 61-77.

Klovan, J.E. and A.T. Miesch, 1976. Extended CABFAC and Qmode computer programs for Q-mode factor analysis of compositional data. Computers in Geosciences, 1: 161-178.

Kominz, M.A., G.R. Heath, T.-L. Ku and N.G. Pisias, 1979. Bruhnes time scales and the interpretation of climatic change. Earth and Planetary Science Letters, 45: 394-410.

Levitus, S., 1982. Climatological Atlas of the World Ocean. Rockville Md: NOAA Professional Paper 13. 173 pgs.

Mankinen, E.A. and G.B. Dalrymple, 1979. Revised geomagnetic polarity time scale for the interval 0-5 my B.P. Journal of Geophysical Research, 84 (B2): 615-626.

Martinson, D.G., 1982. An inverse approach to signal correlation with applications to deep sea strati graphy and chronosratigraphy. Unpublished Ph.D. dissertation, Columbia University. 343 pgs.

Martinson, D.G., W. Menke, and P. Stoffa, 1982. An inverse approach to signal correlation. Journal of Geophysical Research, 87 (B6): 4807-4818.

Martinson, D.G., N.G. Pisias, J.D. Hays, J. Imbrie, T.C. Moore, Jr. and N.J. Shackelton, 1987. Age dating and the orbital theory of the Ice Ages: Development of a high-resolution 0 to 300,000 year chronostratigraphy. Quaternary Research 27: 1-29.

Mayer, L., F. Theyer, et al., Initial Reports of the Deep Sea Drilling Project, 85: Washington (U.S. Government Printing Office), pp. 33-224.

McIntyre, A., W.F. Ruddiman, K. Karlin, and A.C. Mix, 1989. Surface water response of the equatorial Atlantic ocean to orbital forcing. Paleoceanography 4(1):1955.

McPhaden, M.J., 1986. The Equatorial Undercurrent: 100 years of discovery. EOS: Transactions, American Geophysical Union, 67 (40): 762-764.

Mix, A., 1987. The oxygen-isotope record of glaciation. In: W.F. Ruddiman and H.E. Wright, eds., The Geology of North America, V. K-3: North America and Adjacent Oceans During the Last Deglaciation. Boulder, Colorado: Geological Society of America. pp. 111-135.

Molina-Cruz, A., 1977a. Radiolarian assemblages and their relationship to the oceanography of the subtropical southeastern Pacific. Marine Micropaleontology, 2: 315-352.

Molina-Cruz, A., 1977b. The relation of the southern trade winds to upwelling processes during the last 75,000 years. Quaternary Research, 8: 324-338.

Moore, T.C., Jr., 1978. The distribution of radiolarian assemblages in the modern and ice-age Pacific. Marine Micropaleontology 3: 229-266.

Moore, T.C., Jr., L.H. Burckle, K. Geitzenauer, B.Luz, A. Molina-Cruz, J.H. Robertson, H. Sachs, C. Sancetta, J. Theide, P.Thompson, and C. Wenkam, 1980. The reconstruction of sea surface temperatures in the Pacific Ocean of 18,000 B.P. Marine Micropaleontology 5: 215-247.

Morley, J.J., 1980. Analysis of the abundance variations of the subspecies of Cycladophora davisiana. Marine Micropaleontology, 6: 581-598.

Nicolis, C. Self-oscillations, external forcings, and climate predictability. In: A.L. Berger, J. Imbrie, J. Hays, G. Kukla and B. Saltzman (eds.), Milankovitch and Climate, Part 1. D. Riedel Publishing Co., Dordrecht, pp. .

Nigrini, C.A., 1985. Radiolarian biostratigraphy in the central equatorial Pacific, Deep Sea Drilling Project Leg 85. In: L. Mayer, F. Theyer, et al., Initial Reports of the Deep Sea Drilling Project, 85: Washington (U.S. Government Printing Office), pp. 511-522.

Nigrini, C.A., 1968. Radiolaria from eastern tropical Pacific sediments. Micropaleontology, 14: 51-63.

Nigrini, C. and G. Lombari, 1984. A Guide to Miocene Radiolaria. Cushman Foundation for Foraminiferal Research Special Publication Number 22.

Nigrini, C., and T.C. Moore, Jr., 1979. A Guide to Modern Radiolaria. Cushman Foundation for Foraminiferal Research Special Publication Number 16.

Oerlemans, J., 1982. Glacial cycles and ice-sheet modelling. Climatic Change, 4 (4): 353-374.

Philander, S.G.H., 1973. Equatorial Undercurrent: measurements and theories. Reviews of Geophysics and Space Physics, 11 (3): 513-570.

Pickard, G.L. and W.J. Emery, 1982. Descriptive Physical Oceanography: An Introduction. Oxford: Pergamon Press, Inc. 249 pgs.

Pisias, N.G., 1983. Geologic time series from deep sea sediments: time scales and distortion by bioturbation. Marine Geology, 51: 99-113.

Pisias, N.G. and M. Leinen, 1984. Milankovitch forcing of the oceanic system: Evidence from the Northwest Pacific. In: A.L. Berger, J. Imbrie, J. Hays, G. Kukla and B. Saltzman (eds.), Milankovitch and Climate, Part 1. D.Riedel Publishing Co., Dordrecht, pp. 307-330.

Pisias, N.G. and A.C. Mix, 1988. Aliasing of the geologic record and the search for long period Milankovitch cycles. Paleoceanography, 3: 613-619.

Pisias and Moore, 1981. The evolution of Pleistocene climate: A time series approach. Earth and Planetary Science Letters, (52): 450-458.

Pisias, N.G., D.W. Murray, and A.K. Roelofs, 1986. Radiolarian and silicoflagellate response to ocean ographic changes associated with the 1983 El Niño. Nature, 320 (6059): 259-262.

Pisias, N.G., and W.L. Prell, 1985. High resolution carbonate records from the hydraulic piston cored section of site 572. In: L. Mayer, F. Theyer, et al., Initial Reports of the Deep Sea Drilling Project, 85: Washington (U.S. Government Printing Office), pp. 711-722.

Prell, W.L., 1985. Pliocene stable isotope and carbonate stratigraphy (Holes 572C and 573A): Paleoceanographic data bearing of the question of Pliocene glaciation. In: L. Mayer, F. Theyer, et al., Initial Reports of the Deep Sea Drilling Project, 85: Washington (U.S. Government Printing Office), pp. 723-734.

Prell, W.L., 1984. Covariance patterns of foraminiferal dO^{18}: an evaluation of Pliocene ice volume changes near 3.2 million years ago. Science 226: 692-694.

Raymo, M.E., W.F. Ruddiman, J. Backman, B.M. Clement, and D.G. Martinson, in press. Late Pliocene variation in Northern Hemisphere Ice sheets and North Atlantic Deep Water circulation.

Rea, D.K. and H. Schrader, 1985. Late Pliocene onset of glaciation: Ice rafting and diatom stratigraphy of North Pacific DSDP cores. Palaeogeography, Palaeoclimatology, Palaeoecology, 49: 313-325.

Robinson, M.K., 1976. Atlas of North Pacific Monthly Mean Temperatures and Mean Salinities of the Surface Layer. Naval Oceano graphic Office, Washington D.C.

Roelofs, A.K. and N.G. Pisias, 1986. Revised technique for preparing quantitative radiolarian slides from deep-sea sediments. Micropaleontology, 24 (1): 182-185.

Romine, K. and T.C. Moore, 1981. Radiolarian assemblage distributions and paleoceanography of the eastern equatorial Pacific ocean during the last 127,000 years. Palaeogeography, Palaeoclimatology, Palaeoecology, 35: 281-314.

Saltzman, B. and A. Sutera, 1984. a model of the internal feedback system involved in late Quaternary climatic variations. Journal of Atmospheric Science, 41: 736-745.

Schramm, C.T., 1985. Implications of radiolarian as semblages for late Quaternary paleoceanography of the eastern equatorial Pacific. Quaternary Research, 24: 204-218.

Shackelton, N.J., J. Backman, H. Zimmerman, D.V. Kent, M.A. Hall, D.G. Roberts, D. Schnitker, J.G. Baldauf, A. Desprairies, R. Homrighausen, P. Huddlestun, J.B. Keene, A.J. Kaltenback, K.A.O. Krumsiek, A.C. Morton, J.W. Murray, and J. Westberg- Smith, 1984. Oxygen isotope calibration of the onset of ice-rafting and history of glaciation in the North Atlantic region. Nature, 307: 620-623.

Shackelton, N.J., and M.A. Hall, 1984. Oxygen and carbon isotope stratigraphy of DSDP Hole 552A: Plio-Pleistocene glacial history In: D.G. Roberts, D. Schnitker et al., Initial Reports of the Deep Sea Drilling Project, 81: Washington (U.S. Government Printing Office), pp. 599-610.

Shackelton, N.J. and N.D. Opdyke, 1977. Oxygen isotope and paleomagnetic evidence for early Northern Hemisphere glaciation. Nature, 270: 216-219.

van Andel, T.H., G.R. Heath, and T.C. Moore, Jr., 1975. Cenozoic history and paleoceanography of the Central Equatorial Pacific Ocean. Geological Society of America Memoir 143.

Wyrtki, K., 1974. Equatorial currents in the Pacific 1950 to 1970 and their relations to the trade winds. Journal of Physical Oceanography, 4: 372-380.

Wyrtki, K., 1966. Oceanography of the eastern equatorial Pacific ocean. Oceanography and Marine Biology Annual Review, 4: 33- 68.

Wyrtki, K., 1965. Surface currents of the eastern tropical Pacific Ocean. Bulletin of the Inter-American Tropical Tuna Commission, 9: 271-304.

Wyrtki, K. and B. Kilonsky, 1984. Mean water and current structure during the Hawaii-to-Tahiti Shuttle Experiment. Journal of Physical Oceanography, 14: 242-254.

APPENDICES

Appendix A

DSDP Site 572 data

CORE	COMPOSITE SBD (M)	AGE (MY)	CARBONATE (%)	FEB SST C	AUG SST C
572a-4-1	29.2000	1.7917	73.3600	23.8782	21.9423
572a-4-1	29.2800	1.8056	73.6900	26.7994	23.4578
572a-4-1	29.3800	1.8230	73.8500	27.3273	23.0755
572a-4-1	29.5000	1.8439	73.1100	27.5786	23.2071
572a-4-1	29.6000	1.8613	73.1100	25.7963	22.4486
572a-4-1	29.7400	1.8857	63.0900	25.7697	21.7359
572a-4-1	29.7870	1.8938	74.0100	------	------
572a-4-1	29.8427	1.9035	74.9700	24.8094	19.5469
572a-4-1	29.9155	1.9162	70.7000	24.6746	21.0319
572a-4-1	29.9935	1.9297	72.3200	------	------
572a-4-1	30.1215	1.9520	75.1300	24.0353	19.7262
572a-4-1	30.3044	1.9838	72.2000	24.2334	18.9909
572a-4-2	30.6400	1.9998	------	23.6193	17.9427
572a-4-2	30.9760	2.0117	63.0800	23.1970	18.6559
572a-4-2	31.1808	2.0249	65.1200	23.4793	17.1936
572a-4-2	31.3212	2.0344	71.8600	25.6237	21.1660
572a-4-2	31.3991	2.0395	73.0200	23.6521	20.3316
572a-4-2	31.5194	2.0472	78.6600	25.2448	21.4583
572a-4-2	31.5300	2.0479	------	25.0021	21.9720
572a-4-2	31.5488	2.0491	76.3800	24.9283	21.5753
572a-4-2	31.5916	2.0519	76.2800	25.9940	23.8443
572a-4-2	31.6501	2.0555	76.4100	24.8104	20.7684
572a-4-2	31.7040	2.0581	77.8900	25.1764	20.9283
572a-4-2	31.7225	2.0590	78.0100	24.8079	20.0309
572a-4-2	31.7447	2.0601	77.9000	23.5336	17.9044
572a-4-3	31.7693	2.0613	75.9100	------	------
572a-4-3	31.7892	2.0622	74.5100	23.9967	18.2728
572a-4-3	31.8123	2.0633	78.1600	24.1522	20.4122
572a-4-3	31.8367	2.0645	76.3700	25.7370	22.2481
572a-4-3	31.8661	2.0659	78.1400	24.8820	21.2036
572a-4-3	31.8895	2.0671	78.3400	------	------
572a-4-3	31.9325	2.0692	80.5500	24.1701	20.7017
572a-4-3	31.9679	2.0712	79.8900	------	------
572a-4-3	32.0834	2.0789	80.3700	24.5239	19.3839
572a-4-3	32.1352	2.0823	83.6000	25.9587	21.3764
572a-4-3	32.2515	2.0901	84.8200	25.9743	21.7417
572a-4-3	32.4500	2.1074	------	24.9420	20.6433
572a-4-3	32.6718	2.1224	81.7700	25.4582	20.7449
572a-4-3	32.9513	2.1368	77.5700	26.1785	21.2495
572a-4-4	33.3165	2.1523	81.2400	24.3832	21.0687
572a-4-4	33.4977	2.1624	80.5700	24.4648	16.8926
572a-4-4	33.6555	2.1722	79.3300	26.3307	23.7106
572a-4-4	33.7673	2.1796	77.5300	------	------
572a-4-4	33.8546	2.1855	76.5900	24.6328	21.0833
572a-4-4	33.9352	2.1910	79.4100	24.9790	21.1872
572a-4-4	34.0305	2.1975	71.1700	26.4633	23.1324
572a-4-4	34.1254	2.2049	68.4000	23.0412	19.9023
572a-4-4	34.1806	2.2092	70.5100	24.4981	20.3187
572a-4-4	34.2414	2.2139	73.0800	26.2350	22.1278
572a-4-4	34.3012	2.2185	75.9700	24.0276	18.7359
572a-4-4	34.3544	2.2223	68.3800	23.9665	19.4706
572a-4-4	34.4448	2.2283	76.4800	24.4781	20.7979
572a-4-4	34.5588	2.2359	74.3600	26.0503	22.8846
572a-4-4	34.6719	2.2433	76.7000	24.4631	22.0639
572a-4-5	34.7917	2.2511	80.7900	23.8964	20.1488
572a-4-5	34.9172	2.2592	80.2500	25.3475	21.4204
572a-4-5	35.0157	2.2633	79.5800	24.6360	20.2677
572a-4-5	35.1277	2.2676	80.5300	26.0395	22.0062
572a-4-5	35.2120	2.2708	85.2100	27.2250	23.9053
572a-4-5	35.2985	2.2742	82.4800	24.4129	20.4095
572a-4-5	35.3869	2.2801	82.1800	25.1251	20.8553

CORE	COMPOSITE SBD (M)	AGE (MY)	CARBONATE (%)	FEB SST C	AUG SST C
572a-4-5	35.5370	2.2917	85.5600	23.5407	19.1560
572a-4-5	35.6038	2.2963	86.2900	25.1347	18.7970
572a-4-5	35.6866	2.3009	88.3900	24.5147	18.8696
572a-4-5	35.7601	2.3049	87.1900	24.9579	20.0713
572a-4-5	35.8458	2.3096	85.7400	25.0107	20.4016
572a-4-5	35.9368	2.3146	85.5800	24.1667	18.2446
572a-4-5	36.0333	2.3216	81.3400	24.5139	19.7609
572a-5-1	36.3521	2.3451	70.2700	24.5264	21.0119
572a-5-1	36.4745	2.3502	80.9000	26.3436	22.7613
572a-5-1	36.5728	2.3543	86.5700	24.4121	18.8784
572a-5-1	36.6765	2.3586	76.5300	25.2562	22.7979
572a-5-1	36.7634	2.3628	73.3500	25.9594	23.1386
572a-5-1	36.8769	2.3688	76.1600	25.7404	22.4878
572a-5-1	36.9407	2.3721	75.4000	------	------
572a-5-1	37.0226	2.3765	71.9500	24.6909	21.3680
572a-5-1	37.0864	2.3798	70.0100	24.1630	21.2327
572a-5-1	37.1546	2.3831	68.8800	22.8889	20.8960
572a-5-1	37.2219	2.3863	78.9000	20.5881	17.3481
572a-5-1	37.2905	2.3895	78.5200	24.4438	21.1834
572a-5-1	37.3530	2.3925	76.8600	24.0673	21.1848
572a-5-1	37.4327	2.3963	77.6000	23.9558	20.8494
572a-5-1	37.5017	2.3996	76.8600	25.6898	22.8204
572a-5-2	37.5922	2.4087	75.7700	24.3427	19.4474
572a-5-2	37.7010	2.4200	78.6900	25.7639	21.0785
572a-5-2	37.7810	2.4240	81.0700	25.4906	21.7024
572a-5-2	37.8934	2.4297	77.1700	25.5493	21.6620
572a-5-2	38.0198	2.4360	69.8700	23.4159	18.7744
572a-5-2	38.1784	2.4468	76.0900	25.4461	20.8308
572a-5-2	38.3213	2.4592	71.6500	24.0535	21.4507
572a-5-2	38.5025	2.4657	74.9300	21.3068	21.2426
572a-5-2	38.6468	2.4706	80.7600	25.8644	22.1535
572a-5-2	38.7914	2.4754	81.1000	25.5503	21.3076
572a-5-2	38.9334	2.4802	79.0300	22.0568	17.7173
572a-5-2	39.0684	2.4873	79.3100	26.0463	22.0614
572a-5-2	39.1867	2.4935	79.6500	------	------
572a-5-2	39.3136	2.5010	77.8100	25.4176	20.9115
572a-5-2	39.4005	2.5250	85.8300	25.3285	21.8337
572a-5-3	39.5073	2.5322	87.4500	24.6902	20.7549
572a-5-3	39.6253	2.5400	86.6000	24.3911	20.3159
572a-5-3	39.7395	2.5473	81.7500	25.1294	20.8120
572a-5-3	39.8627	2.5543	78.5900	23.8619	20.5979
572a-5-3	40.0074	2.5626	84.0300	23.6165	19.7855
572a-5-3	40.2412	2.5717	88.0700	24.1181	19.9018
572a-5-3	40.4671	2.5796	59.0800	25.0922	22.5565
572a-5-3	40.8733	2.5965	81.7800	25.5870	21.6002
572a-5-3	41.1775	2.6096	85.8900	25.0093	20.2433
572a-5-3	41.4381	2.6199	84.1500	25.4141	20.4311
572a-5-3	41.5843	2.6400	86.2500	26.9748	23.9490
572a-5-3	41.6922	2.6500	85.5400	25.3520	22.0560
572a-5-3	41.8752	2.6626	88.0300	------	------
572a-5-4	41.9449	2.6689	87.7800	24.9503	18.9554
572a-5-4	42.0557	2.6812	86.1500	27.3002	24.9660
572a-5-4	42.1811	2.6901	84.5000	25.8626	22.1084
572a-5-4	42.3401	2.6989	83.4200	25.2375	22.2090
572a-5-4	42.5271	2.7117	85.8500	26.4462	23.5764
572a-5-4	42.7168	2.7269	85.5300	26.7442	24.4738
572a-5-4	42.8774	2.7351	86.7700	26.3817	22.3770
572a-5-4	43.0011	2.7415	81.1200	26.2392	23.1319
572a-5-4	43.0970	2.7480	82.9900	26.8429	24.3434
572a-5-4	43.1414	2.7529	83.1800	26.4577	23.2229
572a-5-4	43.1843	2.7577	80.5300	24.4076	21.3042
572a-5-4	43.2238	2.7621	73.8700	26.9356	23.9373

CORE	COMPOSITE SBD (M)	AGE (MY)	CARBONATE (%)	FEB SST C	AUG SST C
572a-5-4	43.2573	2.7656	76.0800	26.4605	23.6677
572a-5-4	43.2901	2.7681	75.8200	26.6450	23.3627
572a-5-4	43.3201	2.7705	75.7900	25.6058	22.9837
572a-5-4	43.3485	2.7727	74.7100	25.0119	21.9187
572a-5-5	43.3743	2.7748	72.9500	24.4914	20.4644
572a-5-5	43.3978	2.7766	77.0000	24.2676	21.0609
572a-5-5	43.4207	2.7784	74.6400	23.9449	20.2866
572a-5-5	43.4443	2.7802	79.9000	25.1229	21.1309
572a-5-5	43.4662	2.7820	76.4400	24.1064	20.8139
572a-5-5	43.4882	2.7837	76.6400	25.4043	21.9638
572a-5-5	43.5077	2.7852	84.0400	23.7381	21.0069
572a-5-5	43.5378	2.7876	80.7800	24.4080	20.3670
572a-5-5	43.5602	2.7893	69.4400	24.4957	19.6261
572a-5-5	43.5927	2.7919	76.3000	24.5386	21.6281
572a-5-5	43.6336	2.7951	72.3500	25.6470	22.1607
572a-5-5	43.6881	2.7994	73.6800	25.5288	21.5736
572a-5-5	43.7690	2.8056	72.8400	25.2573	20.8445
572a-5-5	43.9123	2.8148	76.9900	23.5877	18.9685
572a-5-5	44.2281	2.8378	73.0200	23.4399	19.8076
572a-5-6	44.6982	2.8663	89.5300	24.6311	21.9219
572a-5-6	45.0633	2.8944	76.4300	24.8405	21.4196
572a-5-6	45.1501	2.8997	72.6800	23.7478	19.1637
572a-5-6	45.2177	2.9038	72.5800	20.4768	15.5955
572a-5-6	45.2640	2.9066	77.5900	23.9247	20.4871
572a-5-6	45.3022	2.9089	75.2400	22.2462	17.9728
572a-5-6	45.3278	2.9107	66.3600	21.8766	15.6418
572a-5-6	45.3579	2.9133	72.4800	24.1158	18.1138
572a-5-6	45.3768	2.9149	66.8500	22.8737	18.5832
572a-5-6	45.3999	2.9169	64.2000	25.5123	19.7969
572a-5-6	45.4234	2.9190	59.8200	24.9940	20.6179
572a-5-6	45.4488	2.9212	52.4500	23.4521	18.7945
572a-5-6	45.4929	2.9250	59.8000	23.7445	19.5638
572a-5-6	45.5509	2.9300	63.2200	26.3940	21.9943
572a-5-6	45.6400	2.9344	58.3600	24.7668	18.8759
572a-5-7	45.8048	2.9424	64.0200	23.7824	19.7387
572a-5-7	46.2400	2.9622	68.5700	24.0177	20.5095
572a-5-7	46.3000	2.9648	63.9300	26.5987	21.9990
572a-5-7	46.4000	2.9691	62.8300	24.7142	20.4289
572c-6-1	48.5900	3.1421	73.7400	24.3154	18.7308
572c-6-1	48.6900	3.1486	69.3300	24.4759	16.6852
572c-6-1	48.7900	3.1550	70.1900	23.4653	18.0700
572c-6-1	48.8900	3.1583	76.2500	24.8148	20.9807
572c-6-1	49.0000	3.1620	74.3900	25.9682	21.0547
572c-6-1	49.0900	3.1650	79.4500	23.5446	18.9581
572c-6-1	49.1900	3.1683	82.5200	25.7111	20.9652
572c-6-1	49.3100	3.1723	77.7600	26.6274	22.7945
572c-6-1	49.3900	3.1750	78.4900	26.7732	23.4715
572c-6-1	49.5100	3.1917	80.1500	26.9269	24.0624
572c-6-1	49.5900	3.2017	82.1700	26.2908	22.5844
572c-6-1	49.6900	3.2100	75.5900	26.9637	22.8459
572c-6-1	49.7900	3.2183	70.9900	26.1873	21.6308
572c-6-1	49.8900	3.2278	82.0400	25.8527	20.4879
572c-6-2	50.0300	3.2415	81.6400	26.3290	21.3775
572c-6-2	50.1000	3.2459	78.4500	26.3469	20.9649
572c-6-2	50.2000	3.2515	82.4700	26.3954	23.1266
572c-6-2	50.3000	3.2572	78.2100	25.7603	20.6700
572c-6-2	50.3900	3.2625	73.7800	25.3446	22.1351
572c-6-2	50.4700	3.2669	76.6700	24.1555	20.6707
572c-6-2	50.6000	3.2740	76.8100	25.6366	21.7257
572c-6-2	50.6900	3.2789	77.9700	25.8425	21.9843
572c-6-2	50.8000	3.2853	86.1100	24.5869	20.8098
572c-6-2	50.8900	3.2906	88.6900	23.9784	19.8685

CORE	COMPOSITE SBD (M)	AGE (MY)	CARBONATE (%)	FEB SST C	AUG SST C
572c-6-2	50.9900	3.2965	82.1600	24.6705	21.3538
572c-6-2	51.0900	3.3036	84.3800	27.0749	22.7582
572c-6-2	51.1900	3.3126	81.2400	24.9462	20.3275
572c-6-2	51.2900	3.3216	79.2300	25.8359	20.9264
572c-6-2	51.4000	3.3323	80.0200	25.6826	21.0109
572c-6-3	51.5200	3.3440	81.1600	26.1375	23.4911
572c-6-3	51.6200	3.3508	78.5600	26.4240	23.5276
572c-6-3	51.6900	3.3553	72.5700	27.2554	24.1789
572c-6-3	51.7900	3.3618	61.6500	25.5552	21.7022
572c-6-3	51.8900	3.3674	64.1700	24.4608	20.0478
572c-6-3	51.9900	3.3721	65.2400	24.7532	19.3156
572c-6-3	52.0900	3.3769	65.5800	26.1189	19.4599
572c-6-3	52.2000	3.3821	70.5200	25.9069	22.0263
572c-6-3	52.3200	3.3895	76.6800	26.3551	21.9022
572c-6-3	52.3900	3.3948	74.3900	25.3148	20.6955
572c-6-3	52.5100	3.4039	73.2900	25.7123	22.0869
572c-6-3	52.5900	3.4100	80.8400	25.1441	20.6210
572c-6-3	52.6900	3.4165	87.5100	24.0637	18.1831
572c-6-3	52.7900	3.4229	83.0200	25.2929	20.3081
572c-6-3	52.8900	3.4293	82.7200	26.2759	23.3227
572c-6-3	52.9900	3.4342	83.1900	24.7825	19.6649
572c-6-4	53.1000	3.4393	76.9600	25.7846	20.3167
572c-6-4	53.2000	3.4440	74.2600	27.0993	22.9614
572c-6-4	53.2900	3.4481	74.5000	26.8199	23.8835
572c-6-4	53.3900	3.4540	54.0400	------	------
572c-6-4	53.5000	3.4613	51.9100	------	------
572c-6-4	53.5900	3.4673	76.9200	26.2477	22.5244
572c-6-4	53.6900	3.4721	81.8200	24.9177	21.5681
572c-6-4	53.8300	3.4771	75.3000	26.1233	21.9777
572c-6-4	53.9300	3.4807	71.1000	26.3051	22.7173
572c-6-4	54.0100	3.4836	59.3400	26.3593	23.9420
572c-6-4	54.0900	3.4873	61.0300	24.3618	21.0331
572c-6-4	54.1900	3.4931	78.2700	24.5015	21.5977
572c-6-4	54.3000	3.4995	83.3600	------	------
572c-6-4	54.3900	3.5048	83.6200	25.6925	22.9980
572c-6-4	54.4800	3.5100	88.3500	------	------
572c-6-5	54.5900	3.5128	83.8000	24.8218	20.3870
572c-6-5	54.6900	3.5152	85.1100	25.1345	21.6343
572c-6-5	54.7900	3.5177	79.1900	25.4257	21.8720
572c-6-5	54.8900	3.5202	65.4600	24.3222	19.6431
572c-6-5	54.9900	3.5227	69.1000	23.8525	20.4007
572c-6-5	55.0900	3.5253	78.6500	24.8084	18.5199
572c-6-5	55.1900	3.5278	79.9900	25.9223	22.3251
572c-6-5	55.2800	3.5300	83.7900	26.2842	22.1061
572c-6-5	55.3900	3.5360	78.1000	25.6987	21.7297
572c-6-5	55.4800	3.5408	74.9400	26.3337	23.7448
572c-6-5	55.5900	3.5468	66.9700	25.4775	21.5128
572c-6-5	55.6900	3.5520	72.5200	24.5723	21.0705
572c-6-5	55.7900	3.5572	72.9500	24.2841	21.0084
572c-6-5	55.8900	3.5623	72.6100	23.5875	17.7367
572c-6-5	55.9900	3.5674	71.1600	25.1385	21.3226
572c-6-6	56.0900	3.5726	72.2900	25.0363	21.8870
572c-6-6	56.1900	3.5779	77.1200	24.2738	22.1860
572c-6-6	56.2900	3.5832	71.1600	25.8002	22.8340
572c-6-6	56.3900	3.5884	75.2300	24.7428	21.7219
572c-6-6	56.4900	3.5937	82.8500	24.3854	20.9010
572c-6-6	56.6000	3.5996	75.6100	25.2217	20.3369
572c-6-6	56.6900	3.6044	66.8700	25.8217	21.1540
572c-6-6	56.7800	3.6092	59.7900	25.8918	21.9313
572c-6-6	56.8900	3.6150	56.9800	25.4489	21.6648
572c-6-6	56.9900	3.6203	58.6900	25.9248	23.5348
572c-6-6	57.0900	3.6255	66.6300	25.8756	22.9215

CORE	COMPOSITE SBD (M)	AGE (MY)	CARBONATE (%)	FEB SST C	AUG SST C
572c-6-6	57.1900	3.6308	64.8700	26.8672	23.7916
572c-6-6	57.3000	3.6376	61.5700	27.3874	24.4533
572c-6-6	57.3900	3.6456	49.0000	26.2560	23.6310
572c-6-7	57.5200	3.6580	72.5800	26.0641	23.7583
572c-6-7	57.5900	3.6650	75.9300	26.3350	23.2687
572c-6-7	57.6900	3.6763	74.9100	27.0460	24.9063
572c-6-7	57.7800	3.6875	72.9900	27.4779	23.8970
572c-6-7	57.8900	3.6964	76.7200	24.9667	21.1771
572c-7-1	58.1200	3.7129	60.1700	24.7298	22.7400
572c-7-1	58.1900	3.7179	51.0800	25.0707	22.4593
572c-7-1	58.3000	3.7257	49.8400	25.4910	21.4801
572c-7-1	58.4000	3.7329	51.4600	25.2530	21.5023
572c-7-1	58.4900	3.7430	63.0200	25.8921	21.8869
572c-7-1	58.5900	3.7563	62.2100	25.8195	23.4418
572c-7-1	58.6900	3.7687	63.9200	26.9297	23.7597
572c-7-1	58.7900	3.7817	65.4300	25.6225	22.8991
572c-7-1	58.8900	3.7950	73.5000	25.8337	21.9337
572c-7-1	59.0100	3.8076	74.2500	23.5276	20.2207
572c-7-1	59.0900	3.8161	74.1000	26.2575	22.4378
572c-7-1	59.1900	3.8276	72.0600	26.1545	22.7480
572c-7-1	59.2900	3.8390	70.7300	25.7650	22.1817
572c-7-1	59.3900	3.8504	68.7700	25.2970	22.7941
572c-7-1	59.4900	3.8630	69.9300	25.8105	22.0636
572c-7-1	59.5800	3.8750	67.3800	25.9247	22.5733
572c-7-2	59.6900	3.8919	63.3400	25.5865	21.7481
572c-7-2	59.7900	3.9083	62.8500	25.8655	21.1523
572c-7-2	59.8900	3.9225	62.5300	26.1096	21.8652
572c-7-2	59.9900	3.9350	69.6400	25.9863	22.2389
572c-7-2	60.0900	3.9467	73.5400	25.8475	20.8378
572c-7-2	60.1900	3.9578	73.6900	26.2449	21.7168
572c-7-2	60.2900	3.9650	73.5100	25.6433	22.1434
572c-7-2	60.3900	3.9712	69.1200	27.2176	23.3130
572c-7-2	60.4900	3.9785	71.7000	26.5761	22.1619
572c-7-2	60.5900	3.9872	81.9400	27.4225	25.2496
572c-7-2	60.7000	3.9972	82.3500	26.7708	22.9877
572c-7-2	60.7900	4.0072	80.0900	26.2059	23.1508
572c-7-2	60.8900	4.0183	78.2200	27.0623	24.3022
572c-7-2	60.9900	4.0294	79.3400	24.0848	21.7579
572c-7-2	61.0900	4.0419	81.8900	------	------
572c-7-3	61.1900	4.0558	77.4300	25.1387	21.3916
572c-7-3	61.2900	4.0661	81.7800	25.5072	21.4074
572c-7-3	61.3900	4.0748	83.7400	26.6686	23.0240
572c-7-3	61.4900	4.0844	76.3700	26.0972	22.9969
572c-7-3	61.5900	4.0956	82.4000	26.9604	22.8125
572c-7-3	61.7000	4.1078	86.1200	26.6204	23.3747
572c-7-3	61.7900	4.1178	84.6200	26.9536	22.6061
572c-7-3	61.8900	4.1289	84.0300	27.3762	22.3285
572c-7-3	61.9900	4.1400	84.6700	26.1941	23.4167
572c-7-3	62.0900	4.1543	83.3400	26.2558	22.5182
572c-7-3	62.1900	4.1652	78.7700	26.6977	24.5572
572c-7-3	62.3000	4.1748	84.2300	26.2142	21.5684
572c-7-3	62.3900	4.1833	83.2300	25.9431	22.2915
572c-7-3	62.4900	4.1944	77.0400	26.2492	21.5469
572c-7-4	62.6200	4.2070	85.1800	26.4069	22.4063
572c-7-4	62.6900	4.2130	81.1600	27.0033	22.9440
572c-7-4	62.7900	4.2218	78.0600	26.2119	22.0441
572c-7-4	62.8900	4.2309	80.9600	26.7521	22.6952
572c-7-4	62.9800	4.2391	79.6700	26.1607	20.4193
572c-7-4	63.0900	4.2467	71.5100	25.1385	17.6012
572c-7-4	63.2000	4.2540	77.5200	26.3690	21.8006
572c-7-4	63.2900	4.2600	80.4100	25.7103	20.6448
572c-7-4	63.3900	4.2680	86.2500	26.6014	22.1186

CORE	COMPOSITE SBD (M)	AGE (MY)	CARBONATE (%)	FEB SST C	AUG SST C
572c-7-4	63.4900	4.2760	59.4600	25.6029	20.2472
572c-7-4	63.5900	4.2849	87.7600	26.5180	20.7448
572c-7-4	63.6900	4.2947	86.4600	26.8264	21.8202
572c-7-4	63.7900	4.3041	------	25.0774	18.1264
572c-7-4	63.8900	4.3121	------	26.6389	22.1939
572c-7-4	63.9900	4.3200	------	25.5630	20.6880
572c-7-5	64.1200	4.3337	81.6500	26.7826	22.1454
572c-7-5	64.1900	4.3411	77.4600	25.1813	20.7016
572c-7-5	64.2900	4.3522	64.8500	27.7624	24.2199
572c-7-5	64.3900	4.3633	67.4000	26.1197	20.7846
572c-7-5	64.4900	4.3744	68.0400	26.6137	22.7406
572c-7-5	64.5900	4.3869	77.5800	25.5390	21.1242
572c-7-5	64.7000	4.4022	77.5200	25.7160	21.7065
572c-7-5	64.7900	4.4128	79.2000	25.4415	20.7304
572c-7-5	64.9300	4.4276	71.1900	24.6265	21.0413
572c-7-5	65.0300	4.4363	80.8200	25.1761	20.0199
572c-7-5	65.1100	4.4433	78.6500	25.3403	21.5875
572c-7-5	65.1900	4.4502	82.3800	26.4130	21.6078
572c-7-5	65.2900	4.4589	82.8300	26.5846	23.3405
572c-7-5	65.3900	4.4683	83.6000	26.9431	23.5809
572c-7-5	65.4900	4.4794	83.7000	26.2046	21.1244
572c-7-6	65.6200	4.4939	------	25.5376	20.4143
572c-7-6	65.6900	4.5017	------	25.6138	22.5292
572c-7-6	65.8000	4.5120	------	25.3578	22.4391
572c-7-6	65.9000	4.5206	------	24.5677	21.4868
572c-7-6	66.0200	4.5294	------	24.7246	22.0783
572c-7-6	66.1000	4.5344	------	25.4299	23.3076
572c-7-6	66.2000	4.5406	------	24.2861	18.8660
572c-7-6	66.2900	4.5472	------	25.8182	20.6728
572c-7-6	66.4100	4.5606	------	25.0185	20.8519
572c-7-6	66.4900	4.5706	------	26.2941	21.8438
572c-7-6	66.7000	4.5997	------	24.9489	19.9247
572c-7-6	66.8000	4.6136	------	25.3667	20.0026
572c-7-6	66.9100	4.6289	------	24.0516	17.4538
572c-7-6	67.0000	4.6414	------	24.4947	18.7718
572c-7-7	67.1200	4.6581	------	25.3914	20.2774
572c-7-7	67.2000	4.6692	------	24.2388	16.5925
572c-7-7	67.3000	4.6831	------	25.0177	21.4285
572c-7-7	67.4000	4.6970	------	26.6926	22.7238
572c-7-7	67.4900	4.7095	------	25.4436	21.2177
572c-7-7	67.5700	4.7206	------	28.0743	25.3795
572c-8-1	67.8000	4.7525	------	25.6946	20.9521
572c-8-1	67.9900	4.7789	------	25.3606	19.1522
572c-8-1	68.0900	4.7928	------	27.2853	22.6133
572c-8-1	68.1900	4.8067	------	25.1981	20.2288
572c-8-1	68.2900	4.8206	------	25.5439	20.4110
572c-8-1	68.3900	4.8345	------	26.5784	21.8331
572c-8-1	68.4900	4.8483	------	26.7256	21.6921
572c-8-1	68.5900	4.8622	------	27.2706	24.2397
572c-8-1	68.6900	4.8761	------	25.2072	20.4007
572c-8-1	68.7900	4.8900	------	23.5006	18.5670
572c-8-1	68.8900	4.9039	------	24.2097	18.5423
572c-8-1	68.9800	4.9164	------	27.6880	25.8466
572c-8-1	69.0900	4.9317	------	24.4730	18.7085

Appendix B

Results of 572a depth mapping function

core	original SBD, m	%CaCO3	composite SBD, m
572-4-1	29.0000	73.3600	29.2000
572-4-1	29.0800	73.6900	29.2800
572-4-1	29.1800	73.8500	29.3800
572-4-1	29.3000	73.1100	29.5000
572-4-1	29.4000	73.1100	29.6000
572-4-1	29.5000	63.0900	29.7400
572-4-1	29.5900	74.0100	29.7870
572-4-1	29.6900	74.9700	29.8427
572-4-1	29.8000	70.7000	29.9155
572-4-1	29.8900	72.3200	29.9935
572-4-1	29.9900	75.1300	30.1215
572-4-1	30.0800	72.2000	30.3044
572-4-2	30.2900	63.0800	30.9760
572-4-2	30.3900	65.1200	31.1808
572-4-2	30.5000	71.8600	31.3212
572-4-2	30.5900	73.0200	31.3991
572-4-2	30.8000	78.6600	31.5194
572-4-2	30.8700	76.3800	31.5488
572-4-2	30.9900	76.2800	31.5916
572-4-2	31.1900	76.4100	31.6501
572-4-2	31.4100	77.8900	31.7040
572-4-2	31.4900	78.0100	31.7225
572-4-2	31.5900	77.9000	31.7447
572-4-3	31.7000	75.9100	31.7693
572-4-3	31.7900	74.5100	31.7892
572-4-3	31.8900	78.1600	31.8123
572-4-3	31.9900	76.3700	31.8367
572-4-3	32.1000	78.1400	31.8661
572-4-3	32.1800	78.3400	31.8895
572-4-3	32.3100	80.5500	31.9325
572-4-3	32.4000	79.8900	31.9679
572-4-3	32.6200	80.3700	32.0834
572-4-3	32.6900	83.6000	32.1352
572-4-3	32.8000	84.8200	32.2515
572-4-3	33.0000	81.7700	32.6718
572-4-3	33.0800	77.5700	32.9513
572-4-4	33.2000	81.2400	33.3165
572-4-4	33.2900	80.5700	33.4977
572-4-4	33.4000	79.3300	33.6555
572-4-4	33.5000	77.5300	33.7673
572-4-4	33.5900	76.5900	33.8546
572-4-4	33.6800	79.4100	33.9352
572-4-4	33.7900	71.1700	34.0305
572-4-4	33.9000	68.4000	34.1254
572-4-4	34.0000	70.5100	34.1806
572-4-4	34.1100	73.0800	34.2414
572-4-4	34.2100	75.9700	34.3012
572-4-4	34.3000	68.3800	34.3544
572-4-4	34.3900	76.4800	34.4448
572-4-4	34.4900	74.3600	34.5588
572-4-4	34.5900	76.7000	34.6719
572-4-5	34.6900	80.7900	34.7917
572-4-5	34.8000	80.2500	34.9172
572-4-5	34.8900	79.5800	35.0157
572-4-5	35.0000	80.5300	35.1277
572-4-5	35.0900	85.2100	35.2120
572-4-5	35.1900	82.4800	35.2985
572-4-5	35.3000	82.1800	35.3869
572-4-5	35.5000	85.5600	35.5370
572-4-5	35.5900	86.2900	35.6038
572-4-5	35.7000	88.3900	35.6866
572-4-5	35.7900	87.1900	35.7601
572-4-5	35.8900	85.7400	35.8458

core	original SBD, m	%CaCO3	composite SBD, m
572-4-5	35.9900	85.5800	35.9368
572-4-5	36.0900	81.3400	36.0333
572-5-1	36.3900	70.2700	36.3521
572-5-1	36.5000	80.9000	36.4745
572-5-1	36.5900	86.5700	36.5728
572-5-1	36.6900	76.5300	36.6765
572-5-1	36.7800	73.3500	36.7634
572-5-1	36.9100	76.1600	36.8769
572-5-1	36.9900	75.4000	36.9407
572-5-1	37.1000	71.9500	37.0226
572-5-1	37.1900	70.0100	37.0864
572-5-1	37.2900	68.8800	37.1546
572-5-1	37.3900	78.9000	37.2219
572-5-1	37.4900	78.5200	37.2905
572-5-1	37.5800	76.8600	37.3530
572-5-1	37.6900	77.6000	37.4327
572-5-1	37.7800	76.8600	37.5017
572-5-2	37.8900	75.7700	37.5922
572-5-2	38.0100	78.6900	37.7010
572-5-2	38.0900	81.0700	37.7810
572-5-2	38.1900	77.1700	37.8934
572-5-2	38.2900	69.8700	38.0198
572-5-2	38.4000	76.0900	38.1784
572-5-2	38.4900	71.6500	38.3213
572-5-2	38.6000	74.9300	38.5025
572-5-2	38.6900	80.7600	38.6468
572-5-2	38.7900	81.1000	38.7914
572-5-2	38.8900	79.0300	38.9334
572-5-2	38.9900	79.3100	39.0684
572-5-2	39.0900	79.6500	39.1867
572-5-2	39.2000	77.8100	39.3136
572-5-2	39.2800	85.8300	39.4005
572-5-3	39.3800	87.4500	39.5073
572-5-3	39.4900	86.6000	39.6253
572-5-3	39.5900	81.7500	39.7395
572-5-3	39.6900	78.5900	39.8627
572-5-3	39.7900	84.0300	40.0074
572-5-3	39.9100	88.0700	40.2412
572-5-3	39.9900	59.0800	40.4671
572-5-3	40.1000	81.7800	40.8733
572-5-3	40.1900	85.8900	41.1775
572-5-3	40.2900	84.1500	41.4381
572-5-3	40.3900	86.2500	41.5843
572-5-3	40.4900	85.5400	41.6922
572-5-3	40.7000	88.0300	41.8752
572-5-4	40.7800	87.7800	41.9449
572-5-4	40.8900	86.1500	42.0557
572-5-4	40.9900	84.5000	42.1811
572-5-4	41.0900	83.4200	42.3401
572-5-4	41.1900	85.8500	42.5271
572-5-4	41.2900	85.5300	42.7168
572-5-4	41.3900	86.7700	42.8774
572-5-4	41.4900	81.1200	43.0011
572-5-4	41.6100	82.9900	43.0970
572-5-4	41.6900	83.1800	43.1414
572-5-4	41.7900	80.5300	43.1843
572-5-4	41.8900	73.8700	43.2238
572-5-4	41.9900	76.0800	43.2573
572-5-4	42.0900	75.8200	43.2901
572-5-4	42.1900	75.7900	43.3201
572-5-4	42.2900	74.7100	43.3485
572-5-5	42.3900	72.9500	43.3743
572-5-5	42.4900	77.0000	43.3978

core	original SBD, m	%CaCO3	composite SBD, m
572-5-5	42.5900	74.6400	43.4207
572-5-5	42.6900	79.9000	43.4443
572-5-5	42.7900	76.4400	43.4662
572-5-5	42.9000	76.6400	43.4882
572-5-5	42.9900	84.0400	43.5077
572-5-5	43.1100	80.7800	43.5378
572-5-5	43.1900	69.4400	43.5602
572-5-5	43.2900	76.3000	43.5927
572-5-5	43.3900	72.3500	43.6336
572-5-5	43.4900	73.6800	43.6881
572-5-5	43.5900	72.8400	43.7690
572-5-5	43.6900	76.9900	43.9123
572-5-5	43.7900	73.0200	44.2281
572-5-6	43.8800	89.5300	44.6982
572-5-6	44.0100	76.4300	45.0633
572-5-6	44.0900	72.6800	45.1501
572-5-6	44.1900	72.5800	45.2177
572-5-6	44.2900	77.5900	45.2640
572-5-6	44.4000	75.2400	45.3022
572-5-6	44.4900	66.3600	45.3278
572-5-6	44.6100	72.4800	45.3579
572-5-6	44.6900	66.8500	45.3768
572-5-6	44.7900	64.2000	45.3999
572-5-6	44.8900	59.8200	45.4234
572-5-6	44.9900	52.4500	45.4488
572-5-6	45.0900	59.8000	45.4929
572-5-6	45.1900	63.2200	45.5509
572-5-6	45.2900	58.3600	45.6400
572-5-7	45.3900	64.0200	45.8048
572-5-7	45.5000	68.5700	46.2400
572-5-7	45.6000	63.9300	46.3000
572-5-7	45.7000	62.8300	46.4000